# Diffusion along mean motion resonance for the restricted planar three body problem

Jacques Féjoz, Marcel Guàrdia, Vadim Kaloshin & Pablo Roldán

September 2, 2011

# 1 Introduction and main result

The stability of the Solar System is a longstanding problem. Over the centuries, mathematicians and astronomers have spent an inordinate amount of time and energy proving stronger and stronger stability theorems for dynamical systems closely related to the Solar System, generally within the frame of the Newtonian $N$-body problem:

$$\ddot{q}_i = \sum_{j \neq i} m_j \frac{q_j - q_i}{\|q_j - q_i\|^3}, \quad q_i \in \mathbf{R}^2, \quad i = 0, 1, ..., N-1, \tag{1}$$

and its planetary subproblem, where $m_0$ (thought of as that of the Sun) is much larger than the other masses $m_i$.

The theorem of Lagrange and Laplace entails that the observed variations in the motion of Jupiter and Saturn come from resonant terms of large amplitude and long period, but with zero average [**?**, p. 164]. Yet it is a mistake, which Laplace made, to infer the topological stability of the planetary system, since the theorem deals only with an approximation of the first order with respect to the masses of the planets and the eccentricities and inclinations. Another key result is Arnold's theorem, which proves the existence of a set of positive Lebesgue measure filled by invariant tori in planetary systems, provided that the masses of the planets are small [**?**, **?**]. However, in the phase space the gaps left by the invariant tori leave room for instability.

It was a big surprise when the numerical computations of Sussman, Wisdom and Laskar showed that over the life span of the Sun, or even over a few hundred thousands years, collisions and ejections of inner planets are probable (because of the exponential divergence of solutions, only a probabilistic result seems within the reach of numerical experiments); see for example [**?**, **?**], or [**?**] for a recent account. Our Solar System, as well as newly discovered extra-solar systems, are now widely believed to be unstable, and the general conjecture about the $N$-body problem is quite the opposite of what it used to be:

**Conjecture 1.1** (Global instability of the $N$-body problem)**.** *In restriction to any energy level of the $N$-body problem, the non-wandering set is nowhere dense. (One can reparameterize orbits so as to have a complete flow, despite collisions.)*

According to Herman [**?**], this is the oldest open problem in dynamical systems (see also [**?**]). This conjecture would imply that bounded orbits form a *nowhere dense set* and that no topological stability holds, in a very strong sense. It is largely confirmed by numerical experiments. In our Solar System, Laskar for instance has shown that collisions between Mars and Venus could occur within a few billion years. The coexistence of a nowhere dense set of positive measure of bounded quasiperiodic motions with an open and dense set of initial conditions with unbounded orbits is a remarkable conjecture.

Currently the above conjecture is largely out of reach. A more modest but still much challenging goal is a local version of the conjecture:

**Conjecture 1.2** (Instability of the planetary problem)**.** *If the masses of the planets are small enough, the wandering set accumulates on the set of circular, coplanar, Keplerian motions.*

There have been some prior attempts to prove such a conjecture. For instance, Moeckel discovered an instability mechanism in the 5-body problem [**?**]. But his proof of diffusion was limited by the so-called big gaps problem between hyperbolic invariant tori. A somehow opposite strategy was developed by Bolotin and McKay, using the Poincaré orbits of the second species to show the existence of symbolic dynamics in the three-body problem, hence of chaotic orbits, but considering far from integrable, non-planetary conditions; see for example [**?**].

In this paper we prove the existence of large instabilities in a realistic planetary system and describe the associated instability mechanism. Thus, we provide a step towards the proof of Conjecture 1.2. The instability mechanism shown in this paper is related to a generalized version of the Mather mechanism [**?**, **?**, **?**, **?**, **?**]. Some parts of the proof rely on high-accuracy numerical computations.

## 1.1 The Restricted elliptic planar three-body problem

Consider the planetary problem (1) assuming $m_0 \gg m_1 \gg m_i,\ i = 2, \ldots, N-1$. The equations of motion can be written as

$$\ddot{q}_i = m_0 \frac{q_0 - q_i}{\|q_0 - q_i\|^3} + m_1 \frac{q_1 - q_i}{\|q_1 - q_i\|^3} + \sum_{j \neq i, j>1} m_j \frac{q_j - q_i}{\|q_j - q_i\|^3}. \tag{2}$$

Neglecting the last sum we obtain the so called *Restricted problem*:

$$\ddot{q}_i = m_0 \frac{q_0 - q_i}{\|q_0 - q_i\|^3} + m_1 \frac{q_1 - q_i}{\|q_1 - q_i\|^3}. \tag{3}$$

This problem can also be obtained by taking $m_j \to 0$. Then, the massless bodies $i \geq 2$ are influenced by, without themselves influencing the *primaries* $i = 0, 1$.

Taking $N = 3$, this model is often used to approximate the dynamics of Sun-Jupiter-Asteroid or Sun-Earth-Satellite problems and it is the simplest one to have instabilities. If we also assume that the massless body moves in the same plane as the pair of primaries, we have the *Restricted planar three-body problem*. Normalize the total mass to one and call the three bodies the Sun (mass $1 - \mu$), Jupiter (mass $0 < \mu \ll 1$) and the Asteroid (zero mass). If the energy of the primaries is negative, they describe two ellipses with the same eccentricity, say $e_0 \geq 0$. The Hamiltonian of the asteroid is

$$K(q, p, t) = \frac{\|p\|^2}{2} - \frac{1-\mu}{\|q + \mu q_0(t)\|} - \frac{\mu}{\|q - (1-\mu) q_0(t)\|} \tag{4}$$

where $q, p \in \mathbb{R}^2$ and $-\mu q_0(t)$ and $(1-\mu) q_0(t)$ correspond to elliptic motions of the Sun and Jupiter respectively. Without loss of generality one can assume that $q_0(t)$ has semi major axis equal to 1 and period $2\pi$. For $e_0 \geq 0$ this system has two and a half degrees of freedom.

When $e_0 = 0$, the primaries describe uniform circular motions aroung their center of mass (circular restricted planar three-body problem). Hence in a frame rotating with the primaries, the system becomes autonomous, and thus has only 2 degrees of freedom. Its energy in the rotating frame is a first integral, called *the Jacobi constant*. It is defined by

$$J = \frac{\|p\|^2}{2} - \frac{1-\mu}{\|q + \mu q_0(t)\|} - \frac{\mu}{\|q - (1-\mu) q_0(t)\|} - \frac{\|q\|^2}{2}. \tag{5}$$

Aforementioned KAM theory applies to both the circular and the elliptic problems [**?**, **?**] and asserts that if the mass of Jupiter is small enough, there is a set of initial conditions of positive Lebesgue measure leading to quasiperiodic motions.

If Jupiter has a circular motion, since the system has only 2 degrees of freedom, KAM invariant tori are 2-dimensional and separate the 3-dimensional energy surfaces. But in the elliptic problem, a priori 3-dimensional KAM tori do not prevent orbits to wander on a 5-dimensional phase space. In this paper we prove the existence of a wide enough set of wandering orbits in the restricted planar elliptic three-body problem.

Let us write Hamiltonian (4) as

$$K(q, p, t) = K_0(q, p) + K_1(q, p, t, \mu)$$

with

$$\begin{aligned} K_0(q, p) &= \frac{\|p\|^2}{2} - \frac{1}{\|q\|} \\ K_1(q, p, t, \mu) &= \frac{1}{\|q\|} - \frac{1-\mu}{\|q + \mu q_0(t)\|} - \frac{\mu}{\|q - (1-\mu) q_0(t)\|}. \end{aligned}$$

One can see that $K_1 = \mathcal{O}(\mu)$ uniformly away from collisions. Then, notice that there is a competition between the integrability $K_0$ and the non-integrability $K_1$, without which there would be no wandering. In this present work we consider a realistic value of the mass ratio, $\mu = 10^{-3}$. For brevity in what

follows we abbreviate *the restricted planar circular (resp. elliptic) three-body problem to the circular (resp. elliptic) problem.*

Here is the main result of this paper.

**Theorem 1.** *Let us consider the elliptic problem with mass ratio $\mu = 10^{-3}$ and eccentricity of Jupiter $e_0 > 0$. Then, for $e_0$ small enough there exist $T > 0$ and a trajectory whose eccentricity $e(t)$ satisfies that*

$$e(0) < 0.48 \quad \textit{and} \quad e(T) > 0.67.$$

There is a more precise result, which is more difficult to state at this stage (see Theorem 2). Let us say that along the above trajectory, the semi major axis $a(t)$ remains almost constant, that is,

$$|a(t) - 7^{2/3}| \leq 14\mu \quad \text{for } t \in [0, T]$$

and that

$$|J(T) - J(0)| > 0.1,$$

where $J$ is the Jacobi constant defined in (5).

When Jupiter performs circular motion the Jacobi constant is an integral of motion and then KAM theory prevents global instabilities. We consider the eccentricity $e_0$ as a small parameter so that we can compare the dynamics of the elliptic problem with the dynamics of the circular one.

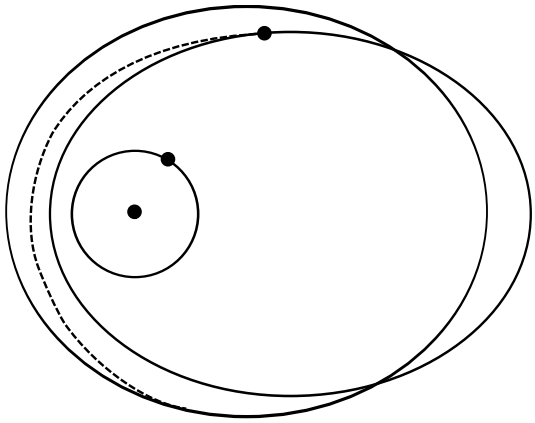

Figure 1: Transition from the osculating ellipse of eccentricty $e = 0.48$ to the ellipse of eccentricty $e = 0.67$. The dashed line schematically shows the transition. Nevertheless, the actual diffusing orbit is very complicated and diffusion is very slow.

In Theorem 1, we do not know what would happen asymptotically if we let $\mu \to 0$ (our estimates worsen). On the other hand, Theorem 1 holds for realistic values of $\mu$, which is out of reach of many qualitative results of perturbation theory where parameters are conveniently assumed to be as small as needed.

## 1.2 Mechanisms of instability

The result obtained in Theorem 1 gives an example of large instability for this mechanical system. It can be interpreted as an example of Arnold diffusion (see [**?**]). Nevertheless, Arnold diffusion usually refers to nearly integrable systems whereas Hamiltonian (4) cannot be considered as close to integrable since $\mu = 10^{-3}$ is fixed. The mechanism of diffusion used in this paper is somewhat similar to the so-called Mather problem ([**?**, **?**, **?**, **?**]). This analogy will be specified in Section 3.2.

Arguably, the main source of the existence of instabilities are *resonances*. One of the most natural resonances in the elliptic problem (even a three-body problem) is the *mean motion orbital resonances*[1].

[1]The mean motions are the frequencies of the Keplerian revolution of Jupiter and the Asteroid around the Sun: in our case the Asteroid makes one full revolution while Jupiter makes seven revolutions.

Along such a resonance, Jupiter and the Asteroid will regularly be in the same relative position. Over a long time interval, Jupiter's influence could thus a priori pile up and, despite its small amplitude due to the small mass of Jupiter, could modify the eccentricity of the Asteroid, instead of averaging out. According to third Kepler's Law, these resonances take place when $a^{3/2}$ is close to a rational, where $a$ is the semi major axis of instant ellipse of the Asteroid. In our case we consider $a^{3/2}$ *close to 7*. This resonance is convenient for the proof. Nevertheless, one should expect that the same mechanism takes place for a large number of mean motion orbital resonances.

The semi major axis $a$ and the eccentricity $e$ describe completely an instant ellipse of the Asteroid (up to orientation). Therefore, geometrically Theorem 1 says that the Asteroid evolves from a Keplerian ellipse of eccentricity $e = 0.48$ to one of eccentricity $e = 0.67$, without changing much its semi major axis (see Figure 1). In Figure 2 we consider the plane $(a, e)$, which describe the ellipse of the Asteroid. Then diffusing orbits given by Theorem 1 correspond to a nearly horizontal line.

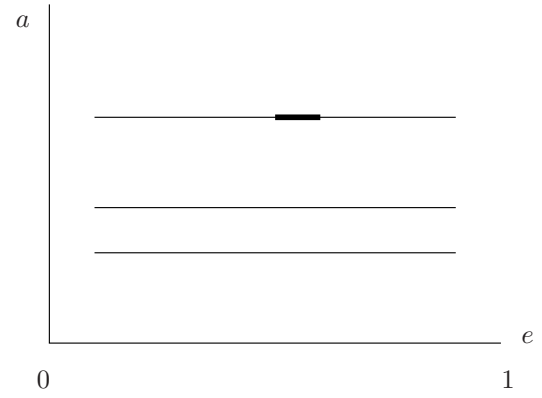


Figure 2: In this graphic we show the diffusion path that we study in the $(a, e)$ plane. The horizontal lines represent the resonances along which we drift. The thicker line is the diffusion path whose existence we are able to prove in this paper.

## 1.3 Presence of instabilities in the Asteroid belt: The Kirkwood gaps

### 1.3.1 The Asteroid belt

One place in the Solar system where one can apply the dynamics of this problem is the Asteroid belt. The Asteroid belt is located between the orbits of Mars and Jupiter and it consists of 1.7 millions of objects ranging from asteroids of 950 kilometers size to dust particles. Taking into account that the mass of Jupiter is approximately 2960 masses of Mars, away from encounters with Mars, dynamics of Asteroids is well approximated by the Restricted problem.

Denote by $\mu = m_1/(m_0 + m_1)$ the mass ratio. For $\mu = 0$ (namely, neglecting Jupiter influence) bounded orbits of the Asteroids are ellipses. Up to orientation they are characterized by their semimajor axis $a$ and eccentricity $e$.

A famous result of Lagrange [**?**] says that, for $\mu > 0$ small, $|a(t) - a(0)| \lesssim \mu$ for all $|t| \lesssim 1/\mu$. Niederman shows that well away from collisions time estimate can be improved to ...

Nevertheless, if one looks at the Asteroid distribution in terms of the semimajor axis of the osculating ellipse, one encounters several gaps, which are called *Kirkwood gaps*. It is believed that the existence of these gaps is due to instability mechanisms.

### 1.3.2 Kirkwood gaps and Wisdom's ejection mechanism

Call *mean motion resonance* when ratio of period of Jupiter and period of Asteroid is rational. Then, the Kirkwood gaps correspond to the ratios $1:3,\ 2:5,\ 3:7$. Here we present an heuristic explanation

of this phenomenon.

It is conjectured and confirmed by numerical data [**?**], that eccentricity of Asteroids placed in the Kirkwood gaps changes by a magnitude of order of one. Notice that in the real data (see Figure ...) eccentricity of most Asteroids in the Asteroid belt is between 0 and 0.18.

As eccentricity of Asteroid changes its perihelion $a(1-e)$ gets closer and closer to the origin (see figure ...). In particular, Asteroid starts to have close encounters with orbits of Mars. Eventually Mars and Asteroid come close and Asteroid gets ejected from the Asteroid belt.

What is surprising is that the change of eccentricity of Asteroid is only possible to elliptic motions of Jupiter. Indeed, for circular motions of Jupiter the problem becomes of two degrees of freedom and there are invariant two-dimensional tori separating energy surfaces.

Heuristically the main conclusion is that if eccentricity of Asteroid changes by a magnitude of order of one under the Restricted problem Sun-Jupiter-Asteroid, then the Asteroid might come into zones where the Restricted problem does not describe dynamics well.

The main result of the paper is that in a certain mean motion resonance there are unstable motions. In this paper, since the proof relies on numerical computations, we only present results for one particular resonance, but we are confident that this mechanism of instability applies to other resonances as long as orbits of unperturbed problem stay away from collisions. Thus, the instability mechanism showed in this paper gives a possible reason of the existence of the Kirkwood gaps. Another instability mechanism using the adiabatic invariant theory, can be seen in [**?**].

## 1.4 Main steps of the proof

The diffusing orbit of the elliptic problem we are looking for lies in a neighborhood of a (3-dimensional) normally hyperbolic invariant cylinder $\Lambda$ and its local invariant manifolds, which exist near our mean motion resonance. The vertical component of the cylinder can be parameterized by the eccentricity of the Asteroid and the horizontal ones by its mean longitude and time.

If the stable and unstable invariant manifolds of $\Lambda$ intersect transversally, the elliptic problem induces two different dynamics on the cylinder (see Sections 4.4 and 4.5): *the inner and the outer ones*. The inner dynamics is simply the restriction of the Newtonian flow to $\Lambda$. The outer dynamics is obtained by a limiting process: it can be observed asymptotically by starting very close to the cylinder and to its unstable manifold, traveling all the way up to a homoclinic intersection, and coming back close to the cylinder and along its stable manifold. Since the system has different homoclinic orbits to the cylinder, one can define several different outer dynamics. In our diffusing mechanism we use two different outer maps. The reason is that each of the outer maps are not defined in the whole cylinder and then we need the two of them to achieve diffusion (see Section 3).

The proof consists in the following four steps:

1. Prove existence of the normally hyperbolic invariant cylinder $\Lambda$.
2. Establish transversality of the stable and unstable invariant manifolds of this cylinder.
3. Compare the inner and outer dynamics on $\Lambda$ and, in particular, check that they do not have common invariant circles.
4. Construct diffusing orbits by shadowing a carefully chosen composition of the outer and inner maps.

This program faces difficulties at every step.

### 1.4.1 Existence of the normally hyperbolic invariant cylinder $\Lambda$.

The first difficulty comes from the proper degeneracy of the Newtonian potential: at the limit $\mu = 0$ (no Jupiter), the Asteroid has a one-frequency, Keplerian motion, whereas symplectic geometry would allow for a three-frequency motion (as with any potential other than the Newtonian potential $1/r$ and the elastic potential $r^2$). Due to this degeneracy, switching to $\mu > 0$ is a singular perturbation. In particular, hyperbolicity is small with respect to $\mu$.

### 1.4.2 Transversal of the stable and unstable invariant manifolds of the cylinder $\Lambda$.

The second step, establishing the transversality of the invariant manifolds of $\Lambda$ is a delicate problem. Asymptotically when $\mu \ll 1$, the difference between the invariant manifolds becomes exponentially small with respect to $\mu$, that is of order $\exp(-c/\sqrt{\mu})$ for some constant $c > 0$. Despite inordinate efforts of splitting specialists, all the known techniques fail here, because the relevant Poincaré-Melnikov integral is not algebraic. This instability mechanism relies on such precise information on the flow, that in details it is discontinuous with respect to any reasonable topology. This step simplifies dramatically in the study of generic systems.

At the expense of creating other difficulties, setting $\mu = 10^{-3}$ avoids this splitting problem, since for this value of the parameter one can see that the splitting of separatrices is not extremely small and therefore, can be detected by means of a computer with a convincing accuracy. Besides, $\mu = 10^{-3}$ is a realistic value of the mass ratio for the Sun-Jupiter model. Since the splitting of the separatrices varies smoothly with respect to the eccentricity $e_0$ of the primaries, it suffices to estimate the splitting numerically for $e_0 = 0$, i.e. in the circular problem. *This is a key point for the numerical computation*, which thus remains relatively simple. On the other hand, in the following two steps it will be crucial to have $e_0 > 0$, without which the KAM tori would separate energy levels.

Finally, recall that the cylinder $\Lambda$ has two branches of both stable and unstable invariant manifolds. In certain regions the intersections between one of the branches of the stable and unstable invariant manifolds is tangential, which does not allow to define the outer map. Nevertheless, then one can check that the other two branches intersect transversally so that we can define a different outer map. Thus, we will combine the two outer maps depending which branches of the invariant manifolds intersect transversally.

### 1.4.3 Calculation of asymptotic formulas for the outer and inner maps

Now we turn to the third step. Using classical perturbation theory and the specific properties of the underlying system one can reduce the inner and (the two different) outer dynamics to three two-dimensional symplectic maps of the form

$$\mathcal{F}^{\text{in}}_{e_0} : \begin{pmatrix} I \\ t \end{pmatrix} \mapsto \begin{pmatrix} I + e_0 \left( A^+(I,\mu) e^{it} + A^-(I,\mu) e^{-it} \right) + \mathcal{O}\left(\mu e_0^2\right) \\ t + \mu \mathcal{T}_0(I,\mu) + \mathcal{O}(\mu e_0) \end{pmatrix} \tag{6}$$

and

$$\mathcal{F}^{\text{out},*}_{e_0} : \begin{pmatrix} I \\ t \end{pmatrix} \mapsto \begin{pmatrix} I + e_0 \left( B^{*,+}(I,\mu) e^{it} + B^{*,-}(I,\mu) e^{-it} \right) + \mathcal{O}\left(\mu e_0^2\right) \\ t + \mu \omega^*(I,\mu) + \mathcal{O}(\mu e_0) \end{pmatrix}, \ * = \text{f}, \text{b}, \tag{7}$$

where $(I, t)$ are conjugate variables which parameterize a certain connected component of the 3-dimensional normally hyperbolic invariant cylinder $\Lambda$ intersected with a certain transversal Poincaré section and $A^{\pm}, \mathcal{T}_0, B^{*,\pm}, \omega^*$ are analytic functions. The superindexes f and b stand for the forward and bacward heteroclinic orbits that are used to define the outer maps. The choice of this notation will be clear later on in Section 3. Note that these maps are real-analytic and therefore $A^-$ and $B^{*,-}$ are the complex conjugates of $A^+$ and $B^{*,+}$ respectively.

### 1.4.4 Nondegeneracy implying existence of diffusing orbits

As we will see in Section 5, the existence of diffusing orbits can be established provided the analytic functions

$$\mathcal{K}^{*,+}(I,\mu) = B^{*,+}(I,\mu) - \frac{e^{i\mu\omega^*(I,\mu)} - 1}{e^{i\mu\mathcal{T}_0(I,\mu)} - 1} A^+(I,\mu)$$

do not vanish for all $I \in [I_-, I_+]$ for which the corresponding outer map is defined. Since $A^{\pm}$ and $B^{*,\pm}$ are complex conjugate, we do not write the complex conjugate $\mathcal{K}^{j,-}(I,\mu)$. Numerically, one can check that $\mathcal{K}^{j,+}(I,\mu) \neq 0$ in their domain of definition. It turns out that $\mathcal{K}^{j,+}(I,\mu) \neq 0$ implies absence of common invariant curves for the inner and outer maps. This reduces the proof of Theorem 1 to shadowing, made in step 4, and thus it leads to the existence of diffusing orbits. Moreover, it turns out that for this problem *no large gaps* appear. This fact is not so surprising taking into account that the elliptic problem has three time scales.

Finally, let us point out that the complex functions $\mathcal{K}^{j,+}(I,\mu)$ can be regarded as a 2-dimensional real-valued function depending analytically on $(I,\mu)$. If the dependence in $\mu$ is non-trivial, a complex valued function $\mathcal{K}^{j,+}(I,\mu)$ does not vanish at any point of their domain of definition except for a finite number of $\mu$'s.

### 1.5 Nature of numerics

In this section we outline which parts of the mechanism are based on numerics.

- On each 3-dimensional energy surface the circular problem has a well-defined Poincare map $F_J : \Sigma_J \to \Sigma_J$ of a 2-dimensional cylinder $\Sigma_J$ for a range of $J$'s. For each $J$ in some interval $[J_-, J_+]$ we establish the existence of a saddle periodic orbit $F_J^7(p_J) = p_J$.
- We show that for all $J \in [J_-, J_+]$ we have two transversal intersections of $W^s(p_J)$ and $W^u(p_J)$. Surprisingly (at least to the authors) "symmetric" intersection points exhibit tangencies for some $J$'s. Nevertheless, since there are two symmetric intersection points, it is rather easy to check the transversality of one of them for each $J \in [J_-, J_+]$.
- Each transversal intersection $q_J$ gives rise to a homoclinic orbit, denoted $\gamma_J$. For each $J \in [J_-, J_+]$ we compute several Melnikov integrals of certain quantities related to $\Delta H_{ell}$ along $\gamma_J$ and $p_J$. Out of these integrals we compute the leading terms of the dynamics of the elliptic problem and verify a necessary condition for diffusion.

At no point of numerics we study rely on numerics which is anywhere close to error of calculations. PAU, AQUESTA FRASE S'HA DE CANVIAR.

## 2 Setting of the problem and notations

The model of the Sun, Jupiter and a massless Asteroid in cartesian coordinates is given by the Hamiltonian (4). First, let us consider the case $\mu = 0$, that is, we consider Jupiter with zero mass. In that case, Jupiter and Asteroid do not make influence on each other and therefore the system is reduced to two uncoupled 2-body problems, the Sun-Jupiter and the Sun-Asteroid, which are integrable.

We want to study the existence of instability in one particular resonance of this system, which appears when the period of Asteroid is seven times the period of Jupiter. One can consider the so-called Delaunay variables, which we denote by $(\ell, L, \hat{g}, G)$, which are angle-action coordinates of the Sun-Asteroid system. The variable $\ell$ is the mean anomaly, $L$ is the square of the semi major axis, $\hat{g}$ is the argument of the perihelion and $G$ is the angular momentum. These variables can be obtained from the Cartesian coordinates as follows (see [**?**] for more details and background, or [**?**, Appendix] for a straightforward definition). First define polar coordinates for the position:

$$q = (r\cos\phi, r\sin\phi).$$

Then, the actions of Delaunay coordinates are defined implicitly by

$$-\frac{1}{2L^2} = \frac{\|p\|^2}{2} - \frac{1}{\|q\|} \tag{8}$$

$$G = -J - \frac{1}{2L^2} \tag{9}$$

(recall that $\mu = 0$ for these definitions). Using these actions, the eccentricity of Asteroid can be expressed as

$$e = \sqrt{1 - \frac{G^2}{L^2}}. \tag{10}$$

To define the angles, let $v$ and $\hat{g}$ be the true anomaly and the argument of the perihelion so that

$$\phi = v + \hat{g}. \tag{11}$$

Then, from $v$ one can obtain the eccentric anomaly $u$ using

$$\tan\frac{v}{2} = \sqrt{\frac{1+e}{1-e}}\tan\frac{u}{2}. \tag{12}$$

From the eccentric anomaly, the mean anomaly is given by the Kepler equation

$$u - e\sin u = \ell. \tag{13}$$

In the Delaunay coordinates, the Hamiltonian (4) can be split into the Keplerian part $-1/2L^2$, the circular part of the perturbing function $\mu\Delta H_{circ}$ and the remainder which vanishes when $e_0 = 0$:

$$\hat{H}(L,\ell,G,\hat{g},t) = -\frac{1}{2L^2} + \mu\Delta H_{\rm circ}(L,\ell,G,\hat{g}-t,t,\mu) + \mu e_0\Delta H_{\rm ell}(L,\ell,G,\hat{g}-t,t,\mu,e_0). \tag{14}$$

It turns out that for $e_0 = 0$, the circular problem only depends on $\hat{g} - t$. To simplify the comparison with the circular problem, we consider rotating Delaunay coordinates, in which $\Delta H_{\rm circ}$ is autonomous. This means to define the new angle $g = \hat{g} - t$ and a new variable $I$ conjugate to time $t$. Then, we have

$$H(L,\ell,G,g,I,t) = -\frac{1}{2L^2} - G + \mu\Delta H_{\rm circ}(L,\ell,G,g,\mu) + \mu e_0\Delta H_{\rm ell}(L,\ell,G,g,t,\mu,e_0) + I. \tag{15}$$

In these new variables, the difference of number of degrees of freedom of the elliptic and circular problems becomes more apparent. When $e_0 = 0$ the system is autonomous and then $I$ is constant, which corresponds to the conservation of the Jacobi constant (5). Therefore, the circular problem reduces to 2 degrees of freedom. Moreover, it will later be crucial to see the circular problem as an approximation of the elliptic one, in order to reduce the Herculean (and doubtful) numerical computations of a direct approach to the corresponding lower dimensional, and thus simpler, computations of the circular problem.

Recall that we consider the $1:7$ mean motion orbit resonance between Jupiter and Asteroid. That is, the period of Asteroid being approximately seven times the period of Jupiter. In rotating Delaunay variables, this corresponds to

$$\dot{\ell} \sim \frac{1}{7} \quad \text{and} \quad \dot{g} \sim -1. \tag{16}$$

A nearby resonance is

$$\dot{\ell} \sim \frac{1}{7} \quad \text{and} \quad \dot{t} \sim 1,$$

but we will stick to the previous one.

The resonance takes place when $L \sim 7^{1/3}$. We will study the dynamics in a large neighborhood of this resonance and we will see that one can drift along it. Namely, we will find trajectories that keep $L$ close to $7^{1/3}$ while the $G$-component changes noticeably. Using (10), one can see that $e$ also changes by an order of one. In this setting, Theorem 1 can be rephrased as follows.

**Theorem 2.** *There exist $e_0^* > 0$ such that for $0 < e_0 < e_0^*$, there exist $T > 0$ and an orbit of the Hamiltonian System with Hamiltonian* (15) *which satisfies*

$$G(0) < G_0 \text{ and } G(T) > G_1$$

*whereas*

$$\left|L(t) - 7^{1/3}\right| \leq 7\mu,$$

By definition the Hamiltonian (15) is autonomous and thus preserved. Therefore, we will restrict ourselves to a level of energy which, without loss of generality, can be taken as $H = 0$. Therefore, since $|I - G| = \mathcal{O}(\mu)$, for orbits satisfying $\left|L(t) - 7^{1/3}\right| \leq 7\mu$, drift in $G$ is equivalent to drift in $I$.

The proof of this theorem is structured as follows.

In Section 3, we study the dynamics in the circular problem, that is $e_0 = 0$ and the underlying Hamiltonian (15) becomes

$$H_{\rm circ}(L,\ell,G,g) = -\frac{1}{2L^2} - G + \mu\Delta H_{\rm circ}(L,\ell,G,g,\mu). \tag{17}$$

*Theorem* 3 says that for an interval of Jacobi energies $[J_-, J_+]$ the circular problem has a smooth family of hyperbolic periodic orbits $\lambda_J$, whose stable and unstable manifolds intersect transversally for each $J \in [J_-, J_+]$. This theorem implies (Corollary 3.1) existence of a normally hyperbolic invariant cylinder. Later in the section (Subsections 3.1 and 3.2) we calculate the aforementioned circular outer and inner maps for the circular problem (see (6) and (7)).

Then in Section 4 we consider the elliptic case $e_0 > 0$ as a perturbation of the circular case.

*Theorem* 4 says that the family of periodic orbits $\{\lambda_J\}_{J\in[J_-.J_+]}$ give rise to a normally hyperbolic invariant cylinder $\Lambda_{e_0}$ whose stable and unstable manifolds intersect transversally for each $J \in [J_- + \delta, J_+ - \delta]$ with small $\delta > 0$. These objects give rise to the inner and outer maps. *Theorem* 5 provides expansions for the inner and outer maps (see formulas (42) and (45) respectively).

Finally, in Section 5 in *Theorem* 6 we complete the proof of Theorem 2. This is done by comparing the inner and the two outer maps in Lemma 5.2 and constructing a transition chain of tori. It turns out that there are **no large gaps**, due to the specific structure of times scales and the Fourier series involved. This a priori contrasts with the typical situation of dynamics near a resonance (see e.g. [**?**]).

**Notation 2.1.** *From now on, we will omit the dependence on $\mu$ (keeping in mind at various points the question of what would happen if we let $\mu$ vary). Recall that we are taking a realistic value of $\mu = 10^{-3}$.*

# 3 The circular problem

The circular problem is given by the Hamiltonian (15) with $e_0 = 0$. Since it does not depend on $t$, $I$ is an integral of motion. Moreover, since we are studying the dynamics in the energy surface $H = 0$, we have $I = -H_{\text{circ}}(\ell, L, g, G)$. Therefore, the variable $I$ equals the opposite of the Jacobi constant (5). For each level $I =$ constant, one can study the dynamics close to the resonance $7\dot{\ell} + \dot{g} \sim 0$. Since $t$ is a cyclic variable, one can consider the two degree of freedom Hamiltonian of the circular problem for which the conservation of energy corresponds to the conservation of the Jacobi constant (5). Moreover, one can see that the circular problem is reversible with respect to the involution

$$\Psi(L, \ell, G, g, I, t) = (L, -\ell, G, -g, I, -t). \tag{18}$$

This symmetry will facilitate several numerical computations.

**Theorem 3.** *Consider the Hamiltonian* (17) *with $\mu = 10^{-3}$. Then, in each energy level $J_- \leq J \leq J_+$, there exists a hyperbolic periodic orbit $\lambda_J = (L_J(t), \ell_J(t), G_J(t), g_J(t))$ of period $T_J$ which satisfies*

$$|T_J - 14\pi| < 60\mu,$$

*smooth in $J$, and*

$$\left| L_J(t) - 7^{1/3} \right| < 7\mu$$

*for certain constant $C > 0$ and all $t \in \mathbb{R}$.*

*Each $\lambda_J$ has two branches of stable and unstable invariant manifolds $W^{s,j}(\lambda_J)$ and $W^{u,j}(\lambda_J)$, $j = 1, 2$. Then, for each $J \in [J_-, J_+]$ either $W^{s,1}(\lambda_J)$ and $W^{u,1}(\lambda_J)$ or $W^{s,2}(\lambda_J)$ and $W^{u,2}(\lambda_J)$ intersect transversally.*

*Proof.* Based on convincing numerical data. See Appendix B. □

We will study the elliptic problem as a perturbation of the circular one. Therefore we do not reduce the dimension of the phase space while studying the inner and outer dynamics of the circular problem. Namely, we consider the *Extended Circular Problem* given by the Hamiltonian (15) with $e_0 = 0$. In other words, we keep the conjugate variables $(I, t)$ even if $t$ is a cyclic variable. Consider the energy level $H = 0$. In this setting the conservation of the Jacobi constant corresponds to the conservation of $I$. Therefore, the periodic orbits obtained in Theorem 3 become invariant two-dimensional tori which belong to hyperplanes $I =$ constant for any $I \in [I_-, I_+] = [-J_+, -J_-]$. Moreover, the union of these 2-dimensional invariant tori form a normally hyperbolic invariant 3-dimensional manifold.

**Corollary 3.1.** *The Hamiltonian* (15) *with* $\mu = 10^{-3}$ *and* $e_0 = 0$ *has an analytic normally hyperbolic invariant* 3*-dimensional manifold* $\Lambda_0$*, which is foliated by two-dimensional invariant tori.*

*Moreover,* $\Lambda_0$ *has two branches of stable and unstable invariant manifolds, which we call* $W^{s,j}(\Lambda_0)$ *and* $W^{u,j}(\Lambda_0)$*,* $j = 1, 2$*. Then, in the invariant planes* $I =$ *constant, for each* $I \in [I_-, I_+]$ *either* $W^{s,1}(\Lambda_0)$ *and* $W^{u,1}(\Lambda_0)$ *or* $W^{s,2}(\Lambda_0)$ *and* $W^{u,2}(\Lambda_0)$ *intersect transversally.*

We define a global Poincaré section and deal with maps to reduce the dimension by one. There are two natural choices: $\{t = 0\}$ and $\{g = 0\}$, since both variables satisfy $\dot{t} \neq 0$ and $\dot{g} \neq 0$. We choose the section $\{g = 0\}$ and call

$$\mathcal{P}_0 : \{g = 0\} \longrightarrow \{g = 0\} \tag{19}$$

this Poincaré map. Since we are studying the resonance (16), the intersection of the cylinder $\Lambda_0$ with the section $\{g = 0\}$ is formed by seven cylinders (see Figure 3). We denote them by $\widetilde{\Lambda}_0^j$, $j = 0, \ldots, 6$. Namely,

$$\Lambda_0 \cap \{g = 0\} = \widetilde{\Lambda}_0 = \cup_{j=0}^{6} \widetilde{\Lambda}_0^j. \tag{20}$$

As a whole $\cup_{j=0}^{6} \widetilde{\Lambda}_0^j$ is a normally hyperbolic invariant manifold for the Poincaré map $\mathcal{P}_0$. One can also consider the Poincaré map $\mathcal{P}_0^7$, namely iterate seven times $\mathcal{P}_0$. Then, for this map, each $\widetilde{\Lambda}_0^j$ is a normally hyperbolic invariant manifold (of course, their union is also a normally hyperbolic invariant manifold for $\mathcal{P}_0^7$). We work with the cylinders $\widetilde{\Lambda}_0^j$ since they have the advantage of having a natural system of coordinates. This system of coordinates will be used later on to study the inner and outer dynamics on them. In particular, we will work with $\widetilde{\Lambda}_0^3$ and $\widetilde{\Lambda}_0^4$. The reason is that in each invariant plane $I =$ constant they are connected by at least one heteroclinic connection (of $\mathcal{P}_0^7$) which is symmetric with respect to the involution (18). We call it a forward heteroclinic orbit if it is asymptotic to $\widetilde{\Lambda}_0^3$ in the past and $\widetilde{\Lambda}_0^4$ in the future and a backward heteroclinic orbit if it is asymptotic to $\widetilde{\Lambda}_0^4$ in the past and to $\widetilde{\Lambda}_0^3$ in the future. We denote by $\mathcal{D}^{\mathrm{f}} \subset [I_-, I_+]$, where f stands for forward, the subset of $[I_-, I_+]$ where $W^u(\widetilde{\Lambda}_0^3)$ and $W^s(\widetilde{\Lambda}_0^4)$ intersect transversally and by $\mathcal{D}^{\mathrm{b}} \subset [I_-, I_+]$, where b stands for backward, the subset of $[I_-, I_+]$ where $W^s(\widetilde{\Lambda}_0^3)$ and $W^u(\widetilde{\Lambda}_0^4)$ intersect transversally. By Corollary 3.1 we have that $\mathcal{D}^{\mathrm{f}} \cup \mathcal{D}^{\mathrm{b}} = [I_-, I_+]$.

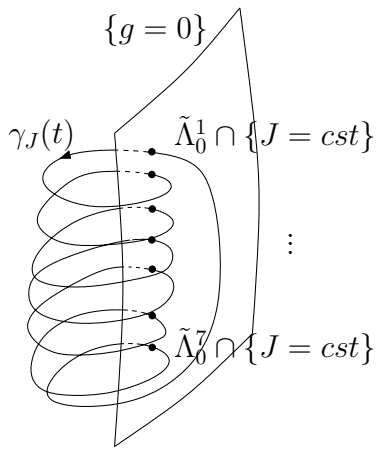


Figure 3: The periodic orbit obtained at each energy level intersects seven times the Poincaré section $\{g = 0\}$, as it is shown schematically in this picture. Then, when one considers the Poincaré map $\mathcal{P}_0$, the normally hyperbolic invariant manifold $\widetilde{\Lambda}_0$ has seven connected components $\widetilde{\Lambda}_0^0, \ldots, \widetilde{\Lambda}_0^6$.

**Corollary 3.2.** *The Poincaré map* $\mathcal{P}_0^7$ *defined in* (19)*, which is induced by the Hamiltonian* (15) *with* $\mu = 10^{-3}$ *and* $e_0 = 0$*, has seven analytic normally hyperbolic invariant manifolds* $\widetilde{\Lambda}_0^j$*,* $j = 0, \ldots, 6$*. They are foliated by one-dimensional invariant curves. Moreover, there exist analytic functions* $\mathcal{G}_0^j$ :

$[I_-, I_+] \times \mathbb{T} \to (\mathbb{R} \times \mathbb{T})^3$ *which can be expressed in coordinates as*

$$\mathcal{G}_0^j(I,t) = \left(\widetilde{\mathcal{G}}_0^j(I), 0, I, t\right) = \left(\mathcal{G}_0^{j,L}(I), \mathcal{G}_0^{j,\ell}(I), \mathcal{G}_0^{j,G}(I), 0, I, t\right), \tag{21}$$

*that parameterize* $\widetilde{\Lambda}_0^j$*, namely,*

$$\widetilde{\Lambda}_0^j = \left\{\mathcal{G}_0^j(I,t) : (I,t) \in [I_-, I_+] \times \mathbb{T}\right\}.$$

*The manifolds* $W^u(\widetilde{\Lambda}_0^3)$ *and* $W^s(\widetilde{\Lambda}_0^4)$ *intersect transversally provided* $I \in \mathcal{D}^{\mathrm{f}}$ *and* $W^s(\widetilde{\Lambda}_0^3)$ *and* $W^u(\widetilde{\Lambda}_0^4)$ *intersect transversally provided* $I \in \mathcal{D}^{\mathrm{b}}$*. Moreover, one of the points of these intersections belong to the symmetry axis of* (18)*. Let us denote by* $\Gamma_0^*$*,* $* = \mathrm{f}, \mathrm{b}$*, these intersections. Then, there exist functions*

$$\mathcal{C}_0^* : \mathcal{D}^j \times \mathbb{R} \to (\mathbb{R} \times \mathbb{T})^3, \quad (I,t) \mapsto \mathcal{C}_0^*(I,t), \ \ * = \mathrm{f}, \mathrm{b}$$

*which parameterize them:*

$$\Gamma_0^* = \left\{\mathcal{C}_0^*(I,t) = (\mathcal{C}_0^{*,L}(I), \mathcal{C}_0^{*,\ell}(I), \mathcal{C}_0^{*,G}(I), 0, I, t) : (I,t) \in \mathcal{D}^* \times \mathbb{T}\right\}, \ \ * = \mathrm{f}, \mathrm{b}.$$

The 0 that appears in the parameterizations $\mathcal{G}$ and $\mathcal{C}$ is just the $g$-coordinate. We keep it although we are in the Poincaré section because later on we will use these parameterizations in the full phase space. Corollary 3.1 gives global coordinates $(I,t)$ for each cylinder $\widetilde{\Lambda}_0^j$. These coordinates are symplectic with respect to the canonical symplectic form

$$\Omega_0 = dI \wedge dt, \tag{22}$$

Indeed, one has to consider the pullback of the canonical form $dL \wedge d\ell + dG \wedge dg + dI \wedge dt$ to the cylinders $\widetilde{\Lambda}_0^j$. By Corollary 3.2 we have that in the cylinders: $g = 0$, $\ell = \mathcal{G}_0^{j,\ell}(I)$ and $L = \mathcal{G}_0^{j,L}(I)$. Then, it is easy to see that the pullback of $dL \wedge d\ell + dG \wedge dg + dI \wedge dt$ is just $\Omega_0$.

We consider the inner and the two outer maps in one of these cylinders. We choose $\widetilde{\Lambda}_0^3$. As we have explained before, the reason is that their heteroclinic connections with the following cylinder $\widetilde{\Lambda}_0^4$ intersect the symmetry axis of the involution (18) and therefore they are easier to be studied numerically (see Figure ??). Since $I$ is conserved by the inner and outer maps, these maps are integrable and the variables $(I,t)$ are the action-angle variables. In this way, it will be easier to understand the influence of the ellipticity.

## 3.1 The inner map of the circular problem

We first obtain the inner map. One could define it as the Poincaré map $\mathcal{P}_0$ restricted to the whole normally hyperbolic invariant manifold (20). Nevertheless, to study the diffusion mechanism it is more convenient to consider just one of the cylinders that form (20), for instance $\widetilde{\Lambda}_0^3$. To this end, we can define the inner map $\mathcal{F}_0^{\mathrm{in}} : \widetilde{\Lambda}_0^3 \to \widetilde{\Lambda}_0^3$ as the Poincaré map $\mathcal{P}_0^7$ restricted to $\widetilde{\Lambda}_0^3$, which leaves it invariant. We use the global coordinates $(I,t)$ of $\widetilde{\Lambda}_0^3$ to express it.

Since $I$ is an integral of motion, this inner map is of the form

$$\mathcal{F}_0^{\mathrm{in}} : \begin{pmatrix} I \\ t \end{pmatrix} \mapsto \begin{pmatrix} I \\ t + \mu\mathcal{T}_0(I) \end{pmatrix}, \tag{23}$$

where the function $\mathcal{T}_0$ is independent of $t$ due to the fact that the inner map preserves the differential form (22), which does not depend on $t$, and that $I$ is a first integral. In fact, $14\pi + \mu\mathcal{T}_0(I)$ is the period of the periodic orbit obtained in Theorem 3 on the corresponding energy surface. It can be seen numerically that this map is twist.

**Lemma 3.1.** *The inner map* $\mathcal{F}_0^{\mathrm{in}}$ *defined in* (23) *is a symplectic twist map, that is*

$$\partial_I \mathcal{T}_0(I) \neq 0 \qquad \textit{for } I \in [I_-, I_+].$$

*Moreover, the function* $\mathcal{T}_0(I)$ *satisfies*

$$0 < \mu\mathcal{T}_0(I) < \pi. \tag{24}$$

*Proof.* Based on convincing numerical data. See Appendix B. □

In Section 3.2, the function $\mathcal{T}_0(I)$ will be written by means of an integral (see (35)).

The information contained in this lemma will be crucial in Section 5 to prove the existence of a transition chain of invariant tori.

## 3.2 The outer map of the circular problem

The outer map has been also called scattering map (see for instance [**?**]). In order to define the outer map we use the perturbative structure of the problem. Let $\mathcal{P}_0$ be a map of a compact manifold $M$ endowed with a smooth metric $\rho$. Let $\Lambda_0 \subset M$ be a normally hyperbolic invariant manifold of $\mathcal{P}_0$. Assume that dynamics on $\Lambda_0$ has zero Lyapunov exponents, e.g. for any $z \in \Lambda_0$ we have $\lim \ln \|dP^n(z)v\|/n = 0$ for any $v \in T_z\Lambda_0$.

Assume that an invariant manifold $\Lambda_0$ is normally hyperbolic and its stable and unstable invariant manifolds intersect transversally. Then, the outer map is defined as follows[2].

Since $\Lambda_0$ is normally hyperbolic it is persistent under small perturbation of $\mathcal{P}_0$.

**Definition 3.1.** *Fix $\lambda > 1$ and a small perturbation $\mathcal{P}$ of $\mathcal{P}_0$. Let $\Lambda \subset M$ be a normally hyperbolic invariant manifold of $\mathcal{P}$. Assume that $\gamma \subset W^s_\Lambda \cap W^u_\Lambda$ is a homoclinic manifold and that the intersection of $W^s_\Lambda$ and $W^u_\Lambda$ is transversal along $\gamma$, that is*

$$\begin{aligned} T_z W^s_\Lambda + T_z W^u_\Lambda = T_z M, \quad & \text{for } z \in \gamma \\ T_z W^s_\Lambda \cap T_z W^u_\Lambda = T_z \gamma, \quad & \text{for } z \in \gamma. \end{aligned}$$

*Then, we say that $\mathcal{S}(x_-) = x_+$, if there exists a point $z \in \gamma$ such that for some $C > 0$ we have*

$$\operatorname{dist}(\mathcal{P}^n(z), \mathcal{P}^n(x_\pm)) < C\lambda^{-|n|} \qquad \text{for all } n \in \mathbb{Z}^\pm.$$

**Remark 3.1.** *Since $\Lambda$ is normally hyperbolic, for each point $x \in \Lambda$ there are strong stable and unstable manifolds $W^{ss}(x)$ and $W^{su}(x)$. Then $\mathcal{S}(x_-) = x_+$ holds only if $W^{su}(x_-) \cap W^{ss}(x_+) \neq \emptyset$ and the intersection occurs on $\gamma$. Due to smooth dependence on initial conditions $\mathcal{S}$ is smooth.*

*In the case when Lyapunov exponents on inner dynamics $\mathcal{P}$ are not close to one, $\lambda$ has to exceed maximal Lyapunov exponent to have domination of convergence toward $\Lambda$ over motion inside of $\Lambda$. Otherwise, one cannot distinguish if an orbit converges to a point on a stable manifold of a periodic point of the restriction $P|_\Lambda$ or it converges to this periodic point.*

One could apply this definition to the normally hyperbolic invariant manifold $\cup_{j=1}^7 \widetilde{\Lambda}_0^j$. Nevertheless, since it does not have a good global system of coordinates is more convenient to proceed as we have done for the inner map in the previous section. Namely, we look for an outer map which sends $\widetilde{\Lambda}_0^3$ to itself. Now one has to be more careful since one cannot consider the outer maps induced by the Poincaré map $\mathcal{P}_0^7$. Indeed, for $\mathcal{P}_0^7$, the cylinder $\widetilde{\Lambda}_0^3$ is a normally hyperbolic invariant manifold but the homoclinic points obtained in Theorem 3.1 now correspond to heteroclinic connections between $\widetilde{\Lambda}_0^3$ and $\widetilde{\Lambda}_0^4$ and between $\widetilde{\Lambda}_0^4$ and $\widetilde{\Lambda}_0^3$. To overcome this problem we will compose the heteroclinic outer maps $\mathcal{S}^*$, $* = \mathrm{f}, \mathrm{b}$ with the Poincaré map $\mathcal{P}_0$ as many times as necessary so that the composition goes from $\widetilde{\Lambda}_0^3$ to itself.

Therefore, this new outer maps $\mathcal{F}_0^{\mathrm{out},\pm}$ that we consider connect $\widetilde{\Lambda}_0^3$ to itself and are defined as

$$\begin{aligned} \mathcal{F}_0^{\mathrm{out,f}} &= \mathcal{P}_0^6 \circ \mathcal{S}^{\mathrm{f}} : \widetilde{\Lambda}_0^3 \longrightarrow \widetilde{\Lambda}_0^3 \\ \mathcal{F}_0^{\mathrm{out,b}} &= \mathcal{S}^{\mathrm{b}} \circ \mathcal{P}_0 : \widetilde{\Lambda}_0^3 \longrightarrow \widetilde{\Lambda}_0^3 \end{aligned} \tag{25}$$

where $\mathcal{S}^{\mathrm{f}}$ is the outer map which connects $\widetilde{\Lambda}_0^3$ and $\widetilde{\Lambda}_0^4$ through $W^u(\widetilde{\Lambda}_0^3) \cap W^s(\widetilde{\Lambda}_0^4)$ and $\mathcal{S}^{\mathrm{b}}$ is the outer map which connects $\widetilde{\Lambda}_0^4$ and $\widetilde{\Lambda}_0^3$ through $W^u(\widetilde{\Lambda}_0^4) \cap W^s(\widetilde{\Lambda}_0^3)$. Note that here we are abusing notation since the

[2]This definition can be modified to generalize the outer map to any normally hyperbolic invariant manifold with transversal stable and unstable invariant manifolds

forward and backwards outer maps are only defined provided $I \in \mathcal{D}^{\mathrm{f}}$ and $I \in \mathcal{D}^{\mathrm{b}}$ respectively and not in the whole cylinder $\widetilde{\Lambda}_0^3$.

The outer map is always exact symplectic (see [**?**]). Then in the circular problem, since $I$ is preserved, the outer maps have to be of the form

$$\mathcal{F}_0^{\mathrm{out},*} : \begin{pmatrix} I \\ t \end{pmatrix} \mapsto \begin{pmatrix} I \\ t + \mu\omega^*(I) \end{pmatrix}, \quad * = \mathrm{f}, \mathrm{b}. \tag{26}$$

The outer map can be defined either with discrete or continuous time. Since the Poincaré-Melnikov theory is considerably simpler for flows than for maps, we compute $\mathcal{F}_0^{\mathrm{out},*}$ using continuous time. Moreover, in Section 4.5 we will use also flows to study the outer map of the elliptic problem as a perturbation of (26). The outer map given by the Hamiltonian (15) with $e_0 = 0$ does not preserve the section $\{g = 0\}$ but the inner map does. In order to fix this problem, we reparameterize the flow so that the inner and outer map preserve this section.

This reparameterization corresponds to identifying the variable $g$ with time and is given by,

$$\begin{array}{lll} \frac{d}{ds}\ell = & \frac{\partial_L H}{-1+\mu\partial_G \Delta H_{\mathrm{circ}}} & \frac{d}{ds}L = -\frac{\partial_\ell H}{-1+\mu\partial_G \Delta H_{\mathrm{circ}}} \\ \frac{d}{ds}g = & 1 & \frac{d}{ds}G = -\frac{\partial_g H}{-1+\mu\partial_G \Delta H_{\mathrm{circ}}} \\ \frac{d}{ds}t = & \frac{1}{-1+\mu\partial_G \Delta H_{\mathrm{circ}}} & \frac{d}{ds}I = 0 \end{array} \tag{27}$$

where $H$ is Hamiltonian (15) with $e_0 = 0$. Notice that this reparameterization implies the change of direction of time. However, the geometric objects stay the same. In particular, the new flow still possesses the normally invariant cylinder obtained in Corollary 3.1 and its invariant manifolds.

We will refer to this system as a *reduced circular problem*. We call it reduced because we identify $g$ with the time $s$. Moreover, the $t$-component (and in fact, all the others) only depends on the other coordinates. Denote by $\Phi_0^{\mathrm{circ}}$ the flow associated to the $(L, \ell, G, g)$ components of equation (27) (which are independent of $t$ and $I$). Componentwise it can be written as

$$\Phi_0^{\mathrm{circ}}\{s, (L, \ell, G, g)\} = \left(\Phi_0^L\{s, (L, \ell, G, g)\}, \Phi_0^\ell\{s, (L, \ell, G, g)\}, \Phi_0^G\{s, (L, \ell, G, g)\}, g + s\right). \tag{28}$$

Then, the outer map can be computed as follows.

Let

$$\begin{aligned} \gamma_I^*(\sigma) &= \Phi_0^{\mathrm{circ}}\{\sigma, (\mathcal{C}_0^{*,L}(I), \mathcal{C}_0^{*,\ell}(I), \mathcal{C}_0^{*,G}(I), 0)\}, \quad * = \mathrm{f}, \mathrm{b} \\ \gamma_I^j(\sigma) &= \Phi_0^{\mathrm{circ}}\{\sigma, (\mathcal{G}_0^{j,L}(I), \mathcal{G}_0^{j,\ell}(I), \mathcal{G}_0^{j,G}(I), 0)\} \end{aligned} \tag{29}$$

be trajectories of the circular problem. The first ones have the initial conditions at the homoclinic points obtained in Theorem 3 with action $I$ since $\mathcal{C}_0^{\mathrm{f,b}}$ are the parameterizations of the intersections of the invariant manifolds of $\widetilde{\Lambda}_0^3$ and $\widetilde{\Lambda}_0^4$, given in Corollary 3.2. The second ones have the initial condition in the fixed points of the Poincaré map $\mathcal{P}_0^7$, which are parameterized by $\mathcal{G}_0^3$ and $\mathcal{G}_0^4$ given in Corollary 3.2.

**Lemma 3.2.** *The functions $\omega^{\mathrm{f,b}}(I)$ involved in the definition of the outer maps in* (26) *can be defined as*

$$\omega^*(I) = \omega_{\mathrm{out}}^*(I) + \omega_{\mathrm{in}}^*(I),$$

*where*

$$\omega_{\mathrm{out}}^*(I) = \omega_+^*(I) - \omega_-^*(I) \tag{30}$$

*with*

$$\begin{aligned} \omega_+^*(I) &= \lim_{N \to +\infty} \left( \int_0^{14N\pi} \frac{(\partial_G \Delta H_{\mathrm{circ}}) \circ \gamma_I^*(\sigma)}{-1 + \mu(\partial_G \Delta H_{\mathrm{circ}}) \circ \gamma_I^*(\sigma)}\, d\sigma + N\mathcal{T}_0(I) \right) \\ \omega_-^*(I) &= \lim_{N \to -\infty} \left( \int_0^{14N\pi} \frac{(\partial_G \Delta H_{\mathrm{circ}}) \circ \gamma_I^*(\sigma)}{-1 + \mu(\partial_G \Delta H_{\mathrm{circ}}) \circ \gamma_I^*(\sigma)}\, d\sigma + N\mathcal{T}_0(I) \right), \quad * = \mathrm{f}, \mathrm{b} \end{aligned} \tag{31}$$

$$\begin{aligned}\omega^{\mathrm{f}}_{\mathrm{in}}(I) &= \int_0^{-12\pi} \frac{(\partial_G \Delta H_{\mathrm{circ}}) \circ \gamma_I^4(\sigma)}{-1+\mu(\partial_G \Delta H_{\mathrm{circ}}) \circ \gamma_I^4(\sigma)}\, d\sigma \\ \omega^{\mathrm{b}}_{\mathrm{in}}(I) &= \int_0^{-2\pi} \frac{(\partial_G \Delta H_{\mathrm{circ}}) \circ \gamma_I^3(\sigma)}{-1+\mu(\partial_G \Delta H_{\mathrm{circ}}) \circ \gamma_I^3(\sigma)}\, d\sigma,\end{aligned} \tag{32}$$

*where $\mathcal{T}_0(I)$ is the function in* (23).

Note that the minus sign that appears in the limits of integration of the integrals involved in the definition of functions $\omega^*_{\mathrm{in}}(I)$ is due to the fact that the reparameterized flow (27) reverses time. Using that the circular problem is symmetric with respect to (18) and that the homoclinic points $\mathcal{C}_0^{\mathrm{f}}$ and $\mathcal{C}_0^{\mathrm{b}}$ belong to the symmetry axis, one can easily see that $\omega^*_- = -\omega^*_+$, $* = \mathrm{f}, \mathrm{b}$.

The geometric interpretation of $\omega^{\mathrm{f,b}}(I)$ is that the $t$-shift occurs since the homoclinic orbits approach different points of the same invariant curve in the future and in the past. This shift is equivalent to the shift in $t$ that appears in the Mather Problem [**?**]. See, for instance, formula (2.1) in Theorem 2.1 of [**?**] and the constants $a$ and $b$ used in formula (1.4) of [**?**].

*Proof.* We compute $\omega^{\mathrm{f}}(I)$. The other case can be done analogously. Since the $t$-component of the reduced circular system (27) does not depend on $t$, its behavior is given by

$$\begin{aligned}\Phi_0^t\{s,(L,\ell,G,g,t)\} &= t + \widetilde{\Phi}_0\{s,(L,\ell,G,g)\} \\ &= t + \int_0^s \frac{1}{-1+\mu\partial_G \Delta H_{\mathrm{circ}}\left(\Phi_0^{\mathrm{circ}}\{\sigma,(L,\ell,G,g)\}\right)}\, d\sigma\end{aligned} \tag{33}$$

Note that, using this flow, the inner map on (23) is just the $(-14\pi)$-time map in the time $s$. Then, the original period of the periodic orbits obtained in Theorem 3, can be expressed using this new flow as

$$14\pi + \mu\mathcal{T}_0(I) = \int_0^{-14\pi} \frac{1}{-1+\mu(\partial_G \Delta H_{\mathrm{circ}}) \circ \gamma_I^3(\sigma)}\, d\sigma. \tag{34}$$

This allows us to define the function $\mathcal{T}_0(I)$ in (23) through integrals as

$$\mathcal{T}_0(I) = \int_0^{-14\pi} \frac{(\partial_G \Delta H_{\mathrm{circ}}) \circ \gamma_I^3(\sigma)}{-1+\mu(\partial_G \Delta H_{\mathrm{circ}}) \circ \gamma_I^3(\sigma)}\, d\sigma. \tag{35}$$

Consider now a point $(\mathcal{C}_0^{\mathrm{f},L}(I), \mathcal{C}_0^{\mathrm{f},\ell}(I), \mathcal{C}_0^{\mathrm{f},G}(I), 0, I, t)$ in $W^u(\widetilde{\Lambda}_0^3) \cap W^s(\widetilde{\Lambda}_0^4) \cap \{g = 0\}$. Since the first four components are independent of $t$, $(\mathcal{C}_0^{\mathrm{f},L}(I), \mathcal{C}_0^{\mathrm{f},\ell}(I), \mathcal{C}_0^{\mathrm{f},G}(I), 0, I, t)$ is forward asymptotic (in the reparameterized time) to a point

$$\left(\mathcal{G}_0^{3,L}(I), \mathcal{G}_0^{3,\ell}(I), \mathcal{G}_0^{3,G}(I), 0, I, t + \mu\omega^{\mathrm{f}}_+(I)\right)$$

and backward asymptotic (in the reparameterized time) to a point

$$\left(\mathcal{G}_0^{4,L}(I), \mathcal{G}_0^{4,\ell}(I), \mathcal{G}_0^{4,G}(I), 0, I, t + \mu\omega^{\mathrm{f}}_-(I)\right).$$

Using (33), the functions $\omega^{\mathrm{f}}_{\pm}(I)$ can be defined as

$$\begin{aligned}\omega^{\mathrm{f}}_+(I) &= \lim_{T\to+\infty} \int_0^T \left( \frac{1}{-1+\mu(\partial_G \Delta H_{\mathrm{circ}}) \circ \gamma_I^{\mathrm{f}}(\sigma)} - \frac{1}{-1+\mu(\partial_G \Delta H_{\mathrm{circ}}) \circ \gamma_I^3(\sigma)} \right) d\sigma \\ \omega^{\mathrm{f}}_-(I) &= \lim_{T\to-\infty} \int_0^T \left( \frac{1}{-1+\mu(\partial_G \Delta H_{\mathrm{circ}}) \circ \gamma_I^{\mathrm{f}}(\sigma)} - \frac{1}{-1+\mu(\partial_G \Delta H_{\mathrm{circ}}) \circ \gamma_I^4(\sigma)} \right) d\sigma.\end{aligned} \tag{36}$$

Moreover, since the system is $14\pi$-periodic in the time $s$ due to the identification of $s$ with $g$, it is more convenient to write these in integrals as

$$\omega_+^{\mathrm{f}}(I) = \lim_{N\to+\infty} \int_0^{14N\pi} \left( \frac{1}{-1+\mu(\partial_G \Delta H_{\mathrm{circ}})\circ\gamma_I^{\mathrm{f}}(\sigma)} - \frac{1}{-1+\mu(\partial_G \Delta H_{\mathrm{circ}})\circ\gamma_I^{3}(\sigma)} \right) d\sigma.$$

$$\omega_-^{\mathrm{f}}(I) = \lim_{N\to-\infty} \int_0^{14N\pi} \left( \frac{1}{-1+\mu(\partial_G \Delta H_{\mathrm{circ}})\circ\gamma_I^{\mathrm{f}}(\sigma)} - \frac{1}{-1+\mu(\partial_G \Delta H_{\mathrm{circ}})\circ\gamma_I^{4}(\sigma)} \right) d\sigma.$$

Then, taking (34) into account, one obtains

$$\omega_\pm^{\mathrm{f}}(I) = \lim_{N\to\pm\infty} \left( \int_0^{14N\pi} \frac{1}{-1+\mu(\partial_G \Delta H_{\mathrm{circ}})\circ\gamma_I^{\mathrm{f}}(\sigma)}\, d\sigma + N(14\pi + \mathcal{T}_0(I)) \right),$$

from which the formulas for $\omega_\pm^{\mathrm{f}}$ in (31) follow.

Finally we have to compute $\omega_{\mathrm{in}}^{\mathrm{f}}(I)$. This term corresponds to the contribution of $\mathcal{P}_0^6$ to the outer map in formula (25). Then, taking into account that $t$ is defined modulo $2\pi$ is straightforward to obtain $\omega_{\mathrm{in}}^{\mathrm{f}}(I)$ in (31). □

# 4 The elliptic problem

We devote this section to study the elliptic problem. Namely, we obtain perturbative expansions of the inner and outer maps. To this end, we use Poincaré-Melnikov techniques applied to the reduced elliptic problem, which is given by

$$\begin{aligned}
\tfrac{d}{ds}\ell &= \frac{\partial_L H}{-1+\mu\partial_G\Delta H_{\mathrm{circ}}+\mu e_0\partial_G\Delta H_{\mathrm{ell}}} & \tfrac{d}{ds}L &= -\frac{\partial_\ell H}{-1+\mu\partial_G\Delta H_{\mathrm{circ}}+\mu e_0\partial_G\Delta H_{\mathrm{ell}}} \\
\tfrac{d}{ds}g &= 1 & \tfrac{d}{ds}G &= -\frac{\partial_g H}{-1+\mu\partial_G\Delta H_{\mathrm{circ}}+\mu e_0\partial_G\Delta H_{\mathrm{ell}}} \\
\tfrac{d}{ds}t &= \frac{1}{-1+\mu\partial_G\Delta H_{\mathrm{circ}}+\mu e_0\partial_G\Delta H_{\mathrm{ell}}} & \tfrac{d}{ds}I &= -\frac{\mu e_0\partial_t\Delta H_{\mathrm{ell}}}{-1+\mu\partial_G\Delta H_{\mathrm{circ}}+\mu e_0\partial_G\Delta H_{\mathrm{ell}}}.
\end{aligned} \tag{37}$$

This system is a perturbation of (27). The study of the inner map can be done both dealing with this system or the system associated to the Hamiltonian (14). Nevertheless, to simplify the exposition we use only (37) for both the inner and outer maps. We also consider the Poincaré map associated with this system and the section $\{g=0\}$,

$$\mathcal{P}_{e_0} : \{g=0\} \longrightarrow \{g=0\}, \tag{38}$$

which is a perturbation of (19).

There are two main results in this section:

- existence of a normally hyperbolic invariant manifold with transversal intersections of invariant manifolds for the elliptic problem (Theorem 4)
- computation of expansions of the inner and outer maps associated to it (Theorem 5).

The above theorems are stated in the next section. Theorem 4 replies on Corollary 3.2, because we study the elliptic problem as a perturbation of the circular one. The proof of Theorem 5 consists of several steps. In Section 4.2 we analyze the $e_0$-expansion of the elliptic Hamiltonian, and from it, in Section 4.3, we deduce properties of the $e_0$-expansion of the flow associated to system (37). In Section 4.4 we do perturbative analysis of the normally hyperbolic invariant cylinders $\widetilde{\Lambda}_{e_0}^j$, which are the perturbation of the cylinders $\widetilde{\Lambda}_0^j$ obtained in Corollary 3.2. This analysis allow us to obtain perturbative in $e_0$ formulas for the inner map derived. Finally, in Section 4.5 we apply the above expansions and compute the outer maps using Poincaré-Melnikov techniques. These expansions allows us to give perturbative formulas of the inner and outer maps of the elliptic problem, which are defined in $\widetilde{\Lambda}_{e_0}^3$, which is $e_0$-close to the cylinder $\widetilde{\Lambda}_0^3$ obtained in Corollary 3.2.

## 4.1 The normally hyperbolic invariant cylinder and specific form of the inner and outer maps for the elliptic problem

For $e_0$ small enough the system associated to the Hamiltonian (15) has a normally hyperbolic invariant cylinder $\Lambda_{e_0}$, which is $e_0$-close to $\Lambda_0$ given in Corollary 3.1. Analogously, the Poincaré map $\mathcal{P}_{e_0}$ associated to this system as the section $\{g = 0\}$ has a normally hyperbolic invariant cylinder $\widetilde{\Lambda}_{e_0} = \Lambda_{e_0} \cap \{g = 0\}$. Moreover, it is formed by seven connected components $\widetilde{\Lambda}^j_{e_0}$, $j = 0, \dots, 6$, which are $e_0$-close to the cylinders $\widetilde{\Lambda}^j_{e_0}$ obtained in Corollary 3.2.

Recall that in Corollary 3.2, we have seen that in the invariant planes $I =$ constant there where forward and backward transveral heteroclinic connections between $\widetilde{\Lambda}^3_0$ and $\widetilde{\Lambda}^4_0$ provided $I \in \mathcal{D}^{\mathrm{f}}$ and $I \in \mathcal{D}^{\mathrm{b}}$ respectively. For the elliptic problem and $e_0$ small enough we will have transversal heteroclinic connections in slightly smaller domains. To this end, we define

$$\mathcal{D}^*_\delta = \{I \in \mathcal{D}^* : \mathrm{dist}(I, \partial\mathcal{D}^*) > \delta\}, \ \ * = \mathrm{f}, \mathrm{b}. \tag{39}$$

**Theorem 4.** *For any $\delta > 0$, there exists $e_0^* > 0$ such that for $0 < e_0 < e_0^*$ the map $\mathcal{P}^7_{e_0}$, where $\mathcal{P}_{e_0}$ is the Poincaré map associated to Hamiltonian (15) and section $\{g = 0\}$, has seven normally hyperbolic locally[3] invariant manifolds $\widetilde{\Lambda}^j_{e_0}$, which are $e_0$-close in the $\mathcal{C}^1$ sense to $\widetilde{\Lambda}^j_0$. Moreover, there exist functions $\mathcal{G}^j_{e_0} : [I_- + \delta, I_+ - \delta] \times \mathbb{T} \to (\mathbb{R} \times \mathbb{T})^3$, $j = 0, \dots, 6$ which can be expressed in coordinates as*

$$\mathcal{G}^j_{e_0}(I, t) = \left(\mathcal{G}^{j,L}_{e_0}(I, t), \mathcal{G}^{j,\ell}_{e_0}(I, t), \mathcal{G}^{j,G}_{e_0}(I, t), 0, I, t\right), \tag{40}$$

*that parameterize $\widetilde{\Lambda}^j_{e_0}$. In other words $\widetilde{\Lambda}^j_{e_0}$ is a graph over $(I, t)$ defined as*

$$\widetilde{\Lambda}^j_{e_0} = \{\mathcal{G}_{e_0}(I, t) : (I, t) \in [I_- + \delta, I_+ - \delta] \times \mathbb{T}\}.$$

*The invariant manifolds $W^u(\widetilde{\Lambda}^3_{e_0})$ and $W^s(\widetilde{\Lambda}^4_{e_0})$ intersect transversally provided $I \in \mathcal{D}^{\mathrm{f}}_\delta$ and the invariant manifolds $W^u(\widetilde{\Lambda}^4_{e_0})$ and $W^s(\widetilde{\Lambda}^3_{e_0})$ intersect transversally provided $I \in \mathcal{D}^{\mathrm{b}}_\delta$. Moreover, one of these intersections is $e_0$-close in the $\mathcal{C}^1$ sense to the manifolds $\Gamma^{\mathrm{f,b}}_0$ defined in Corollary 3.2. Denote $\Gamma^{\mathrm{f,b}}_{e_0}$ these intersections. There exist functions*

$$\mathcal{C}^*_{e_0}(I, t) = \left(\mathcal{C}^{*,L}_{e_0}(I, t), \mathcal{C}^{*,\ell}_{e_0}(I, t), \mathcal{C}^{*,G}_{e_0}(I, t), 0, I, t\right), \ \ * = \mathrm{f}, \mathrm{b}$$

*which parameterize them. Namely,*

$$\Gamma^*_{e_0} = \left\{\mathcal{C}^*_{e_0}(I, t) : (I, t) \in [I_- + \delta, I_+ - \delta] \times \mathbb{T}\right\}, \ \ * = \mathrm{f}, \mathrm{b}.$$

For the elliptic problem, the coordinates $(I, t)$ are symplectic not with respect to the canonical symplectic form $dI \wedge dt$. Indeed if we make the pullback of the canonical form $dL \wedge d\ell + dG \wedge dg + dI \wedge dt$ to the cylinders $\widetilde{\Lambda}^j_{e_0}$, we obtain the symplectic form

$$\Omega^j_{e_0} = \left(1 + e_0 a^j_1(I, t) + e_0^2 a^j_2(I, t) + e_0^3 a^j_{\geq}(I, t)\right) dI \wedge dt, \tag{41}$$

for certain functions $a^j_k : [I_-, I_+] \times \mathbb{T} \to \mathbb{R}$. The functions $a^j_{\geq}$ contain the $e_0^3$ remainder terms, and thus depend on $e_0$ even if we do not write explicitly this dependence to simplify notation.

**Remark 4.1.** *Theorem 4 only guarantees local invariance for $\widetilde{\Lambda}^j_{e_0}$. Namely, boundary might not be invariant. Nevertheless, later in Section 5 we will show the existence of invariant tori in $\widetilde{\Lambda}^j_{e_0}$, which will play the role of boundaries of $\widetilde{\Lambda}^j_{e_0}$. Thanks to these tori, one can choose $\widetilde{\Lambda}^j_{e_0}$ to be invariant. For that reason, from now we will refer $\widetilde{\Lambda}^j_{e_0}$ as a normally hyperbolic invariant manifold.*

We introduce the following notation.

[3] see remark right below

**Notation 4.1.** *For any function $f$ with $2\pi$-periodic dependence on $t$, $\mathcal{N}(f)$ is the subset of the integers corresponding to which $t$-harmonics of $f$ (which may depend on other variables) are non-zero.*

In the invariant cylinder $\widetilde{\Lambda}^3_{e_0}$ given in Theorem 4 one can define inner and outer maps as we have done in $\widetilde{\Lambda}^3_0$ for the circular problem. Next sections are devoted to the perturbative analysis of these maps. We state here their main result.

**Theorem 5.** *The normally hyperbolic invariant manifold $\widetilde{\Lambda}^3_{e_0}$ given in Theorem 4 of the Poincaré map $\mathcal{P}^7_{e_0}$ in (38) has associated inner and outer maps. Moreover*

- *The inner map is of the form*

$$\mathcal{F}^{\rm in}_{e_0}:\begin{pmatrix} I\\ t\end{pmatrix}\mapsto\begin{pmatrix} I+e_0A_1(I,t)+e_0^2A_2(I,t)+\mathcal{O}\left(e_0^3\right)\\ t+\mu\mathcal{T}_0(I)+e_0\mathcal{T}_1(I,t)+e_0^2\mathcal{T}_2(I,t)+\mathcal{O}(e_0^3)\end{pmatrix}. \tag{42}$$

  *and the functions $A_1$, $A_2$, $\mathcal{T}_1$, and $\mathcal{T}_2$ satisfy*

$$\mathcal{N}(A_1)=\{\pm1\},\ \mathcal{N}(A_2)=\{0,\pm1,\pm2\} \tag{43}$$
$$\mathcal{N}(\mathcal{T}_1)=\{\pm1\},\ \mathcal{N}(\mathcal{T}_2)=\{0,\pm1,\pm2\}. \tag{44}$$

- *The outer maps are of the form*

$$\mathcal{F}^{{\rm out},*}_{e_0}:\begin{pmatrix} I\\ t\end{pmatrix}\mapsto\begin{pmatrix} I+e_0B^*(I,t)+\mathcal{O}\left(e_0^2\right)\\ t+\mu\omega^*(I)+\mathcal{O}(e_0)\end{pmatrix},\ *={\rm f,b}. \tag{45}$$

  *and the functions $B^*$ satisfy*

$$\mathcal{N}(B^*)=\{\pm1\}. \tag{46}$$

## 4.2 The $e_0$-expansion of the elliptic Hamiltonian

We obtain expansions of $\Delta H_{\rm ell}$ in (15) with respect to $e_0$. These expansions will be used later in Sections 4.3, 4.4 and 4.5. The most important goal is to see which harmonics in $t$ have the $e_0$ and $e_0^2$ terms of the elliptic perturbation in (15). Note that the circular problem is independent of $t$.

We define the function

$$\mathcal{B}(r,v,g,t)=\frac{1}{\left|re^{i(v+g-t)}-r_0(t)e^{iv_0(t)}\right|}. \tag{47}$$

This function is the potential

$$\frac{1}{|q-q_0(t)|}$$

expressed in terms of $g=\hat{g}-t$, where $\hat{g}$ is the argument of the perihelion, the true anomaly $v$ of the Asteroid defined in (11) and the radius $r$. The functions $r_0(t)$ and $v_0(t)$ are the radius and the true anomaly of Jupiter. The functions $r_0(t)$ and $v_0(t)$ are the only ones involved in the definition of $\mathcal{B}$ which depend on $e_0$.

Then, the perturbation in (14) can be expressed as

$$\begin{aligned}\mu\Delta H_{\rm circ}(L,\ell,G,g)+\mu e_0\Delta H_{\rm ell}(L,\ell,G,g,t)=&-\frac{1-\mu}{\mu}\mathcal{B}\left(-\frac{r}{\mu},v,g,t\right)\\ &-\frac{\mu}{1-\mu}\mathcal{B}\left(\frac{r}{1-\mu},v,g-t,t\right)+\frac{1}{r}\Big|_{(r,v)=(r(L,\ell,G),v(L,\ell,G))}\end{aligned}$$

First we study the expansion of $\mathcal{B}$, and from it, we deduce the one of $\Delta H_{\rm ell}$.

**Lemma 4.1.** *Consider the expansion*

$$\mathcal{B}(r,v,g,t)=\mathcal{B}_0(r,v,g)+e_0\mathcal{B}_1(r,v,g,t)+e_0^2\mathcal{B}_2(r,v,g,t)+\mathcal{O}\left(e_0^3\right) \tag{48}$$

*of the function $\mathcal{B}$ defined in (47). Then,*

- $\mathcal{B}_0$ *satisfies* $\mathcal{N}(\mathcal{B}_0) = \{0\}$.
- $\mathcal{B}_1$ *satisfies* $\mathcal{N}(\mathcal{B}_1) = \{\pm 1\}$ *and is given by*

$$\mathcal{B}_1(r, v, g, t) = -\frac{1}{2\Delta^3(r, v, g)} \left(2\cos t - 3r\cos(v + g + t) + r\cos(v + g - t)\right), \tag{49}$$

*where*

$$\Delta(r, v, g) = \left(r^2 + 1 - 2r\cos(v + g)\right)^{1/2}.$$

- $\mathcal{B}_2$ *satisfies* $\mathcal{N}(\mathcal{B}_2) = \{0, \pm 1, \pm 2\}$.

Note that the elliptic problem is a peculiar perturbation of the circular problem in the sense that the $k$-th $e_0$-order has $t$-harmonics up to order $k$. This fact will be crucial when we will compare the inner and outer dynamics in Section 5.

*Proof.* To prove this lemma we look for the $e_0$-expansions of the functions $r_0(t)$ and $v_0(t)$ involved in the definition of $\mathcal{B}$ in (47). We obtain them using the eccentric, true and mean anomalies of Jupiter.

From the relation $t = u_0 - e_0 \sin u_0$ (see (13)), one can obtain that

$$u_0(t) = t + e_0 \sin t + \frac{e_0^2}{2} \sin 2t + \mathcal{O}\left(e_0^3\right).$$

Then, using $r_0 = 1 - e_0 \cos u_0$,

$$r_0(t) = 1 - e_0 \cos t + e_0^2 \sin^2 t + \mathcal{O}\left(e_0^3\right).$$

For the eccentric anomaly we can use

$$\tan \frac{v_0}{2} = \sqrt{\frac{1 + e_0}{1 - e_0}} \tan \frac{u_0}{2}$$

(see (89)), to obtain

$$v_0 = u_0 + e_0 \sin u_0 + e_0^2 \left(\frac{9}{2} \sin u_0 - 2 \sin 2u_0\right) + \mathcal{O}\left(e_0^3\right)$$

and then

$$v_0(t) = t + 2e_0 \sin t + e_0^2 \left(\frac{9}{2} \sin t - \sin 2t\right) + \mathcal{O}\left(e_0^3\right).$$

Plugging $r_0(t)$ and $v_0(t)$ into (47), it can be easily seen that the expansion (48) satisfies all the properties of $\mathcal{B}_0$, $\mathcal{B}_1$ and $\mathcal{B}_2$ stated in the lemma. □

From the expansion of $\mathcal{B}$, one can easily deduce the expansion of $\Delta H_{\text{ell}}$ in (15).

**Corollary 4.1.** *Let us consider the $e_0$-expansion of the function $\Delta H_{\text{ell}}$ in* (15)*,*

$$\Delta H_{\text{ell}} = \Delta H_{\text{ell}}^1 + e_0 \Delta H_{\text{ell}}^2 + \mathcal{O}\left(e_0^2\right).$$

*Then, the first order is given by*

$$\begin{aligned} \Delta H_{\text{ell}}^1(L, \ell, G, g, t) = &-\frac{1 - \mu}{\mu} \mathcal{B}_1\left(-\frac{r(L, \ell, G)}{\mu}, v(L, \ell, G), g, t\right) \\ &- \frac{\mu}{1 - \mu} \mathcal{B}_1\left(\frac{r(L, \ell, G)}{1 - \mu}, v(L, \ell, G), g, t\right). \end{aligned} \tag{50}$$

*where $\mathcal{B}_1$ is the function defined in Lemma 4.1 and therefore it satisfies*

$$\mathcal{N}\left(\Delta H_{\text{ell}}^1\right) = \{\pm 1\}.$$

*The second order $\Delta H_{\text{ell}}^2$ satisfies*

$$\mathcal{N}\left(\Delta H_{\text{ell}}^2\right) = \{0, \pm 1, \pm 2\}.$$

### 4.3 Perturbative analysis of the flow

To study the inner and outer maps perturbatively, we need first to study the first orders with respect to $e_0$ of the flow $\Phi_{e_0}\{s,(g,I,t)\}$ associated to the vector field (37). Particularly, we want to know their dependence on the variable $t$. Recall that we already know the dependence on $t$ of the 0-order thanks to formulas (28) and (33).

**Lemma 4.2.** *The flow $\Phi_{e_0}\{s,(L,\ell,G,g,I,t)\}$ has a perturbative expansion*

$$\begin{aligned}\Phi^{\text{in}}_{e_0}\{s,(L,\ell,G,g,I,t)\} =&\Phi^{\text{in}}_0\{s,(L,\ell,G,g,I,t)\} + e_0\Phi^{\text{in}}_1\{s,(L,\ell,G,g,I,t)\}\\ &+ e_0^2\Phi^{\text{in}}_2\{s,(L,\ell,G,g,I,t)\} + \mathcal{O}\left(e_0^3\right),\end{aligned}$$

*which satisfies*

$$\mathcal{N}\left(\Phi^{\text{in}}_1\{s,(L,\ell,G,g,I,t)\}\right) = \{\pm 1\} \tag{51}$$

$$\mathcal{N}\left(\Phi^{\text{in}}_2\{s,(L,\ell,G,g,I,t)\}\right) = \{0,\pm 1,\pm 2\}. \tag{52}$$

*Proof.* Let us denote $z=(L,\ell,G,g,I)$ and call $\mathcal{X}_{e_0}$ to the vector field (37), which has expansion

$$\mathcal{X}_{e_0} = \mathcal{X}_0 + e_0\mathcal{X}_1 + e_0^2\mathcal{X}_2 + \mathcal{O}\left(e_0^3\right).$$

We first prove (51). The $e_0$-order $\Phi_1$ is a solution of the ordinary differential equation

$$\frac{d}{ds}\xi = D\mathcal{X}_0\left(\Phi_0\{s,(z,t)\}\right)\xi + \mathcal{X}_1\left(\Phi_0\{s,(z,t)\}\right)$$

with initial condition $\xi(0)=(0,0)$. By (27), $\mathcal{X}_0$ is independent of $t$ and therefore,

$$D\mathcal{X}_0\left(\Phi_0\{s,(z,t)\}\right) = D\mathcal{X}_0\left(\Phi^{\text{circ}}_0(s,z)\right),$$

where $\Phi^{\text{circ}}_0$ has been defined in (28). Then, this term is also independent of $t$. From Corollary 4.1, one can deduce that $\mathcal{N}(\mathcal{X}_1)=\{\pm 1\}$ and therefore $\mathcal{X}_1$ can be written as

$$\mathcal{X}_1(z,t) = \mathcal{X}_1^+(z)e^{it} + \mathcal{X}_1^-(z)e^{-it},$$

Therefore, using formulas (28) and (33), one has that

$$\mathcal{X}_1\left(\Phi_0\{s,(z,t)\}\right) = \left(\mathcal{X}_1^+\left(\Phi^{\text{circ}}_0\{s,z\}\right)e^{i\widetilde{\Phi}_0\{s,z\}}\right)e^{it} + \left(\mathcal{X}_1^-\left(\Phi^{\text{circ}}_0\{s,z\}\right)e^{i\widetilde{\Phi}_0\{s,z\}}\right)e^{-it}.$$

To prove (51), it is enough to use variation of constants formula. Let us consider $M_z(s)$ the fundamental matrix of the linear equation

$$\frac{d}{ds}\xi = D\mathcal{X}_0\left(\Phi^{\text{circ}}_0(s,z)\right)\xi,$$

then

$$\Phi_1\{s,(z,t)\} = \Phi_1^+\{s,z\}e^{it} + \Phi_1^-\{s,z\}e^{-it}$$

with

$$\Phi_1^\pm\{s,z\} = M_z(s)\int_0^s M_z^{-1}(\sigma)\left(\mathcal{X}_1^\pm\left(\Phi^{\text{circ}}_0\{s,z\}\right)e^{\pm i\widetilde{\Phi}_0\{s,z\}\}}\right)d\sigma.$$

The proof of (52) follows the same lines. Indeed, $\Phi_2$ is solution of an equation of the form

$$\frac{d}{ds}\xi = D\mathcal{X}_0\left(\Phi^{\text{circ}}_0\{s,z\}\right)\xi + \Xi(s,g,I,t)$$

with initial condition $\xi(0)=(0,0,0)$. The function $\Xi$ is given in terms of the previous orders of $\mathcal{X}_{e_0}$ and $\Phi_{e_0}$ as

$$\Xi = \frac{1}{2}D^2\mathcal{X}_0\left(\Phi^{\text{circ}}_0\right)\left(\Phi_1\right)^{\otimes 2} + D\mathcal{X}_1\left(\Phi^{\text{circ}}_0\right)\Phi^{\text{in}}_1 + \mathcal{X}_2\left(\Phi^{\text{circ}}_0\right),$$

and then it satisfies $\mathcal{N}(\Xi)=\{0,\pm 1,\pm 2\}$.

Since the homogeneous linear equation is the same as for $\Phi^{\text{in}}_1$ and does not depend on $t$, one can easily see that (52) is satisfied. □

## 4.4 Perturbative analysis of the normally hyperbolic invariant manifold and the inner map

We devote this section to study the normally hyperbolic invariant manifold of the elliptic problem $\widetilde{\Lambda}^3_{e_0}$, given in Theorem 4, and the inner map associated to it. We study the inner map of the elliptic problem perturbatively from (23), taking $e_0$ as a small parameter. We call the inner map $\mathcal{F}^{\rm in}_{e_0} : \widetilde{\Lambda}^3_{e_0} \to \widetilde{\Lambda}^3_{e_0}$, which is defined as the $(-14\pi)$-Poincaré map of the flow $\Phi_{e_0}$, defined in Lemma 4.2, restricted to $\widetilde{\Lambda}^3_{e_0}$.

We want to see which $t$-harmonics the first orders of the inner map has and also we want to compute the first order of the $I$ component. To this end we consider the classical theory of normally hyperbolic invariant manifolds [**?**, **?**]. This theory ensures the existence of the maps $\mathcal{G}^j_{e_0}$ parameterizing the normally hyperbolic manifolds $\widetilde{\Lambda}^j_0$ of the map $\mathcal{P}^7_{e_0}$. Moreover, they can be made unique imposing

$$\pi_I \mathcal{G}^j_{e_0}(I,t) = I,\ \pi_t \mathcal{G}^j_{e_0}(I,t) = t, \tag{53}$$

where $\pi_*$ is the projection with respect to the corresponding component of the function. Since we only need properties of the parameterization of $\widetilde{\Lambda}^3_{e_0}$ and the dynamics on it, we just consider the case $j = 3$. The map $\mathcal{G}^3_{e_0}$ satisfies the invariance equation

$$\widetilde{\mathcal{P}}_{e_0} \circ \mathcal{G}^3_{e_0} = \mathcal{G}^3_{e_0} \circ \mathcal{F}^{\rm in}_{e_0}, \tag{54}$$

where $\widetilde{\mathcal{P}}_{e_0} = \mathcal{P}^7_{e_0}$ and $\mathcal{F}^{\rm in}_{e_0}$ is the inner map of the elliptic problem, namely the Poincaré map $\mathcal{P}^7_{e_0}$ restricted to the cylinder $\widetilde{\Lambda}^3_{e_0}$.

Since we have regularity with respect to parameters, the invariance equation allows us to obtain expansions of both the parameterizations of $\widetilde{\Lambda}^3_{e_0}$ and the inner map $\mathcal{F}^{\rm in}_{e_0}$ with respect to $e_0$. Let us expand $\mathcal{G}^3_{e_0}$ and $\mathcal{F}^{\rm in}_{e_0}$ as

$$\mathcal{G}^3_{e_0} = \mathcal{G}^3_0 + e_0\mathcal{G}^3_1 + e_0^2\mathcal{G}^3_2 + \mathcal{O}\left(e_0^3\right) \tag{55}$$

$$\mathcal{F}^{\rm in}_{e_0} = \mathcal{F}^{\rm in}_0 + e_0\mathcal{F}^{\rm in}_1 + e_0^2\mathcal{F}^{\rm in}_2 + \mathcal{O}\left(e_0^3\right). \tag{56}$$

Then, $\mathcal{G}^3_0$ is the function defined in (21) and $\mathcal{F}^{\rm in}_0$ is the inner map of the circular problem obtained in (23), which is defined in $\widetilde{\Lambda}^3_0$. Recall that

$$\widetilde{\mathcal{P}}_{e_0}(L,\ell,G,0,I,t) = \mathcal{P}^7_{e_0}(L,\ell,G,0,I,t) = \Phi_{e_0}\{-14\pi,(L,\ell,G,0,I,t)\}, \tag{57}$$

where $\Phi_{e_0}$ is the flow considered in Lemma 4.2. Then, we have that

$$\mathcal{N}\left(\widetilde{\mathcal{P}}_1\right) = \{\pm 1\} \quad \text{and} \quad \mathcal{N}\left(\widetilde{\mathcal{P}}_2\right) = \{0, \pm 1, \pm 2\}.$$

Then, expanding equation (54) with respect to $e_0$ allows us to deduce the properties we need about the inner map. They are summarized in the next lemma, which reproduces the part of Theorem 5 referred to the inner dynamics.

**Lemma 4.3.** *The expansions of the functions $\mathcal{G}^3_{e_0}$ and $\mathcal{F}^{\rm in}_{e_0}$ in* (55) *and* (56) *satisfy that*

$$\mathcal{N}\left(\mathcal{G}^3_1\right) = \{\pm 1\} \quad \textit{and} \quad \mathcal{N}\left(\mathcal{G}^3_2\right) = \{0, \pm 1, \pm 2\}$$

*and*

$$\mathcal{N}(\mathcal{F}^{\rm in}_1) = \{\pm 1\} \quad \textit{and} \quad \mathcal{N}(\mathcal{F}^{\rm in}_2) = \{0, \pm 1, \pm 2\}.$$

*Namely, the inner map is of the form,*

$$\mathcal{F}^{\rm in}_{e_0} : \begin{pmatrix} I \\ t \end{pmatrix} \mapsto \begin{pmatrix} I + e_0 A_1(I,t) + e_0^2 A_2(I,t) + \mathcal{O}\left(\mu e_0^3\right) \\ t + \mu\mathcal{T}_0(I) + e_0\mathcal{T}_1(I,t) + e_0^2\mathcal{T}_2(I,t) + \mathcal{O}\left(\mu e_0^2\right) \end{pmatrix}, \tag{58}$$

*and the functions $A_1$, $A_2$ $\mathcal{T}_1$ and $\mathcal{T}_2$ satisfy*

$$\mathcal{N}(A_1) = \{\pm 1\}, \ \mathcal{N}(A_2) = \{0, \pm 1, \pm 2\} \tag{59}$$
$$\mathcal{N}(\mathcal{T}_1) = \{\pm 1\}, \ \mathcal{N}(\mathcal{T}_2) = \{0, \pm 1, \pm 2\}. \tag{60}$$

*Moreover $A_1$ can be split as,*

$$A_1(I,t) = A_1^+(I)e^{it} + A_1^-(I)e^{-it},$$

*with*

$$A_1^\pm(I) = \mp i\mu \int_0^{-14\pi} \frac{\Delta H_{\text{ell}}^{1,\pm} \circ \gamma_I^3(\sigma)}{-1 + \mu \partial_G \Delta H_{\text{circ}} \gamma_I^3(\sigma)} e^{\pm i \widetilde{\gamma}_I^3(\sigma)} d\sigma, \tag{61}$$

*where the functions $\Delta H_{\text{ell}}^{1,\pm}$ are defined as*

$$\Delta H_{\text{ell}}^1(L,\ell,G,g,t) = \Delta H_{\text{ell}}^{1,+}(L,\ell,G,g)e^{it} + \Delta H_{\text{ell}}^{1,\pm}(L,\ell,G,g)e^{-it},$$

*$\gamma_I^3(\sigma)$ has been defined in* (29) *and*

$$\widetilde{\gamma}_I^3(\sigma) = \widetilde{\Phi}_0\{\sigma, (\mathcal{G}_0^{3,L}(I), \mathcal{G}_0^{3,\ell}(I), \mathcal{G}_0^{3,G}(I), 0)\}, \tag{62}$$

*where $\widetilde{\Phi}_0$ has been defined in* (68) *and $\mathcal{G}_0^3$ in Corollary 3.2.*

From the properties of $\mathcal{G}_{e_0}^3$, we can deduce properties of the symplectic form $\Omega_{e_0}^3$ in (41), which is defined in the cylinder $\widetilde{\Lambda}_{e_0}^3$.

**Corollary 4.2.** *The functions $a_1^3$ and $a_2^3$ in the expansion of the symplectic form $\Omega_{e_0}^3$ in* (41)*, which is the pullback of the symplectic form $dL \wedge d\ell + dG \wedge dg + dI \wedge dt$ into the cylinder $\widetilde{\Lambda}_{e_0}^3$, satisfy*

$$\mathcal{N}\left(a_1^3\right) = \{\pm 1\} \quad \textit{and} \quad \mathcal{N}\left(a_2^3\right) = \{0, \pm 1, \pm 2\}.$$

*Proof of Lemma 4.3.* In the proof we omit the superscript 3 of the terms in the expansion of $\mathcal{G}_{e_0}^3$.

Expanding equation (54) with respect to $e_0$, we have that the first terms satisfy

$$\widetilde{\mathcal{P}}_0 \circ \mathcal{G}_0 = \mathcal{G}_0 \circ \mathcal{F}_0^{\text{in}} \tag{63}$$
$$\widetilde{\mathcal{P}}_1 \circ \mathcal{G}_0 + \left(D\widetilde{\mathcal{P}}_0 \circ \mathcal{G}_0\right) \mathcal{G}_1 = \mathcal{G}_1 \circ \mathcal{F}_0^{\text{in}} + \left(D\mathcal{G}_0 \circ \mathcal{F}_0^{\text{in}}\right) \mathcal{F}_1^{\text{in}} \tag{64}$$
$$\begin{aligned}\widetilde{\mathcal{P}}_2 \circ \mathcal{G}_0 + \left(D\widetilde{\mathcal{P}}_1 \circ \mathcal{G}_0\right) \mathcal{G}_1 + \frac{1}{2}\left(D^2\widetilde{\mathcal{P}}_0 \circ \mathcal{G}_0\right) \mathcal{G}_1^{\otimes 2} + \left(D\widetilde{\mathcal{P}}_0 \circ \mathcal{G}_0\right) \mathcal{G}_2 &= \mathcal{G}_2 \circ \mathcal{F}_0^{\text{in}} + \left(D\mathcal{G}_1 \circ \mathcal{F}_0^{\text{in}}\right) \mathcal{F}_1^{\text{in}} \\ &+ \frac{1}{2}\left(D^2\mathcal{G}_0 \circ \mathcal{F}_0^{\text{in}}\right)(\mathcal{F}_1^{\text{in}})^{\otimes 2} + \left(D\mathcal{G}_0 \circ \mathcal{F}_0^{\text{in}}\right) \mathcal{F}_2^{\text{in}}\end{aligned} \tag{65}$$

By the uniqueness condition (53), $\mathcal{G}_1$ is of the form

$$\mathcal{G}_1(g,I,t) = \left(\widetilde{\mathcal{G}}_1(g,I,t), 0, 0, 0\right)$$

with $\widetilde{\mathcal{G}}_1(g,I,t) = (\mathcal{G}_1^L(g,I,t), \mathcal{G}_1^\ell(g,I,t), \mathcal{G}_1^G(g,I,t))$.

Equation (63) corresponds to the inner dynamics of the circular problem. We use equations (64) and (65) to deduce the properties of $\mathcal{F}_1^{\text{in}}$ and $\mathcal{F}_2^{\text{in}}$ respectively. These equations can be solved iteratively and thus we start with (64). Since

$$D\mathcal{G}_0 = \begin{pmatrix} D\widetilde{\mathcal{G}}_0 \\ \text{Id} \end{pmatrix} \text{ and } D\mathcal{G}_i = \begin{pmatrix} D\widetilde{\mathcal{G}}_i \\ 0 \end{pmatrix} \text{ for } i \geq 1, \tag{66}$$

we have that

$$\mathcal{F}_1^{\text{in},*} = \pi_* \left(\widetilde{\mathcal{P}}_1 \circ \mathcal{G}_0 + \left(D\widetilde{\mathcal{P}}_0 \circ \mathcal{G}_0\right) \widetilde{\mathcal{G}}_1\right), \ * = I, t.$$

Replacing this into (64) we obtain an equation for $\mathcal{G}_1$. The equation for every Fourier $t$-coefficient is uncoupled, and therefore, using (57), that $\widetilde{\mathcal{P}}_0$ is independent of $t$ and the uniqueness of $\mathcal{G}_1$, one can deduce that $\mathcal{N}(\mathcal{G}_1) = \{\pm 1\}$. As a consequence we have that $\mathcal{N}(\mathcal{F}_1^{\text{in}}) = \{\pm 1\}$.

Reasoning analogously and using (57) again, one can see that $\mathcal{N}(\mathcal{G}_2) = \{0, \pm 1, \pm 2\}$ and $\mathcal{N}(\mathcal{F}_2^{\text{in}}) = \{0, \pm 1, \pm 2\}$.

Now it only remains to prove formula (61). To this end, let us recall that one can write the $I$-component of the inner equation as

$$\mathcal{F}_{e_0}^{\text{in},I}(I,t) = \Phi_{e_0}^I \left\{-14\pi, \mathcal{G}_{e_0}(I,t)\right\}$$

since it is defined as the $(-14\pi)$-Poincaré map associated to the flow of system (37) restricted to the cylinder $\widetilde{\Lambda}_{e_0}^3$. Recall that the minus sign in the time appears due to the fact that system (37) has the time reversed with respect to the original one. Then, one can apply the Fundamental Theorem of Calculus and use (37) to obtain

$$\begin{aligned}\mathcal{F}_{e_0}^{\text{in},I}(I,t) &= \int_0^{-14\pi} \frac{d}{ds}\Phi_{e_0}^I \left\{s, \mathcal{G}_{e_0}(I,t)\right\} ds \\ &= -\int_0^{-14\pi} \frac{\mu e_0 \partial_t \Delta H_{\text{ell}} \circ \Phi_{e_0} \left\{s, \mathcal{G}_{e_0}(I,t)\right\}}{-1 + \mu \partial_G \Delta H_{\text{circ}} \circ \Phi_{e_0} \left\{s, \mathcal{G}_{e_0}(I,t)\right\} + \mu e_0 \partial_g \Delta H_{\text{ell}} \circ \Phi_{e_0} \left\{s, \mathcal{G}_{e_0}(I,t)\right\}} ds\end{aligned}$$

Then, using the expansions of the Hamiltonian $\Delta H_{\text{ell}}$ in Corollary 4.1, of the flow $\Phi_{e_0}$ in Lemma 4.2 and of $\mathcal{G}_{e_0}$ just obtained,

$$\mathcal{F}_{e_0}^{\text{in},I}(I,t) = -e_0 \int_0^{-14\pi} \frac{\mu \partial_t \Delta H_{\text{ell}}^1 \circ \Phi_0 \left\{s, \mathcal{G}_0(I,t)\right\}}{-1 + \mu \partial_G \Delta H_{\text{circ}} \circ \Phi_0 \left\{s, \mathcal{G}_0(I,t)\right\}} ds + \mathcal{O}\left(e_0^2\right)$$

Namely,

$$A_1(I,t) = -\int_0^{-14\pi} \frac{\mu \partial_t \Delta H_{\text{ell}}^1 \circ \Phi_0 \left\{s, \mathcal{G}_0(I,t)\right\}}{-1 + \mu \partial_G \Delta H_{\text{circ}} \circ \Phi_0 \left\{s, \mathcal{G}_0(I,t)\right\}} ds$$

To deduce the formulas for $A_1^{\pm}$ it is enough to split $\Delta H_{\text{ell}}^1$ as

$$\Delta H_{\text{ell}}^1(L,\ell,G,g,t) = \Delta H_{\text{ell}}^{1,+}(L,\ell,G,g) e^{it} + \Delta H_{\text{ell}}^{1,\pm}(L,\ell,G,g) e^{-it},$$

and recall that by formulas (28) and (33), $\Phi_0$ can be written as

$$\Phi_0 \left\{s, (L,\ell,G,g,I,t)\right\} = \left(\Phi_{\text{circ}} \left\{s, (L,\ell,G,g,I)\right\}, t + \widetilde{\Phi}_0 \left\{s, (L,\ell,G,g,I)\right\}\right).$$

□

## 4.5 The outer map of the elliptic problem

We devote this section to study the outer maps

$$\mathcal{F}_{e_0}^{\text{out},*} : \widetilde{\Lambda}_{e_0}^3 \longrightarrow \widetilde{\Lambda}_{e_0}^3, \quad * = \text{f}, \text{b} \tag{67}$$

for $e_0 > 0$.

Theorem 4 gives the existence of $\mathcal{C}_{e_0}^*$, $* = \text{f}, \text{b}$, transversal intersections of the invariant manifolds of $\widetilde{\Lambda}_{e_0}^3$ and $\widetilde{\Lambda}_{e_0}^4$. The Poincaré map (38) possesses then also a normally hyperbolic invariant manifold $\widetilde{\Lambda}_{e_0} = \cup_{j=0}^6 \widetilde{\Lambda}_{e_0}^j$ and its invariant manifolds intersect transversally at $\widetilde{\Gamma}_{e_0}$.

Then, we can proceed as in Section 3.2 to define the outer maps $\mathcal{F}_{e_0}^{\text{out}}$. We want to study it as a perturbation of the outer map of the circular problem given in (26). To this end we use Poincaré-Melnikov techniques. As we have explained in Section 3.2, the original flow associated to Hamiltonian (14) does not allow us to study perturbatively $\mathcal{F}_{e_0}^{\text{out}}$. Instead, we use the reduced elliptic problem defined in (37).

The results stated in Theorem 5 about the outer map are summarized in the next lemma. We also show how to compute the first order term. To this end, we use the notation used in Section 3.2. In particular, we will use the notation $\gamma_I^{\mathrm{f,b}}(\sigma)$ and $\gamma_I^{3,4}(\sigma)$ defined in (29). Analogously we define their corresponding $t$-component of the flow as

$$\begin{aligned}\widetilde{\gamma}_I^*(\sigma) &= \widetilde{\Phi}_0\{\sigma, (\mathcal{C}_0^{*,L}(I), \mathcal{C}_0^{*,\ell}(I), \mathcal{C}_0^{*,G}(I), 0)\}, \ \ * = \mathrm{f}, \mathrm{b} \\ \widetilde{\gamma}_I^j(\sigma) &= \widetilde{\Phi}_0\{\sigma, (\mathcal{G}_0^{j,L}(I), \mathcal{G}_0^{j,\ell}(I), \mathcal{G}_0^{j,G}(I), 0)\}, \ \ j = 3, 4\end{aligned} \tag{68}$$

where $\widetilde{\Phi}_0$ has been defined in (33) and $\mathcal{C}_0^*$ and $\mathcal{G}_0^j$ have been given in Corollary 3.2.

**Lemma 4.4.** *The outer map defined in* (67) *has the following expansion with respect to* $e_0$*,*

$$\mathcal{F}_{e_0}^{\mathrm{out},*} : \begin{pmatrix} I \\ t \end{pmatrix} \mapsto \begin{pmatrix} I + e_0\left(B^{*,+}(I)e^{it} + B^{*,-}(I)e^{-it}\right) + \mathcal{O}\left(e_0^2\right) \\ t + \mu\omega^*(I) + \mathcal{O}(e_0) \end{pmatrix}, \ \ * = \mathrm{f}, \mathrm{b}. \tag{69}$$

*Moreover, the functions* $B^{*,\pm}(I)$ *can be defined as*

$$\begin{aligned}B^{\mathrm{f},\pm}(I) &= B_{\mathrm{out}}^{\mathrm{f},\pm}(I) + B_{\mathrm{in}}^{\mathrm{f},\pm}(I)e^{\pm i\mu\omega_{\mathrm{out}}^{\mathrm{f}}(I)} \\ B^{\mathrm{b},\pm}(I) &= B_{\mathrm{in}}^{\mathrm{b},\pm}(I) + B_{\mathrm{out}}^{\mathrm{b},\pm}(I)e^{\pm i\mu\omega_{\mathrm{in}}^{\mathrm{b}}(I)}\end{aligned} \tag{70}$$

*where* $\omega_{\mathrm{out}}^{\mathrm{f}}(I)$ *and* $\omega_{\mathrm{in}}^{\mathrm{b}}(I)$ *are the functions defined in* (30) *and* (32) *respectively and*

$$B_{\mathrm{out}}^{\mathrm{f},\pm}(I) = \pm i\mu \lim_{T\to+\infty} \int_0^T \left( \frac{\Delta H_{\mathrm{ell}}^{1,\pm} \circ \gamma_I^{\mathrm{f}}(\sigma)}{-1 + \mu\partial_G \Delta H_{\mathrm{circ}} \circ \gamma_I^{\mathrm{f}}(\sigma)} e^{\pm i\widetilde{\gamma}_I^{\mathrm{f}}(\sigma)} \right. \tag{71}$$

$$\left. - \frac{\Delta H_{\mathrm{ell}}^{1,\pm} \circ \gamma_I^{3}(\sigma)}{-1 + \mu\partial_G \Delta H_{\mathrm{circ}} \circ \gamma_I^{3}(\sigma)} e^{\pm i\left(\widetilde{\gamma}_I^{3}(\sigma) + \mu\omega_+^{\mathrm{f}}(I)\right)} \right) d\sigma \tag{72}$$

$$\mp i\mu \lim_{T\to-\infty} \int_0^T \left( \frac{\Delta H_{\mathrm{ell}}^{1,\pm} \circ \gamma_I^{\mathrm{f}}(\sigma)}{-1 + \mu\partial_G \Delta H_{\mathrm{circ}} \circ \gamma_I^{\mathrm{f}}(\sigma)} e^{\pm i\widetilde{\gamma}_I^{\mathrm{f}}(\sigma)} \right.$$

$$\left. - \frac{\Delta H_{\mathrm{ell}}^{1,\pm} \circ \gamma_I^{4}(\sigma)}{-1 + \mu\partial_G \Delta H_{\mathrm{circ}} \circ \gamma_I^{4}(\sigma)} e^{\pm i\left(\widetilde{\gamma}_I^{4}(\sigma) + \mu\omega_-^{\mathrm{f}}(I)\right)} \right) d\sigma,$$

$$B_{\mathrm{out}}^{\mathrm{b},\pm}(I) = \pm i\mu \lim_{T\to+\infty} \int_0^T \left( \frac{\Delta H_{\mathrm{ell}}^{1,\pm} \circ \gamma_I^{\mathrm{b}}(\sigma)}{-1 + \mu\partial_G \Delta H_{\mathrm{circ}} \circ \gamma_I^{\mathrm{b}}(\sigma)} e^{\pm i\widetilde{\gamma}_I^{\mathrm{b}}(\sigma)} \right.$$

$$\left. - \frac{\Delta H_{\mathrm{ell}}^{1,\pm} \circ \gamma_I^{4}(\sigma)}{-1 + \mu\partial_G \Delta H_{\mathrm{circ}} \circ \gamma_I^{4}(\sigma)} e^{\pm i\left(\widetilde{\gamma}_I^{4}(\sigma) + \mu\omega_+^{\mathrm{b}}(I)\right)} \right) d\sigma \tag{73}$$

$$\mp i\mu \lim_{T\to-\infty} \int_0^T \left( \frac{\Delta H_{\mathrm{ell}}^{1,\pm} \circ \gamma_I^{\mathrm{b}}(\sigma)}{-1 + \mu\partial_G \Delta H_{\mathrm{circ}} \circ \gamma_I^{\mathrm{b}}(\sigma)} e^{\pm i\widetilde{\gamma}_I^{\mathrm{b}}(\sigma)} \right.$$

$$\left. - \frac{\Delta H_{\mathrm{ell}}^{1,\pm} \circ \gamma_I^{3}(\sigma)}{-1 + \mu\partial_G \Delta H_{\mathrm{circ}} \circ \gamma_I^{3}(\sigma)} e^{\pm i\left(\widetilde{\gamma}_I^{3}(\sigma) + \mu\omega_-^{\mathrm{b}}(I)\right)} \right) d\sigma,$$

(74)

$$B_{\mathrm{in}}^{\mathrm{f},\pm}(I) = \mp i\mu \int_0^{-12\pi} \frac{\Delta H_{\mathrm{ell}}^{1,\pm} \circ \gamma_I^{4}(\sigma)}{-1 + \mu\partial_G \Delta H_{\mathrm{circ}} \circ \gamma_I^{4}(\sigma)} e^{\pm i\widetilde{\gamma}_I^{4}(\sigma)} d\sigma \tag{75}$$

$$B_{\mathrm{in}}^{\mathrm{b},\pm}(I) = \mp \int_0^{-2\pi} \frac{\Delta H_{\mathrm{ell}}^{1,\pm} \circ \gamma_I^{3}(\sigma)}{-1 + \mu\partial_G \Delta H_{\mathrm{circ}} \circ \gamma_I^{3}(\sigma)} e^{\pm i\widetilde{\gamma}_I^{3}(\sigma)} d\sigma \tag{76}$$

*where*

$$\Delta H_{\mathrm{ell}}^{1,\pm}(\ell, L, g, G, t) = \Delta H_{\mathrm{ell}}^{1,\pm}(\ell, L, g, G)e^{it} + \Delta H_{\mathrm{ell}}^{1,\pm}(\ell, L, g, G)e^{-it}$$

*has been defined in Corollary 4.1 and* $\omega_\pm^*$ *have been defined in* (31)*.*

*Proof.* To prove the lemma recall that the outer maps are the composition of two maps. Indeed, as we have explained in Section 3.2, they are defined as

$$\mathcal{F}^{\mathrm{out,f}}_{e_0} = \mathcal{P}^6_{e_0} \circ \mathcal{S}^{\mathrm{f}}_{e_0} : \widetilde{\Lambda}^3_0 \longrightarrow \widetilde{\Lambda}^3_0$$
$$\mathcal{F}^{\mathrm{out,b}}_{e_0} = \mathcal{S}^{\mathrm{b}}_{e_0} \circ \mathcal{P}_{e_0} : \widetilde{\Lambda}^3_0 \longrightarrow \widetilde{\Lambda}^3_0.$$

Thus, we will study both maps perturbatively and then the composition of them will lead to the proof of the lemma. We only deal with $\mathcal{F}^{\mathrm{out,f}}_{e_0}$ since the proof for $\mathcal{F}^{\mathrm{out,b}}_{e_0}$ can be done analogously.

To study $\mathcal{S}^{\mathrm{f}}_{e_0} : \widetilde{\Lambda}^3_0 \longrightarrow \widetilde{\Lambda}^4_0$ we use the Definition 3.1 of the (heteroclinic) outer map. Let us consider points $z \in \widetilde{\Gamma}^*_{e_0}$, $x_+ \in \widetilde{\Lambda}^4_{e_0}$ and $x_- \in \widetilde{\Lambda}^3_{e_0}$ such that

$$\mathrm{dist}\left(\mathcal{P}^n_{e_0}(z), \mathcal{P}^n_{e_0}(x_\pm)\right) < C\lambda^{-|n|} \qquad \text{for } n \in \mathbb{Z}^\pm$$

for certain constants $C > 0$ and $\lambda > 1$. Using the parameterizations of $\widetilde{\Gamma}^{\mathrm{f}}_{e_0}$ and $\widetilde{\Lambda}^j_{e_0}$, $j = 3, 4$, given in Theorem 4, we can write the points $z$ and $x_\pm$ in coordinates as $z = \mathcal{C}_{e_0}(I_0, t_0)$, $x_+ = \mathcal{G}^4_{e_0}(I_+, t_+)$ and $x_- = \mathcal{G}^3_{e_0}(I_-, t_-)$. Then, the $I$-component of the outer map is just given by the relation

$$\mathcal{F}^{\mathrm{out},I}_{e_0}(I_-, t_-) = I_+ = I_- + (I_+ - I_-).$$

To measure $I_+ - I_-$ we first consider $I_0 - I_\pm$. Define the flow $\Phi_{e_0}$ associated to the reduced elliptic problem (37). Then, applying Fundamental Theorem of Calculus

$$I_0 - I_+ = \lim_{T\to-\infty} \int_T^0 \left( \frac{d}{ds}\Phi_{e_0}\left\{s, \mathcal{C}^{\mathrm{f}}_{e_0}(I_0, t_0)\right\} - \frac{d}{ds}\Phi_{e_0}\left\{s, \mathcal{G}^4_{e_0}(I_+, t_+)\right\}\right) ds$$
$$I_0 - I_- = \lim_{T\to+\infty} \int_T^0 \left( \frac{d}{ds}\Phi_{e_0}\left\{s, \mathcal{C}^{\mathrm{f}}_{e_0}(I_0, t_0)\right\} - \frac{d}{ds}\Phi_{e_0}\left\{s, \mathcal{G}^3_{e_0}(I_-, t_-)\right\}\right) ds$$

Note that the changed signs in the limits come from the fact that system (37) has the time reversed.

Using the perturbative expansions of $\mathcal{C}^{\mathrm{f}}_{e_0}$ and $\Lambda^j_{e_0}$ given in Theorem 4, equation (37), the perturbative expansion of the Hamiltonian (14) given in Corollary 4.1 and the perturbation of the flow $\Phi_{e_0}$ given in Lemma 4.2, one can see that

$$\begin{aligned} I_0 - I_+ = -e_0 \lim_{T\to-\infty} \int_T^0 \Bigg( & \left.\frac{\mu\partial_t \Delta H^1_{\mathrm{ell}}(L,\ell,G,g,t)}{-1+\mu\partial_G \Delta H_{\mathrm{circ}}(L,\ell,G,g)}\right|_{(L,\ell,G,g,t)=(\Phi_0^{\mathrm{circ}},\Phi_0^t)\left\{s,\mathcal{C}^{\mathrm{f}}_0(I_0,t_0)\right\}} \\ & - \left.\frac{\mu\partial_t \Delta H^1_{\mathrm{ell}}(L,\ell,G,g,t)}{-1+\mu\partial_G \Delta H_{\mathrm{circ}}(L,\ell,G,g)}\right|_{(L,\ell,G,g,t)=(\Phi_0^{\mathrm{circ}},\Phi_0^t)\left\{s,\mathcal{G}^4_0(I_+,t_+)\right\}} \Bigg) ds + \mathcal{O}\left(e_0^2\right) \\ I_0 - I_- = -e_0 \lim_{T\to+\infty} \int_T^0 \Bigg( & \left.\frac{\mu\partial_t \Delta H^1_{\mathrm{ell}}(L,\ell,G,g,t)}{-1+\mu\partial_G \Delta H_{\mathrm{circ}}(L,\ell,G,g)}\right|_{(L,\ell,G,g,t)=(\Phi_0^{\mathrm{circ}},\Phi_0^t)\left\{s,\mathcal{C}^{\mathrm{f}}_0(I_0,t_0)\right\}} \\ & - \left.\frac{\mu\partial_t \Delta H^1_{\mathrm{ell}}(L,\ell,G,g,t)}{-1+\mu\partial_G \Delta H_{\mathrm{circ}}(L,\ell,G,g)}\right|_{(L,\ell,G,g,t)=(\Phi_0^{\mathrm{circ}},\Phi_0^t)\left\{s,\mathcal{G}^3_0(I_-,t_-)\right\}} \Bigg) ds + \mathcal{O}\left(e_0^2\right). \end{aligned}$$

where $\Phi_0^{\mathrm{circ}}$ and $\Phi_0^t$ have been defined in (28) and (33) respectively.

Taking into account that in Corollary 4.1 we have proved that $\Delta H^1_{\mathrm{ell}}$ satisfies $\mathcal{N}\left(\Delta H^1_{\mathrm{ell}}\right) = \{\pm 1\}$, one can easily obtain the formula for $B^{\mathrm{f},\pm}_{\mathrm{out}}$ in (71).

To obtain the formula for $B^{\mathrm{f},\pm}_{\mathrm{in}}$ one can proceed as in the study of the inner map in Section 4.1. Finally, to obtain the formula for $B^{\mathrm{f},\pm}$ is is enough to compose both maps $\mathcal{P}^6_{e_0}$ and $\mathcal{S}^{\mathrm{f}}_{e_0}$. □

# 5 Existence of diffusing orbits

The main result of this section is the following.

**Theorem 6.** *For any $\delta > 0$ there exists $e_0^* > 0$ and $C > 0$ such that for any $0 < e_0 < e_0^*$ the map $\mathcal{P}_{e_0}$ in (38) has a collection of invariant 1-dimensional tori $\{\mathbb{T}_i\}_{i=1}^N \subset \tilde{\Lambda}^3_{e_0}$ such that*

- $\mathbb{T}_1 \cap \{I = I_- + \delta\} \neq \emptyset$ *and* $\mathbb{T}_N \cap \{I = I_+ - \delta\} \neq \emptyset$.
- *Hausdorff* $\operatorname{dist}(\mathbb{T}_i, \mathbb{T}_{i+1}) < Ce_0^{3/2}$
- *These tori form a transition chain. Namely, $W^u_{\mathbb{T}_i} \pitchfork W^s_{\mathbb{T}_{i+1}} \neq \emptyset$ for each $i = 1, \dots, N-1$.*

*Proof.* Once we have computed the first orders in $e_0$ of both the outer and inner maps, we want to understand their properties and compare their dynamics. To make this comparison we will perform two steps of averaging [**?**, **?**]. This change of coordinates will straighten the $I$-component of the inner map at order $\mathcal{O}(e_0^3)$ in such a way that with the new system of coordinates will be easier to compare the dynamics of both maps. Nevertheless, before performing averaging we have to perform a preliminary change of coordinates to straighten the symplectic form $\Omega^3_{e_0}$ to deal with the canonical form $dI \wedge dt$.

**Lemma 5.1.** *There exists a $e_0$-close to the identity change of variables*

$$(I, t) = (I', t') + e_0 \varphi_1 (I', t'), \tag{77}$$

*defined on $\widetilde{\Lambda}^3_{e_0}$, which transforms the symplectic form $\Omega^3_{e_0}$ defined in (41) into the canonical form*

$$\Omega_0 = dI' \wedge dt'.$$

*In the new coordinates,*

- *The inner map $\mathcal{F}^{\text{in}}_{e_0}$ in (42) reads*

$$\mathcal{F}^{\text{in}'}_{e_0} : \begin{pmatrix} I' \\ t' \end{pmatrix} \mapsto \begin{pmatrix} I' + e_0 A_1 (I', t') + e_0^2 A_2' (I', t') + \mathcal{O}\left(\mu e_0^3\right) \\ t' + \mu \mathcal{T}_0 (I') + e_0 \mathcal{T}_1' (I', t') + e_0^2 \mathcal{T}_2' (I', t') + \mathcal{O}\left(\mu e_0^3\right) \end{pmatrix} \tag{78}$$

  *where $A_1$ is the function given in Lemma 4.3 and $A_2'$, $\mathcal{T}_1'$ and $\mathcal{T}_2'$ satisfy*

$$\mathcal{N}(A_2') = \{0, \pm 1, \pm 2\}, \ \mathcal{N}(\mathcal{T}_1') = \{\pm 1\} \ \text{ and } \ \mathcal{N}(\mathcal{T}_2') = \{0, \pm 1, \pm 2\}.$$

- *The outer maps $\mathcal{F}^{\text{out,f}}_{e_0}$ and $\mathcal{F}^{\text{out,b}}_{e_0}$ in (45) read*

$$\mathcal{F}^{\text{out},*'}_{e_0} : \begin{pmatrix} I' \\ t' \end{pmatrix} \mapsto \begin{pmatrix} I' + e_0 B^* (I', t') + \mathcal{O}\left(\mu e_0^2\right) \\ \tau + \mu \omega^*(I') + \mathcal{O}(\mu e_0) \end{pmatrix}, \ * = \text{f}, \text{b}, \tag{79}$$

  *where $B^*$ are the functions given in Lemma 4.4.*

*Proof.* We will see that there exists a change of coordinates of the form

$$\begin{cases} I = I' + e_0^2 f_2 (I', t') + \mathcal{O}\left(e_0^3\right) \\ t = t' + e_0 g_1 (I', t') + e_0^2 g_2 (I', t') + \mathcal{O}\left(e_0^3\right) \end{cases} \tag{80}$$

with

$$\mathcal{N}(g_1) = \{\pm 1\}, \ \mathcal{N}(g_2) = \{0, \pm 1, \pm 2\} \ \text{ and } \ \mathcal{N}(f_2) = \{0, \pm 1, \pm 2\}, \tag{81}$$

which straightens the symplectic form $\Omega^3_{e_0}$. In fact, we look for the inverse change. Namely, we look for a change of variables of the form

$$\begin{cases} I' = I + e_0^2 \widetilde{f}_2 (I, t) + e_0^3 \widetilde{f}_{\geq}(I, t) \\ t' = t + e_0 \widetilde{g}_1 (I, t) \end{cases} \tag{82}$$

such that the pullback of $\Omega_0 = dI' \wedge dt'$ with respect to this change is the symplectic form $\Omega^3_{e_0}$. Even if we do not write it explicitly, $\widetilde{f}_{\geq}$ depends on $e_0$. To obtain this change, it is enough to solve the equations

$$\begin{aligned}\partial_t \widetilde{g}_1 &= a_1^3\\ \partial_I \widetilde{f}_2 &= a_2^3\\ \partial_I \widetilde{f}_{\geq} &= b\end{aligned}$$

where

$$b = a^3_{\geq} - \partial_t \widetilde{g}_1 \partial_I \widetilde{f}_2 - e_0 \partial_t \widetilde{g}_1 \partial_I \widetilde{f}_{\geq} + \partial_I \widetilde{g}_1 \partial_t \widetilde{f}_2 + e_0 \partial_I \widetilde{g}_I \partial_t \widetilde{f}_{\geq}$$

and $a_1^3$, $a_2^3$ and $a^3_{\geq}$ are the functions considered in (41). These equations can be solved iteratively.

Recall that by Corollary 4.2 we have that $\mathcal{N}(a_1^3) = \{\pm 1\}$. Then, one can take $\widetilde{g}_1$ as the primitive of $a_1^3$ with zero average, which satisfies

$$\mathcal{N}\left(\widetilde{g}_1\right) = \{\pm 1\}. \tag{83}$$

The other equations can be solved taking

$$\begin{aligned}\widetilde{f}_2(I,t) &= \int_0^I a_2^3(J,t)dJ\\ \widetilde{f}_{\geq}(I,t) &= \int_0^I b(J,t)dJ.\end{aligned}$$

Note that $b$ depends on $\widetilde{g}_1$ and $\widetilde{f}_2$, which have been already obtained. Since by Corollary 4.2 we have that $\mathcal{N}(a_2^3) = \{0, \pm 1, \pm 2\}$, one can deduce that

$$\mathcal{N}\left(\widetilde{f}_2\right) = \{0, \pm 1, \pm 2\}. \tag{84}$$

To obtain the change (80) it is enough to invert the change (82). Then, formulas (83) and (84) imply (81).

To finish the proof it only remains to check the properties of the inner and outer maps in the new coordinates. To this end one only needs to take into account (81). □

Once we have straightened the symplectic form, we can perform two steps of averaging to the inner map.

**Lemma 5.2.** *There exists a $e_0$-close to the identity symplectic change of variables*

$$(I', t') = (\mathcal{I}, \tau) + e_0 \varphi_2(\mathcal{I}, \tau) \tag{85}$$

*defined on $\widetilde{\Lambda}^3_{e_0}$, which:*

- *Transforms the inner map $\mathcal{F}^{\mathrm{in}'}_{e_0}$ in (78) into*

$$\widetilde{\mathcal{F}}^{\mathrm{in}}_{e_0} : \begin{pmatrix} \mathcal{I} \\ \tau \end{pmatrix} \mapsto \begin{pmatrix} \mathcal{I} + \mathcal{O}\left(\mu e_0^3\right) \\ \tau + \mu \mathcal{T}_0\left(\mathcal{I}\right) + e_0^2 \widetilde{\mathcal{T}}_2\left(\mathcal{I}\right) + \mathcal{O}\left(\mu e_0^3\right) \end{pmatrix} \tag{86}$$

- *Transforms the outer maps $\mathcal{F}^{\mathrm{out,f}'}_{e_0}$ and $\mathcal{F}^{\mathrm{out,b}'}_{e_0}$ in (79) into*

$$\widetilde{\mathcal{F}}^{\mathrm{out},*}_{e_0} : \begin{pmatrix} \mathcal{I} \\ \tau \end{pmatrix} \mapsto \begin{pmatrix} \mathcal{I} + e_0 \widetilde{B}^*(\mathcal{I}, \tau) + \mathcal{O}\left(\mu e_0^2\right) \\ \tau + \mu \omega^*(\mathcal{I}) + \mathcal{O}(\mu e_0) \end{pmatrix}, \quad * = \mathrm{f}, \mathrm{b}, \tag{87}$$

*where*

$$\widetilde{B}^*\left(\mathcal{I}, \tau\right) = \widetilde{B}^{*,+}\left(\mathcal{I}\right) e^{i\tau} + \widetilde{B}^{*,-}\left(\mathcal{I}\right) e^{-i\tau}$$

*with*

$$\widetilde{B}^{*,\pm}(\mathcal{I}) = B^{*,\pm}(\mathcal{I}) - \frac{e^{\pm i\mu\omega^*(\mathcal{I})}-1}{e^{\pm i\mu\mathcal{T}_0(\mathcal{I})}-1}A_1^{\pm}(\mathcal{I}).$$

*Moreover, these functions satisfy*

$$\widetilde{B}^{*,\pm}(\mathcal{I}) \neq 0 \qquad \text{for } \mathcal{I} \in \mathcal{D}^*, \tag{88}$$

*where $\mathcal{D}^*$ are the domains considered in Corollary 3.2.*

Note that we can do two steps of averaging globally in the whole cylinder $\widetilde{\Lambda}_{e_0}$ due to the absence of resonances in the first orders in $e_0$. Namely, there are no *big gaps*. This is quite in contrast with the typical situation in Arnold diffusion (see e.g. [**?**]).

*Proof.* We perform two steps of (symplectic) averaging. To this end we consider a generating function of the form

$$\mathcal{S}(\mathcal{I}, t') = \mathcal{I}t + e_0\mathcal{S}_1(\mathcal{I}, t') + e_0^2\mathcal{S}_2(\mathcal{I}, t'),$$

which defines the change (85) implicitly as

$$\begin{aligned} I &= \mathcal{I} + e_0\partial_{t'}\mathcal{S}_1(\mathcal{I}, t') + e_0^2\partial_t\mathcal{S}_2(\mathcal{I}, t') \\ \tau &= t' + e_0\partial_{\mathcal{I}}\mathcal{S}_1(\mathcal{I}, t') + e_0^2\partial_{\mathcal{I}}\mathcal{S}_2(\mathcal{I}, t'). \end{aligned}$$

By Theorem 3.1 we have (24) and by Theorem 5 we know which $t$-harmonics have the functions $A_i$ and $\mathcal{T}_i$. Then, it is easy to see that the functions $\mathcal{S}_i$ that correspond to two steps of averaging are globally defined in $\widetilde{\Lambda}^3_{e_0}$. Moreover, in these new variables, taking into account that the inner map is exact symplectic, one can see that the inner map is of the form (86).

To obtain a perturbative expression for the outer maps $\widetilde{\mathcal{F}}^{\mathrm{out},*}_{e_0}$, we need to know $\mathcal{S}_1$ explicitly. It is given by

$$\mathcal{S}_1(\mathcal{I}, t) = -\frac{iA_1^+(\mathcal{I})}{e^{i\mu\mathcal{T}_0(\mathcal{I})}-1}e^{it} + \frac{iA_1^-(\mathcal{I})}{e^{-i\mu\mathcal{T}_0(\mathcal{I})}-1}e^{-it}.$$

If we apply this change to the outer maps $\mathcal{F}^{\mathrm{out},*}_{e_0}$ in (69), we obtain (87).

The statement (88) is based on convincing numerical data (see Appendix ??). □

In the new coordinates $(\mathcal{I}, \tau)$ the inner map $\widetilde{\mathcal{F}}^{\mathrm{in}}_{e_0}$ in (86) is a $e_0^3$-close to integrable map. Moreover, thanks to Theorem 3.1 is twist and therefore we can apply KAM theory to proof the existence of invariant curves in $\widetilde{\Lambda}^3_{e_0}$. We use a version of the KAM Theorem from [**?**] (see also [**?**]).

**KAM theorem.** *Let $f : [0,1]\times\mathbb{T} \to [0,1]\times\mathbb{T}$ be an exact symplectic $\mathcal{C}^l$ map with $l > 4$. Assume that $f = f_0 + \delta f_1$, where $f_0(I,\psi) = (I, \psi + A(I))$, $A$ is $\mathcal{C}^l$, $|\partial_I A| > M$ and $\|f_1\|_{\mathcal{C}^l} \leq 1$. Then, if $\delta^{1/2}M^{-1} = \rho$ is sufficiently small, for a set of $\omega$ of Diophantine numbers of exponent $\theta = 5/4$, we can find invariant tori which are the graph of $\mathcal{C}^{l-3}$ functions $u_\omega$, the motion on them is $\mathcal{C}^{l-3}$ conjugate to the rotation by $\omega$, and $\|u_\omega\|_{\mathcal{C}^{l-3}} \leq C\delta^{1/2}$.*

Applying this theorem to the map $\widetilde{\mathcal{F}}^{\mathrm{in}}_{e_0}$ we obtain the KAM tori. Moreover, this theorem ensures that the distance between these tori is no bigger than $e_0^{3/2}$. Then, the results of Lemma 5.2 and KAM theorem lead to the existence of a transition chain of invariant tori.

The transition chain is obtained comparing the outer and inner dynamics. We do this comparison in the coordinates $(\mathcal{I}, \tau)$ given by Lemma 5.2 and therefore we deal with the maps $\widetilde{\mathcal{F}}^{\mathrm{in}}_{e_0}$ and $\widetilde{\mathcal{F}}^{\mathrm{out},*}_{e_0}$ in (86) and (87) respectively.

KAM theorem ensures that there exists a torus $\mathbb{T}_1$ such that $\mathbb{T}_1 \cap \{I = I_- - \delta\} \neq \emptyset$. Then, either $\widetilde{\mathcal{F}}^{\mathrm{out,f}}_{e_0}$ or $\widetilde{\mathcal{F}}^{\mathrm{out,b}}_{e_0}$ are defined for points in $\mathbb{T}_1$. Assume, without loss of generality that $\widetilde{\mathcal{F}}^{\mathrm{out,f}}_{e_0}$ is defined for points in $\mathbb{T}_1$. Then, thanks to (88), $\mathcal{F}^{\mathrm{out,f}}_{e_0}(\mathbb{T}_1)$ satisfies

$$\operatorname{dist}\left(\mathbb{T}_1, \mathcal{F}^{\mathrm{out,f}}_{e_0}(\mathbb{T}_1)\right) \geq Ce_0$$

for a constant $C > 0$ independent of $e_0$. Then, KAM theorem ensures that there exists a torus $\mathbb{T}_2$ such that $\mathbb{T}_2 \cap \mathcal{F}_{e_0}^{\text{out,f}}(\mathbb{T}_1) \neq 0$. Iterating this procedure, choosing at each step either $\widetilde{\mathcal{F}}_{e_0}^{\text{out,f}}$ or $\widetilde{\mathcal{F}}_{e_0}^{\text{out,b}}$, one obtains the transition chain. □

To finish the proof of Theorem 2 it only remains to prove the existence of a diffusing orbit using a shadowing method. We use a result stated in [**?**].

**Lemma 5.3.** *Let $f$ be a $\mathcal{C}^1$ sympletic map in a $2(d+1)$ symplectic manifold. Assume that the map leaves invariant a $\mathcal{C}^1$ $d$-dimensional torus $\tau$ and the motion on the torus is an irrational rotation. Let $\Gamma$ be a $d+1$ manifold intersecting $W_\tau^u$ transversally. Then,*

$$W_\tau^s \subset \overline{\bigcup_{i>0} f^{-i}(\Gamma)}.$$

An immediate consequence of this lemma is that any finite transtion chain can be shadowed by a true orbit, which finishes the proof of Theorem 2.

# A From cartesian to Delaunay and computation of $\partial_G \Delta H_{\rm circ}$

In this appendix we explain an easy way to obtain the rotating Delaunay coordinates from rotating cartesian (or polar) coordinates in the circular problem. First recall that $G$ can be computed as

$$G = r\left(-p_x \sin\phi + p_y \cos\phi\right).$$

In a fixed level of energy $J$, knowing $G$ one can obtain $L$. Recall that

$$J = -\frac{1}{2L^2} - G + \mu \Delta H_{\rm circ}$$

The term $\mu\Delta H_{\rm circ}$ in cartesian only depends on $x$ and $y$, and can be easily computed. Then, one can use this equation to obtain $L$. Knowing $L$ and $G$ we can obtain the eccentricity $e$ by

$$e = \sqrt{1 - \frac{G^2}{L^2}}.$$

Using that $r = L^2(1 - e\cos u)$, one can obtain $u$ and from here $\ell$ using the formula $u - e\sin u = \ell$. On the other hand, from $u$ we can obtain $v$ using

$$\tan\frac{v}{2} = \sqrt{\frac{1+e}{1-e}}\tan\frac{u}{2}.$$

Finally, we can deduce $g$ using that $\phi = v + g$.

We devote the rest of the section to compute $\partial_G \Delta H_{\rm circ}$. Let us define

$$N(r, v, g) = \frac{1}{\left(r^2 + 1 - 2r\cos(v+g)\right)^{1/2}}.$$

Then,

$$\Delta H_{\rm circ}(L,\ell,G,g) = -\frac{1-\mu}{\mu} N\left(-\frac{r(L,\ell,G)}{\mu}, v(L,\ell,G), g\right) - \frac{\mu}{1-\mu} N\left(\frac{r(L,\ell,G)}{1-\mu}, v(L,\ell,G), g\right) + \frac{1}{r(L,\ell,G)}.$$

Therefore

$$\begin{aligned}
\partial_G \Delta H_{\rm circ}(L,\ell,G,g) = &- \left[ -\frac{1-\mu}{\mu^2}\partial_r N\left(-\frac{r(L,\ell,G)}{\mu}, v(L,\ell,G), g\right)\right.\\
&\left. + \frac{\mu}{(1-\mu)^2}\partial_r N\left(\frac{r(L,\ell,G)}{1-\mu}, v(L,\ell,G), g\right)\right]\partial_G r(L,\ell,G)\\
&- \left[\frac{1-\mu}{\mu}\partial_v N\left(-\frac{r(L,\ell,G)}{\mu}, v(L,\ell,G), g\right)\right.\\
&\left. + \frac{\mu}{1-\mu}\partial_v N\left(\frac{r(L,\ell,G)}{1-\mu}, v(L,\ell,G), g\right)\right]\partial_G v(L,\ell,G)\\
&- \frac{1}{r^2}\partial_G r(L,\ell,G).
\end{aligned}$$

In only remains to compute $\partial_G r$ and $\partial_G v$. First, let us point out that

$$\partial_G e = -\frac{G}{eL^2} = \frac{e^2-1}{eG}.$$

On the other hand, using that $\ell = u - e\sin u$, one has that

$$\partial_e u = \frac{\sin u}{1 - e\cos u}.$$

Then, since $r(L,e,\ell) = L^2(1 - e\cos u(e,\ell))$, using that

$$\cos v = \frac{\cos u - e}{1 - e\cos u}, \tag{89}$$

we have that

$$\partial_e r(L,e,\ell) = L^2 \cos v$$

and therefore,

$$\partial_G r(L,\ell,G) = -\frac{G\cos v}{e}.$$

To compute $\partial_G v$ let us point out that $\partial_G v = \partial_e v \partial_G e$. Therefore it only remains to compute $\partial_e v$, we obtain it using formula (89) and

$$\sin v = \frac{\sqrt{1-e^2}\sin u}{1 - e\cos u}.$$

Then,

$$\partial_e v = \frac{\sin v}{1-e^2}\left(2 + e\cos v\right).$$

and therefore,

$$\partial_G v = -\frac{\sin v}{eG}\left(2 + e\cos v\right).$$

# B Numerical study of the normally hyperbolic invariant manifold of the circular problem.

We devote this appendix to the numerical study of the hyperbolic invariant manifold of the circular problem given in Corollary 3.1 and its invariant manifolds. In other words, we show numerical results which justify the properties of the circular problem stated in Theorem 3.

It is well known that in numerical analysis there are several sources of error, such as round-off errors in computer arithmetic, and approximations of ideal mathematical objects (e.g. linear approximation of local stable/unstable manifolds). In our analysis, we will try to evaluate such errors whenever possible, and check that they are appropriately small. We do *not* claim however to give a fully rigorous proof of Theorem 3, which would probably require Computer-Assisted techniques as in [Zgliczynski-Capinski],[...].

Let us make a few comments on the general strategy of our numerical analysis. As mentioned in Section 3, the circular problem has a conserved quantity which corresponds to energy $H$ when the system is expressed in rotating coordinates. Thus it is natural to fix the energy $H = h$ and perform our analysis for a given energy $h$. This allows us to reduce the dimension of the computations by one. Finally, we let $H$ vary and repeat the computations for all $H$ in the range of interest $H \in [H_-, H_+]$.

Another important comment is on the choice of coordinates. For numerics we prefer Cartesian coordinates, since the equations of motion are explicit in these coordinates. Thus we carry out our computations of the hyperbolic structure of the circular problem in Cartesian (section B).

On the other hand, for perturbative analysis we have used Delaunay coordinates throughout this paper. Thus, in section C we explain how to change coordinates from Cartesian to Delaunay, and we carry out our computations of the inner and outer maps of the circular and elliptic problems in Delaunay (section D).

Regarding the integration method, we use a variable-order Taylor method specially generated to integrate the equations of motion and variational equations of the circular problem. The Taylor method has been generated using the "taylor" package of À. Jorba and M. Zou (see `http://www.maia.ub.es/~angel/taylor/`). The main advantage of using a Taylor method is that it is very fast for long-time integrations (without sacrificing accuracy).

## B.1 Computation of the periodic orbits

Consider the circular problem in rotating cartesian coordinates

$$H(x, y, p_x, p_y) = \frac{1}{2}(p_x^2 + p_y^2) + yp_x - xp_y - \frac{1-\mu}{r_1} - \frac{\mu}{r_2}, \tag{90}$$

where

$$r_1^2 = (x - \mu_2)^2 + y^2,$$
$$r_2^2 = (x + \mu_1)^2 + y^2.$$

We follow the convention to place the large mass (Sun) to the left of the origin, and the small mass (Jupiter) to the right. (This is opposite to the astrodynamics convention). Thus we choose $\mu_1 = \mu$ as the small mass, and $\mu_2 = 1 - \mu$ as the large mass. Notice that equation (90) is reversible with respect to the involution

$$R(x, p_x, y, p_y) = (x, -p_x, -y, p_y). \tag{91}$$

Thus, a solution of the system is symmetric if and only if it intersects the symmetry axis $\mathrm{Fix}(R) = \{y = 0,\ p_x = 0\}$. This symmetry will facilitate our numerical computations. Note that the involution $R$ is just the involution (18) expressed in rotating cartesian coordinates.

Let the energy be fixed to $H = h$. We look for a resonant periodic orbit $\gamma_h$ of (90) in the level of energy $h$. As a first approximation to $\gamma_h$, we look for a resonant periodic orbit of the two-body problem, i.e. of the Hamiltonian (17) with $\mu = 0$. Let us denote the approximate periodic orbit by $\tilde{\gamma}_h = (L, \ell, G, g)$. The actions $L$ and $G$ are determined by the resonant condition $L^3 = 7$ and energy condition $-\frac{1}{2L^2} - G = h$. To determine $\tilde{\gamma}_h$ completely, we choose that the Asteroid is initially at the perihelion, i.e. we impose an initial condition $\tilde{\gamma}_h(t = 0) = (L^0, \ell^0, G^0, g^0)$ with mean anomaly $\ell^0 = 0$ and argument of perihelion $g^0 = 0$. Switching to cartesian coordinates, we obtain an initial condition $(x^0, p_x^0, y^0, p_y^0)$ with $p_x^0 = 0$ and $y^0 = 0$.

Next we refine the trajectory $\tilde{\gamma}_h$ into a true periodic orbit $\gamma_h$ for the system (90) with $\mu = \mu_J$. Consider the Poincaré section

$$\Sigma^+ = \{y = 0,\ p_y > 0\}$$

in the circular problem (90), and let $P\colon\ \Sigma^+ \to \Sigma^+$ be the associated Poincaré map. Since we are in rotating coordinates, this section corresponds to collinear configurations of the three bodies.

**Remark B.1.** *In numerical integrations, we use a variable-order Taylor method with local error tolerance $10^{-16}$. Moreover, a point is considered to be on the Poincaré section whenever $|y| < 10^{-16}$ and $p_y > 0$.*

Furthermore, the momentum variable $p_y$ can be eliminated. Assuming that $\partial_{p_y} H \neq 0$, it can be recovered from the other variables using the energy condition $H(x, p_x, y, p_y) = h$. Hence, the Poincaré map is a two-dimensional symplectic map at each energy level, acting only on $(x, p_x)$.

Notice that, in the rotating frame, a 7:1 resonant periodic orbit makes 6 turns around the origin. See Figure 4. In principle, we could look for the periodic orbit as a periodic point $p = (x, p_x)$ of the Poincaré map: $p = P^6(p)$. This would imply solving a system of two equations. Thanks to the reversibility (91), in fact it is only necessary to solve one equation. Notice that our initial condition $(x, p_x)$ is at the symmetry section $\{y = 0,\ p_x = 0\}$, so the periodic orbit must be symmetric. Thus it is enough to impose the condition that the trajectory $\gamma_h(t)$ after *half* the period is again at the symmetry section. Hence we set up the problem as simple one-dimensional root finding: we look for a point $p = (x, 0)$, such that its third iterate $P^3(p)$ has momentum $p_x = 0$:

$$\pi_{p_x}(P^3(p)) = 0.$$

(Here, $\pi_{p_x}\colon \mathbb{R}^2 \to \mathbb{R}$ is the projection onto the $p_x$ component).

In order to solve this problem, we use a a Newton-like method. Specifically, we use a modified version of Powell's Hybrid method (see the GSL manual for details) without scaling. In our computations, the Newton method converges in less than 5 iterations. As a test of the software, we have checked that the rate of convergence of the Newton method is quadratic.

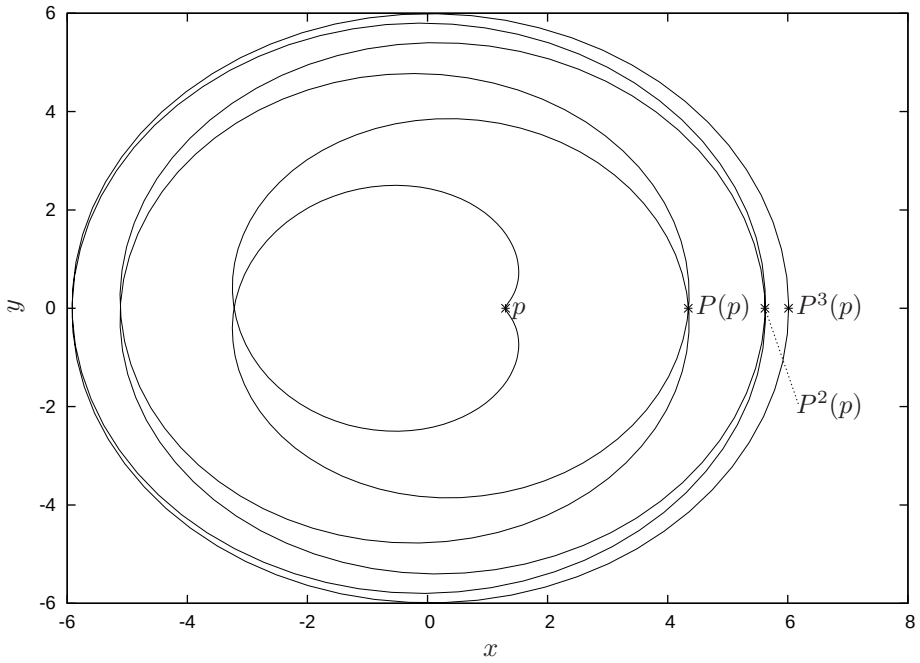


Figure 4: Resonant periodic orbit $\gamma_{-1.6}$ of the circular problem in rotating cartesian coordinates.

**Remark B.2.** *We ask for an accuracy of* $10^{-14}$ *in the Newton method, i.e. a point* $p = (x, 0)$ *is accepted as a root if and only if its third iterate* $P^3(p)$ *has momentum* $|p_x| < 10^{-14}$.

For the Newton method, we need to compute the derivative of the Poincaré map. For each $\xi \in \mathbb{R}^4$, let $u(t, \xi)$ be the solution of the system with initial condition $u(0, \xi) = \xi$. Let $T : \Sigma^+ \to \mathbb{R}$ be the Poincaré return time. The derivative of the Poincaré map at a point $p \in \mathbb{R}^4$ is given by the partial derivative $DP(p) = u_\xi(T(p), p)$. It is well-known that $u_\xi(t, p)$ is the matrix solution of the variational equation

$$\dot{W} = Df(u(t, p))W,$$

where $f$ is the vectorfield of the circular problem. We compute $DP(p)$ by numerically integrating the variational equation using the Taylor method mentioned above.

For illustration, let us show some numerical results corresponding to the energy value $H = -1.6$. The first approximation $\tilde{\gamma}_{-1.6}$ from the two-body problem has initial condition $p^0 = (x^0, p_x^0) = (1.30253\cdots, 0)$. After refining this initial condition via the Newton method, we obtain a resonant periodic orbit $\gamma_{-1.6}$ of the circular problem passing through the point $p = (x, p_x) = (1.29858\cdots, 0)$, with period $T_{-1.6} = 44.01796\cdots \sim 14\pi$. See Figure 4. The periodic orbit $\gamma_{-1.6}$ is symmetric, with the points $p$ and $P^3(p)$ located at the symmetry section (they have $y = 0$ and $p_x = 0$). Notice that, in rotating coordinates, the trajectory of the Asteroid makes 6 turns around the origin before closing up at the point $p$.

Finally, we let $H$ change and, using this procedure, we are able to obtain the resonant periodic orbit for energy levels

$$H \in [\bar{H}_-, \bar{H}_+] = [-2.04, -1.56].$$

See Figure 5. This family of resonant periodic orbits constitutes the normally hyperbolic invariant manifold $\Lambda_0$ given in Corollary 3.1. Notice that the period $T_H$ stays close to the resonant period $14\pi$ of the unperturbed system. From Figure 5, we obtain the bound

$$|T_H - 14\pi| < 60\mu,$$

which is the first bound given in Theorem 3.

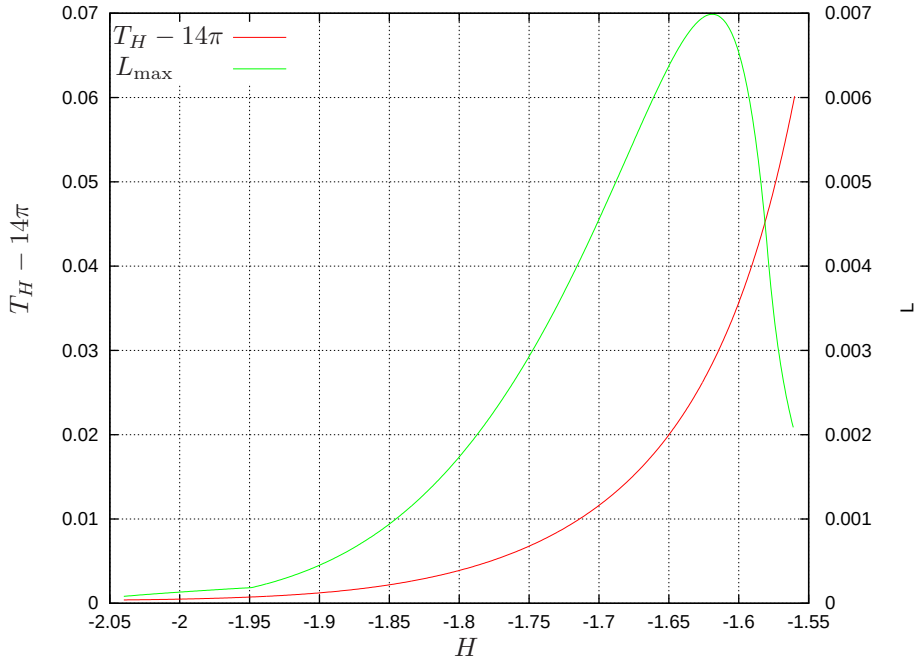


Figure 5: Resonant family of periodic orbits. We show normalized period $T_H - 14\pi$, and maximum deviation of $L$ component with respect to the resonant value $7^{1/3}$ (see equation (92)).

To determine the stability of the periodic orbit $\gamma_h$, we compute the eigenvalues $\lambda$ and $\lambda^{-1}$ of the matrix $DP^6(p)$, where $DP^6(p)$ is the linearization of the iterated Poincaré map $P^6$ about the fixed point $p$. (Since $DP^6(p)$ is a $2 \times 2$ matrix, the eigenvalues are trivial to compute.)

Figure 6 shows the characteristic exponents $\ln(\lambda)$, $\ln(\lambda^{-1})$ as a function of energy. The family of periodic orbits is strongly hyperbolic as $H \to \bar{H}_+$, and weakly hyperbolic as $H \to \bar{H}_-$. Note that one would expect that we are in a nearly integrable regime since $\mu$ is small. Then one would expect the eigenvalues to be close to 1. Nevertheless, in this problem the non-integrability is very noticeable when one increases $\mu$ to $\mu = \mu_J = 10^{-3}$. This is due to the effect of the perturbing body (Jupiter) on the Asteroid, as the Asteroid passes close to it.

Furthermore, we verify that the (square of the) semi-major axis $L$ stays close to the resonant value $7^{1/3}$. Integrating the periodic orbit in Delaunay coordinates $\gamma_H(t) = (L(t), \ell(t), G(t), g(t))$ over one period $T_H$, we compute the quantity

$$L_{\max}(H) = \max_{t \in [0, T_H)} |L_H(t) - 7^{1/3}|. \tag{92}$$

The function $L_{\max}(H)$ is plotted in figure 5. Notice that we obtain the bound

$$|L_H(t) - 7^{1/3}| < 7\mu$$

for all $t \in \mathbb{R}$, which is stated in Theorem 3.

Let us briefly describe the family of periodic orbits $\gamma_H$. For illustration, see Figure 7.

XXXXX PR: We should try to explain the family in terms of bifurcations of periodic orbits. XXXXX

At one endpoint of the family, as $H \to \bar{H}_-$, the periodic orbit $\gamma_H$ tends to a circular orbit of period $14\pi$ centered at the origin and passing far away from the primaries (Sun and Jupiter). Moreover, $\gamma_H$ looses hyperbolicity when $H \to \bar{H}_-$. For instance, the periodic orbit $\tilde{\gamma}(\bar{H}_-)$ of the two-body problem approximation has eccentricity $e(\bar{H}_-) = 0.09989\cdots$.

At the other endpoint of the family, as $H \to \bar{H}_+$, the periodic orbit $\gamma_H$ tends to a homoclinic loop of the Lagrangian equilibrium point $L_2$ that makes 6 turns around the Sun-Jupiter system. (In rotating cartesian coordinates, $L_2$ is located on the $x$ axis at the point $x_2 \simeq 1.068$). This explains the fact that

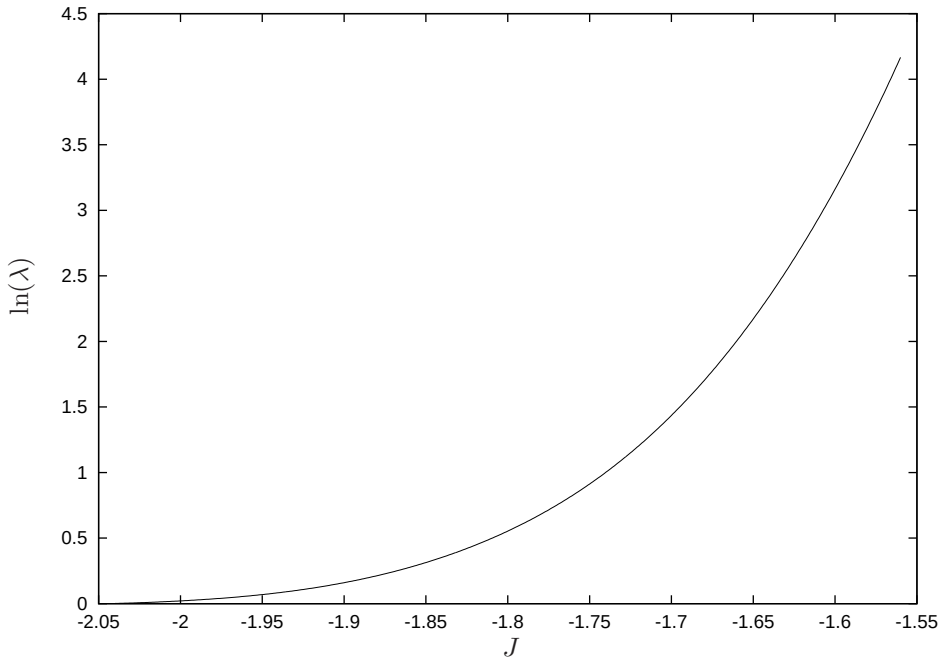


Figure 6: Characteristic exponent $\ln(\lambda)$ as a function of energy level $J$ (the other exponent is $-\ln(\lambda)$).

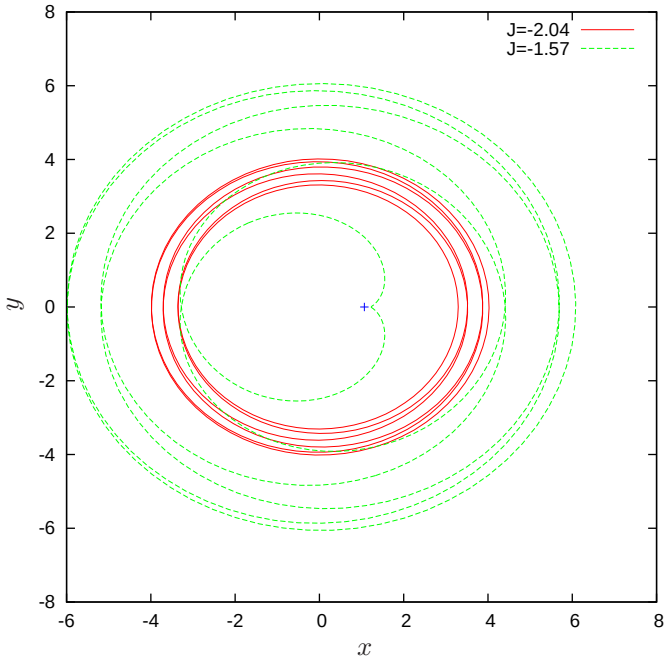


Figure 7: Extremal periodic orbits of the family: circular periodic orbit with $H = \bar{H}_-$ (in red), elliptical periodic orbit with $H = \bar{H}_+$ (in green). The Lagrange equilibrium point $L_2$ is marked with a '+' symbol.

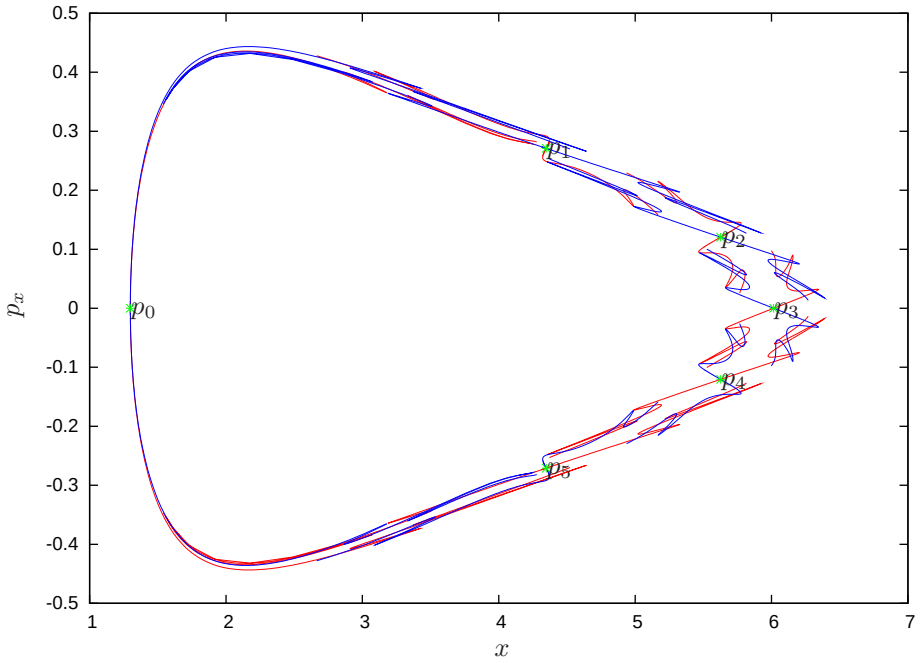


Figure 8: Invariant manifolds of the fixed points $p_0, p_1, \ldots, p_5$ on the section $\Sigma^+$. Unstable manifolds are plotted in red, stable in blue. The fixed points are marked in green.

the period $T_H$ "explodes" as $H \to \bar{H}_+$. Since we are interested in working close to the resonance, we avoid energies $H > \bar{H}_+$ where the period explodes.

## B.2 Computation of invariant manifolds

In this section, we compute the stable and unstable invariant manifolds associated to the periodic orbits found in the previous section.

Consider first a fixed energy level $H = h$. Let $\gamma_h$ be the resonant periodic orbit of the circular problem found in the previous section. To compute the invariant manifolds of the periodic orbit, we continue using the iterated Poincaré map. Thus we look for (one dimensional) invariant manifolds of a hyperbolic fixed point at each energy level. Let $p \in \gamma_h$ be a hyperbolic fixed point of the iterated Poincaré map $\mathcal{P} = P^6$. Let $\lambda$, $\lambda^{-1}$ be the eigenvalues of $D\mathcal{P}(z)$ with $\lambda > 1$, and $v_u, v_s$ be the associated eigenvectors.

Assume that we want to compute the unstable manifold $W^u(p)$. Let $\eta$ be a small displacement in the unstable direction $v_u$. We approximate a piece of the local manifold by the linear segment between the points $p + \eta v_u$ and $\mathcal{P}(p + \eta v_u)$. We call this segment a *fundamental domain*. We discretize the fundamental domain into an array of points, and iterate them by $\mathcal{P}$ to globalize the manifold. (The stable manifold is computed analogously using the inverse map $\mathcal{P}^{-1}$.)

The error commited in the local approximation $\mathcal{P}(p + \eta v_u) = p + \lambda \eta v_u + \mathcal{O}(\eta^2)$ of the manifold is given by

$$\mathrm{err}(\eta) = \|\mathcal{P}(p + \eta v_u) - p - \lambda \eta v_u\| \in \mathcal{O}(\eta^2).$$

**Remark B.3.** *For each energy level $H$, we choose a displacement $\eta = \eta(H)$ such that the local error is* $\mathrm{err}(\eta) < 10^{-12}$.

One can think of $p$ as a fixed point of the iterated Poincaré map $\mathcal{P} = P^6$, or as a 6-periodic point of the Poincaré map $P$. If $p_i = P^i(p)$ are the iterates of $p$ for $i = 0, \ldots, 5$, then $p_i$ are also fixed points of $\mathcal{P}$. They have associated unstable and stable manifolds, which can be obtained from $W^{u,s}(p)$ by iteration.

For illustration, let us show some numerical results corresponding to the energy value $H = -1.6$. Figure 8 shows the manifolds of all iterates $\{p_i\}_{i=0,\ldots,5}$. Notice that the dynamics in Figure 8 is reversible

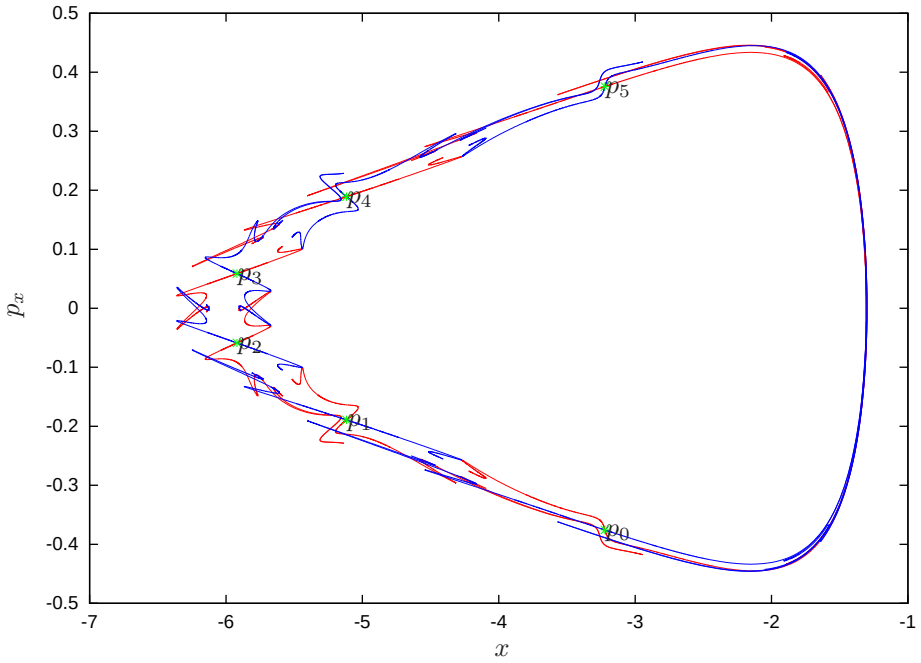


Figure 9: Invariant manifolds on the section $\Sigma^-$.

with respect to the symmetry section $\{y = 0,\ p_x = 0\}$, as discussed in the previous section (equation (91)). Figure 8 shows that the manifolds do intersect transversally at different homoclinic points. We are interested in measuring the splitting angle between the manifolds. Unfortunately, the homoclinic points do not lie on the symmetry axis, which would be very useful in order to compute them.

In order to have the homoclinic points lie on the symmetry axis, we recompute the manifolds on the new Poincaré section

$$\Sigma^- = \{y = 0,\ p_y < 0\}.$$

Numerically, we just transport points on the unstable manifold from section $\Sigma^+$ to section $\Sigma^-$ by the forward flow, and points in the stable manifold by the backward flow. See Figures 9 and 10. Now the points that lie on the symmetry line $p_x = 0$ are homoclinic points.

## B.3 Computation of transversal homoclinic points and splitting angle

In this section, we compute the angle between the invariant manifolds at one of the transversal intersections. We will restrict the range of energy values to

$$H \in [H_-, H_+] = [-1.81, -1.56],$$

or equivalently the range of eccentricities to $e \in [e_-, e_+] = [0.48, 0.66]$. This is the range where we can validate the accuracy of our computations (see section B.4). Below $e_- = 0.48$, the splitting size becomes comparable to the numerical error that we commit in double precision arithmetic.

**Remark B.4.** *In this paper we concentrate on proving the existence of global instabilities in the Restricted three-body problem; we are not so much concerned with finding the* maximal *range of eccentricities along which the Asteroid drifts. Thus we do not investigate the behavior of the splitting below $e_-$. However, we are convinced that the maximal range of eccentricities is larger than $[e_-, e_+]$, in particular that the lower bound can be pushed well below $e_-$. We think that our mechanism of instability applies to this larger range of eccentricities. In fact, it is possible to study such exponentially small splitting using more sophisticated numerical methods, such as multiple-precision arithmetic, and high-order approximation of local invariant manifolds, see for instance [***?***, ***?***, ***?***].*

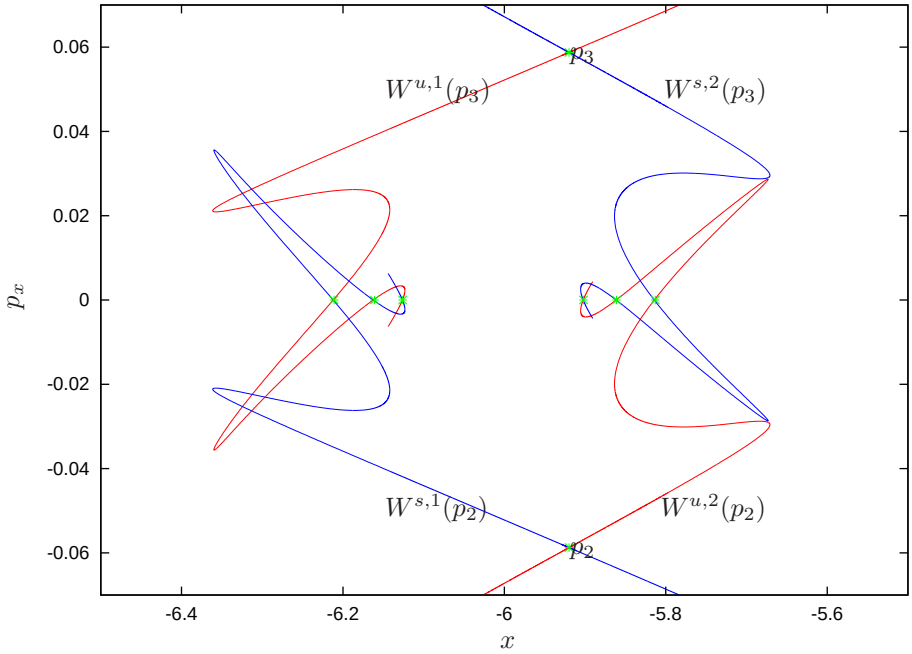


Figure 10: Invariant manifolds of the points $p_2$ and $p_3$ on the section $\Sigma^-$. Due to the symmetry, points that lie on the line $p_x = 0$ (marked in green) are intersection points.

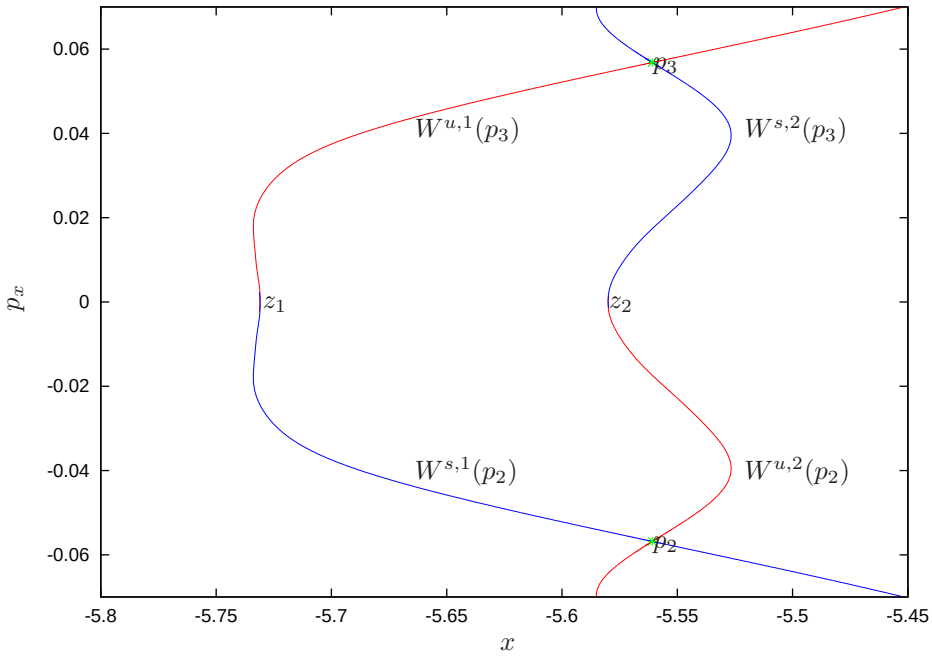


Figure 11: Invariant manifolds of the points $p_2$ and $p_3$ for the energy level $H = -1.74$.

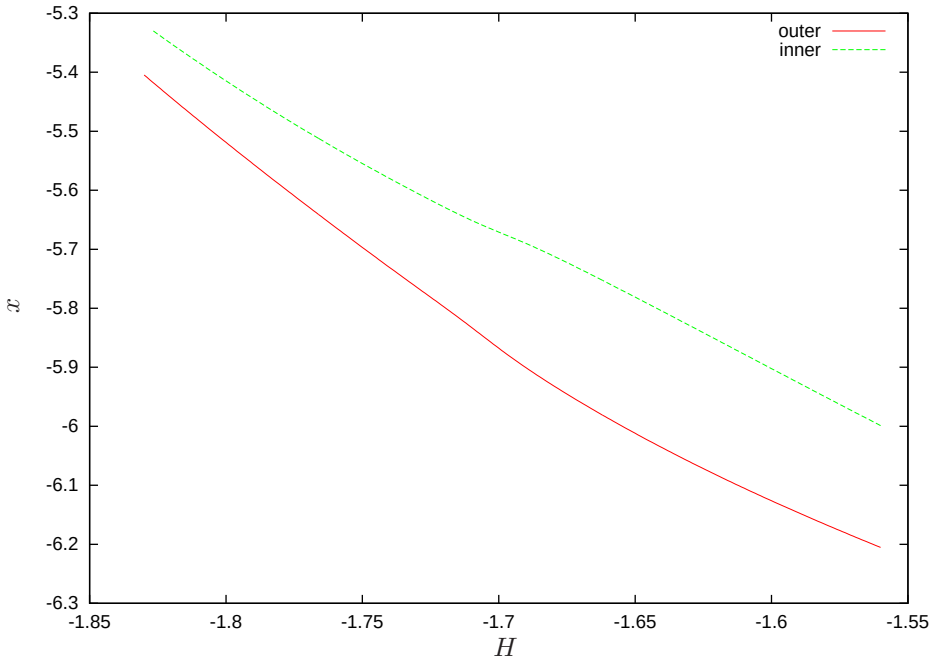


Figure 12: Family of primary intersection points corresponding to outer and inner splitting. For every energy level $H$, we plot the $x$ coordinate of the intersection point $z_1$ and $z_2$ (the $p_x$ coordinate is equal to zero). Notice that both families are continuous.

Consider first a fixed energy level $H = h$ that is close to the unperturbed situation, e.g. $H = -1.74$. The corresponding manifolds are given in Figure 11. In general, there are uncountably many intersection points. For instance, in Figure 10 we show six intersections on the symmetry line. However, when the perturbation is small, there is one distinguished intersection point located "in the middle" of the homoclinic. We call it the *primary* intersection point.

Let us compute the primary intersection point $z_1$ corresponding to the "outer" splitting of the manifolds $W^{u,1}(p_3)$ and $W^{s,1}(p_2)$. For $H = -1.74$, the *primary* intersection $z_1$ corresponds to the *first* intersection of the manifolds with the $p_x = 0$ line, as we grow the manifolds from the fix points. Thanks to the symmetry, it is enough to look for the intersection of $W^{u,1}(p_3)$ with the $p_x = 0$ axis, because $W^{s,1}(p_2)$ must also intersect the axis at the same point.

To compute the intersection point $z_1$, we continue using a linear approximation of the local manifold, and propagate a fundamental domain in the local manifold by iteration. Let $v_u$ be the unstable eigenvector associated to the point $p_3$. Consider the fundamental segment $l_u$ between the points $p_3 + \eta v_u$ and $\mathcal{P}(p_3 + \eta v_u)$, as in the previous section. First we look for the *smallest* natural $n$ such that $\mathcal{P}^n(l_u)$ intersects the $p_x = 0$ axis. Then we use a standard numerical method (bisection-like one-dimensional root finding) to find a point $z_u$ in the fundamental segment $l_u$ such that

$$\pi_{p_x}(\mathcal{P}^n(z_u)) = 0.$$

Thus we obtain the homoclinic point $z_1 = \mathcal{P}^n(z_u)$ in Figure 11. Numerically, we verify that $z_1$ is in the the $p_x = 0$ axis within $10^{-10}$ tolerance.

Finally, we vary energy $H$ and use a continuation method to obtain the family of primary intersections $\{z_1\}_H$, using as seed the primary intersection $z_1(H = -1.74)$ found above. See Figure 12.

**Remark B.5.** *For low energy levels (such as $H = -1.74$), corresponding to weak hyperbolicity, the invariant manifolds behave as if they were close to integrable, and the primary intersection corresponds to the* first *intersection of the manifolds with the $p_x = 0$ axis. For high energy levels (such as $H = -1.6$),*

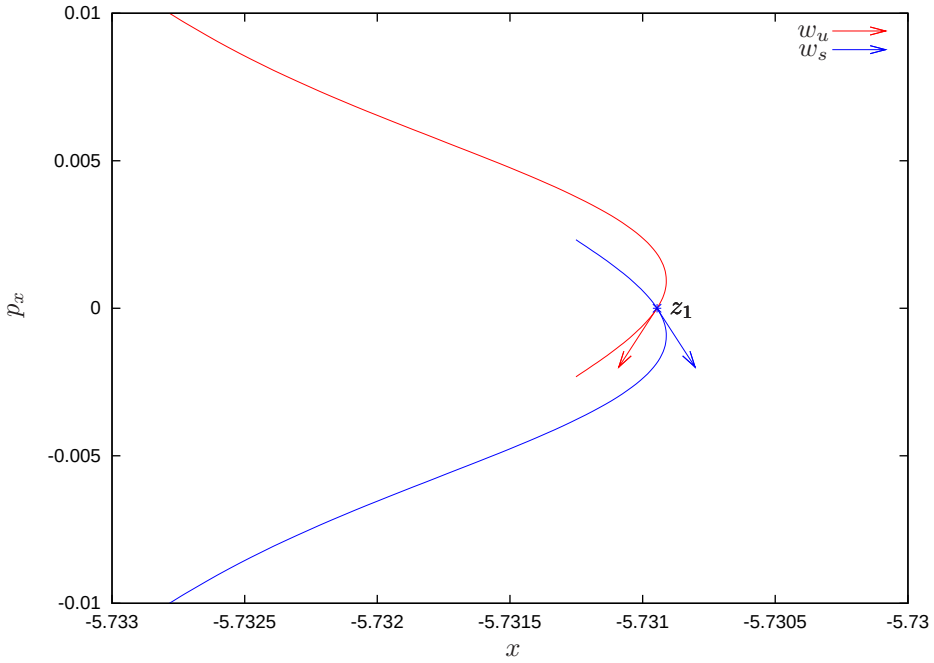


Figure 13: Outer splitting of the manifolds for energy level $H = -1.74$. This is a magnification of Figure 11 at the intersection point $z_1$. We show the vectors $w_u, w_s$ tangent to the unstable and stable manifolds at $z_1$. The splitting angle $\sigma$ is the angle between $w_u$ and $w_s$.

*corresponding to strong hyperbolicity, the manifolds develop some folds, and thus the primary intersection may not correspond to the* first *intersection of the manifolds with the $p_x = 0$ axis. See Figure 10.*

*In practice, we first identify the primary intersection at low energy levels, and then use a continuation method to obtain. the primary family of intersections up to high energy levels.*

Analogously, we compute the family of primary intersections $\{z_2\}_H$ corresponding to the inner splitting. See Figure 12.

Let us now compute the splitting angle between the manifolds $W^{u,1}(p_3)$ and $W^{s,1}(p_2)$ at the point $z_1$. For illustration, we show some numerical results corresponding to the energy value $H = -1.74$. First we need the tangent vectors $w_u$ and $w_s$ to the manifolds at $z_1$. See Figure 13. As found above, let $z_u$ be the point in the unstable fundamental segment that maps to $z_1$, i.e. $\mathcal{P}^n(z_u) = z_1$. Consider the tangent vector $v_u$ to the manifold $W^{u,1}(p_3)$ at the point $z_u$. (Recall that at this point the linear approximation is good enough, so we can use as $v_u$ the unstable eigenvector.) Multiply $v_u$ by the Jacobian of $\mathcal{P}$ at the successive iterates $\mathcal{P}^i(p_u)$, for $i = 0, ..., n-1$. This way, we obtain the tangent vector to the unstable manifold at $z_1$. Let us denote this vector $w_u = (w_1, w_2)$. We normalize it to $||w_u|| = 1$.

Due to reversibility, the vector $w_s$ tangent to the stable manifold at $z_1$ is $w_s = (w_1, -w_2)$. See Figure 13. Notice that we choose the tangent vectors with the appropriate orientation, i.e. with the same orientation as the trajectories on the manifolds.

Thus the oriented splitting angle between $w_u$ and $w_s$ is

$$\sigma = 2 \arctan_2(-w_1, -w_2),$$

where $\arctan_2$ is the arctangent function of two variables, which uses the signs of the two arguments to determine the sign of the result.

Finally, we let $H$ change and, using this procedure, we are able to obtain the splitting angle for energy levels $H \in [H_-, H_+]$. See Figure 14. The splitting angle is nonzero for all energy values except for a discrete set of them. The splitting angle oscillates around zero with decreasing amplitude as $H \to H_-$. Numerically, we find that the zeros of the splitting angle are contained in the intervals listed in Table 1.

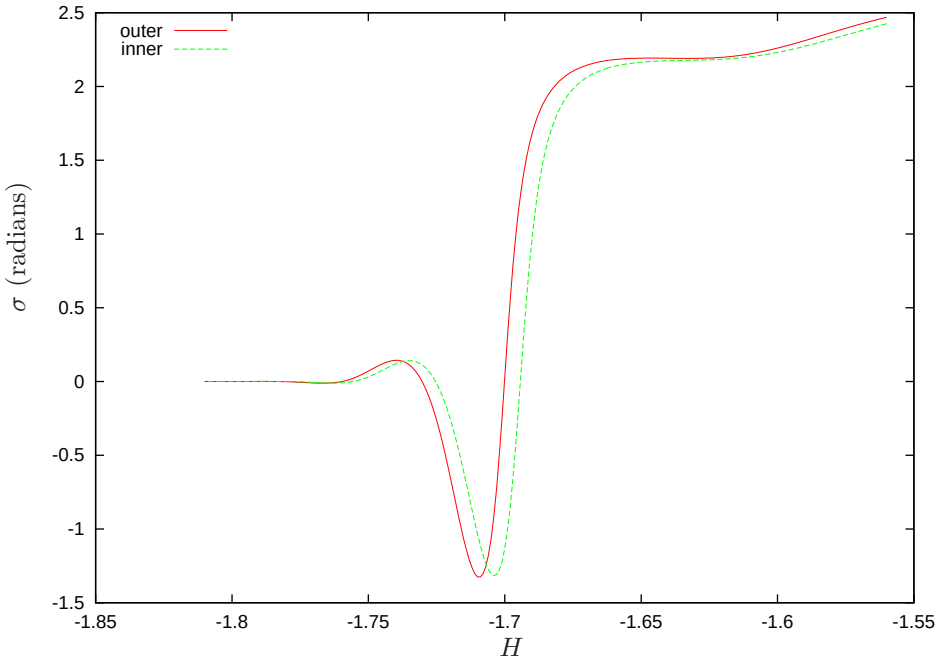


Figure 14: Splitting angle associated to inner and outer splitting.

| inner | outer |
|---|---|
| $(-1.695, -1.694)$ | $(-1.701, -1.700)$ |
| $(-1.726, -1.725)$ | $(-1.731, -1.730)$ |
| $(-1.756, -1.755)$ | $(-1.760, -1.759)$ |
| $(-1.781, -1.780)$ | $(-1.784, -1.783)$ |
| $(-1.802, -1.801)$ | $(-1.805, -1.804)$ |

Table 1: Subintervals of $H \in [H_-, H_+]$ containing the zeros of inner splitting (left column) and outer splitting (right column).

| $p_x$ | $x^u$ | $x^s$ | $x^u - x^s$ |
|---|---|---|---|
| $-0.00002$ | $-5.481541931871417$ | $-5.481541932226887$ | $0.000000000355470$ |
| $-0.00001$ | $-5.481541931790012$ | $-5.481541931967703$ | $0.000000000177691$ |
| $0.00000$ | $-5.481541931822124$ | $-5.481541931822124$ | $0.000000000000000$ |
| $0.00001$ | $-5.481541931967703$ | $-5.481541931790012$ | $-0.000000000177691$ |
| $0.00002$ | $-5.481541932226887$ | $-5.481541931871417$ | $-0.000000000355470$ |

Table 2: Sampling of the manifolds $W^{u,1}(p_3)$ and $W^{s,1}(p_2)$ at different values of $p_x$, and their difference (last column).

Notice that the inner and outer splittings behave similarly. However, they become zero at different values of $H$, as seen in Table 1. Thus, when one of the intersections becomes tangent, the other one is still transversal, and we can always use one of them for diffusion.

## B.4 Accuracy of the Computations

For small eccentricities, the splitting angle $\sigma$ becomes very small. We need to check the validity of $\sigma$, making sure that the size of (accumulated) numerical errors in the computation is smaller than the size of $\sigma$.

The smallest splitting angle in Figure 14, corresponding to $H_- = -1.81$, is

$$\sigma(H_-) = -1.777970294158603 \times 10^{-5}.$$

We check the validity of $\sigma(H_-)$ by recomputing this angle using an alternative numerical method. First we compute the intersection of the manifolds $W^{u,1}(p_3)$ and $W^{s,1}(p_2)$ with the horizontal axis defined by

$$p_x = \frac{j}{10^5}$$

for $j \in (-2, -1, 1, 2)$.

In Table 2 we tabulate the $x$ coordinate of $W^{u,1}(p_3)$ and $W^{s,1}(p_2)$ on these axis, and their difference $d = x^u - x^s$ gives the distance between the manifolds. We apply numerical differentiation to the last column of this table, using central differences centered at $z_1$ with step sizes 0.00002 and 0.00004, and obtain the values:

$$d_1 = \frac{d(0.00001) - d(-0.00001)}{0.00002} = -0.0000177691.$$

$$d_2 = \frac{d(0.00002) - d(-0.00002)}{0.00004} = -0.0000177735.$$

Finally, we use Richardson extrapolation and obtain:

$$d = \frac{4d_1 - d_2}{3} = -0.00001776763333333333.$$

Thus, using this alternative method, we obtain the splitting angle

$$\sigma(H_-) = \text{atan}(-0.00001776763333333333) = -0.00001776763333146364.$$

Compare the splitting angle computed using the two methods. They differ by approximately $10^{-8}$. This gives an estimate of the numerical error commited in our computation of the splitting angle.

We repeat this test for a range of energies $H \in [-1.81, -1.8]$. In Figure 15, we compare the splitting angle $\sigma(H)$ and the estimate of the numerical error $\text{err}(H)$. This error stays below $10^{-7}$, and it is several orders of magnitude smaller than the splitting angle. For higher energy values $H \in [-1.8, -1.56]$, the splitting angle is large, so the numerical error is certainly smaller. Therefore we are confident that the splitting angle has been accurately computed in the range of eccentricities considered, $[H_-, H_+]$.

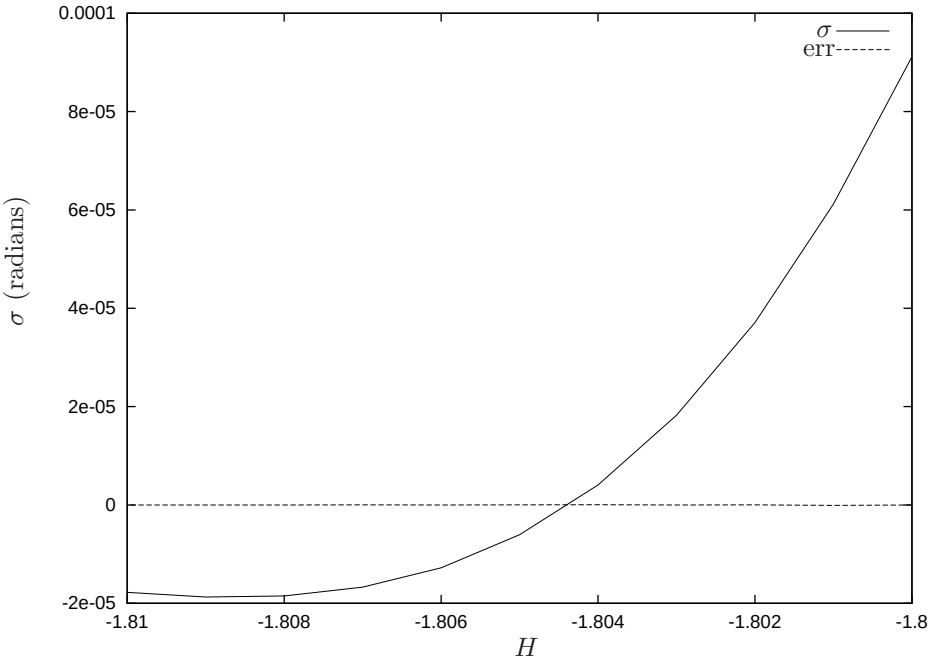


Figure 15: Splitting angle $\sigma(H)$ and estimate of the numerical error $\mathrm{err}(H)$ as a function of energy level $H$.

# C Geometric structure of the resonance in Delaunay coordinates

Explain that the Poincaré sections in Cartesian and Delaunay are very different. Explain that, after we transform periodic points to Delaunay, we have to flow them a little forward or backwards until they lie on the g=0 section.

Show a picture of the resonance (periodic points, inv. manifolds) in Delaunay.

# D Numerical study of the inner and outer dynamics

## D.1 Inner and outer dynamics of the circular problem

In this section, we numerically compute the inner map $\mathcal{F}_0^{\mathrm{in}}$ and the outer maps $\mathcal{F}_0^{\mathrm{out},*}$ of the circular problem, given in Section 3. XXX Change of notation: $H$ instead of $I$. XXX

As seen in Section 3.1, the inner map has the form

$$\mathcal{F}_0^{\mathrm{in}} : \begin{pmatrix} H \\ t \end{pmatrix} \mapsto \begin{pmatrix} H \\ t + \mu \mathcal{T}_0(H) \end{pmatrix}, \tag{93}$$

where $T_H = 14\pi + \mu\mathcal{T}_0(H)$ is the period of the periodic orbit obtained in Theorem 3 on the corresponding energy surface.

Recall that we computed the periodic orbit $\gamma_H$ as well as its period $T_H$ in Section B.1. In particular, Figure 5 shows a plot of the function $T_H - 14\pi = \mu\mathcal{T}_0(H)$. Notice that the derivative of the function $\mathcal{T}_0(H)$ is nonzero for the whole range $[\bar{H}_-, \bar{H}_+]$ of energy values. This shows that the inner map is twist. Moreover, Figure 5 shows that

$$0 < \mu\mathcal{T}_0(H) < 60\mu < \pi.$$

Therefore, the function $\mathcal{T}_0(H)$ satisfies the properties stated in Lemma 3.1

As a test, we have computed the same function $\mathcal{T}_0(H)$ using two different methods. First by computing the period of the periodic orbit, as above. Then by computing the integral expression (35) using numerical integration. The difference in $\mathcal{T}_0(H)$ using both methods is of the order $10^{-12}$.

As seen in Section 3.2, the outer maps have the form

$$\mathcal{F}_0^{\mathrm{out},*} : \begin{pmatrix} H \\ t \end{pmatrix} \mapsto \begin{pmatrix} H \\ t + \mu\omega^*(H) \end{pmatrix}, \quad * = \mathrm{f}, \mathrm{b}. \tag{94}$$

For simplicity, let us only discuss the computation of $\omega^{\mathrm{f}}(H)$ ($\omega^{\mathrm{b}}(H)$ is computed analogously). Recall from Lemma 3.2 that the function $\omega^{\mathrm{f}}(H)$ is defined as

$$\omega^{\mathrm{f}}(H) = \omega^{\mathrm{f}}_{\mathrm{out}}(H) + \omega^{\mathrm{f}}_{\mathrm{in}}(H),$$

where, taking into account that the homoclinic orbit is symmetric with respect to the involution (18),

$$\omega^{\mathrm{f}}_{\mathrm{out}}(H) = \omega^{\mathrm{f}}_{+}(H) - \omega^{\mathrm{f}}_{-}(H) = 2\omega^{\mathrm{f}}_{+}(H) \tag{95}$$

with

$$\omega^{\mathrm{f}}_{+}(H) = \lim_{N\to+\infty} \left( \int_0^{14N\pi} \frac{(\partial_G \Delta H_{\mathrm{circ}}) \circ \gamma^{\mathrm{f}}_H(\sigma)}{-1 + \mu(\partial_G \Delta H_{\mathrm{circ}}) \circ \gamma^{\mathrm{f}}_H(\sigma)}\, d\sigma + N\mathcal{T}_0(H) \right), \tag{96}$$

$$\omega^{\mathrm{f}}_{\mathrm{in}}(H) = \int_0^{-12\pi} \frac{(\partial_G \Delta H_{\mathrm{circ}}) \circ \gamma^{4}_H(\sigma)}{-1 + \mu(\partial_G \Delta H_{\mathrm{circ}}) \circ \gamma^{4}_H(\sigma)}\, d\sigma. \tag{97}$$

To obtain $\omega^{\mathrm{f}}(H)$, we compute the integrals (96) and (97) numerically, using a standard algorithm from the GSL library XXX Add reference XXX. The integrals are computed within a relative error limit $10^{-9}$.

The function $\partial_G \Delta H_{\mathrm{circ}}$ involved in both integrals is given explicitly in Appendix A. The integral $\omega^{\mathrm{f}}_{\mathrm{in}}(H)$ is evaluated on a periodic trajectory $\gamma^4_H(\sigma)$ of the circular problem with initial condition $p_4$, a fixed point of the Poincaré map $\mathcal{P}_0^7$ found in Section C. The integral $\omega^{\mathrm{f}}_{+}(H)$ is evaluated on a homoclinic trajectory $\gamma^{\mathrm{f}}_H(\sigma)$ of the circular problem with initial condition $z_2$, the primary homoclinic point corresponding to the inner splitting found in Section B.3.

Next we make a couple of important remarks about the numerical computation of the integral $\omega^{\mathrm{f}}_{+}(H)$. The key point is that the homoclinic orbit $\gamma^{\mathrm{f}}_H$ was already computed in section B.3 with high accuracy, and we can exploit this information here. Recall that the primary homoclinic point $z_2$ was obtained as the $n$-th iterate of a point $z_u$ in the local fundamental segment $l_u$ under the Poincaré map:

$$z_2 = \{\mathcal{P}_0^7\}^n(z_u). \tag{98}$$

Moreover, recall that the point $z_u$ was chosen to be suitably close to the fixed point $p_3$ for each energy level $H$. See Remark B.3.

Notice that the integral $\omega^{\mathrm{f}}_{+}(H)$ is defined by a limit as $N \to \infty$, i.e. as the homoclinic orbit $\gamma^{\mathrm{f}}_H(\sigma)$ assymptotically approaches the periodic orbit $\gamma^3_H(\sigma)$ in forward time (see equation (36)). Numerically, of course, we should stop integrating at an upper endpoint $N$ large enough such that the integral converges. In practice, we choose the upper endpoint $N = N(H)$ to be the number of iterates $n = n(H)$ in (98). This means that we evaluate the integral along the homoclinic trajectory $\gamma^{\mathrm{f}}_H(\sigma)$ until it reaches the point $z_u$, which is suitably close to the periodic orbit.

Notice also that integrating the homoclinic trajectory $\gamma^{\mathrm{f}}_H(\sigma)$ forwards in the reduced system means integrating it backwards along the unstable manifold in the original system. This is numerically unstable, since numerical errors grow exponentially. In practice, we rewrite the integral (96) using the change of variables $\hat{\sigma} = \sigma - 14N\pi$ so that the homoclinic trajectory is integrated forwards along the unstable manifold, starting from the point $z_u$.

The computed values of the functions $\omega^{\mathrm{f}}$ and $\omega^{\mathrm{b}}$ are shown in Figure 16.

To test the computation of the function $\omega^{\mathrm{f}}_{+}$, we directly verify the definition of the outer map 3.1. Let $z_2 = (L_h, \ell_h, G_h, 0)$ be the primary homoclinic point, and let $p_3 = (L_p, \ell_p, G_p, 0)$ be the periodic

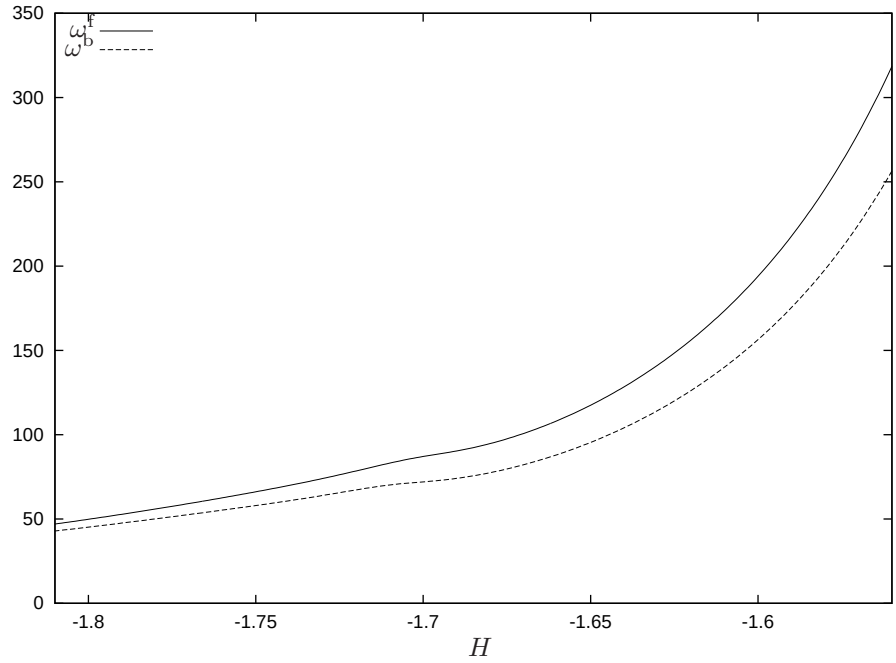


Figure 16: Functions $\omega^{\mathrm{f}}$ and $\omega^{\mathrm{b}}$ involved in the definition of the outer map (94) of the circular problem.

point. Given a point $(L_h, \ell_h, G_h, 0, I, t)$ in the extended circular problem, we check that it is forward assymptotic (in the reparametrized time) to the point $(L_p, \ell_p, G_p, 0, I, t + \omega^{\mathrm{f}}_+)$, where $t \in \mathbb{T}$ is arbitrary. Thus we check that the distance

$$\mathrm{dist}^+(s) = |\Phi_0\{s, (L_h, \ell_h, G_h, 0, I, t)\} - \Phi_0\{s, (L_p, \ell_p, G_p, 0, I, t + \omega^{\mathrm{f}}_+)\}| \xrightarrow{s\to\infty} 0$$

with exponential decay.

The result of the test is shown in Figure 17 for values of the energy $H \in [H_-, H_+]$. Notice that the vertical axis is in logarithmic scale. Let $s = 14N\pi$. We plot the distance $\mathrm{dist}^+$ as a function of $N$ (multiples of the period). The test shows exponential decay of the distance function for all energy values, i.e. straight lines in the plot.

Recall that the periodic orbit $\gamma_H$ becomes more hyperbolic as the energy $H$ increases. Thus, the rate of exponential convergence between the homoclinic and the periodic trajectory also increases, i.e. the straight lines have increasing slope in the plot. As explained above, the length of integration $N = N(H)$ along the homoclinic orbit is suitably chosen for each energy level. For energy values $H \to H_-$, there is exponential decay up to time $s = 40 \cdot (14\pi) \approx 1760$.

## D.2 Inner and outer dynamics of the elliptic problem

In this section, we numerically compute the first orders in $e_0$ of the inner map $\mathcal{F}^{\mathrm{in}}_{e_0}$ and the outer maps $\mathcal{F}^{\mathrm{out},*}_{e_0}$ of the elliptic problem, given in Section 4. In order to compare the inner and outer dynamics of the elliptic problem through Lemma 5.2, only some specific terms in the expansions of the inner and outer maps are necessary. Namely, we only need to compute the term $A_1$ in the expansion of the inner map (58), and the term $B^*$ in the expansion of the outer map (69).

Recall from section 4.4 that $A_1$ can be split as

$$A_1(I, t) = A_1^+(I)e^{it} + A_1^-(I)e^{-it}.$$

Since $A_1^+$ and $A_1^-$ are complex conjugate, it is only necessary to compute one of them. Let us compute

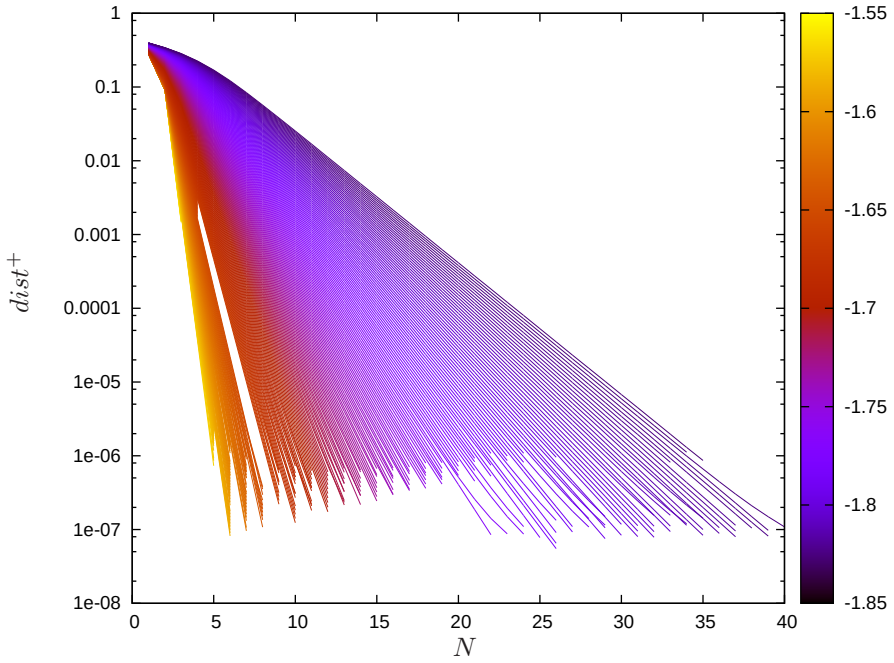


Figure 17: Exponential decay of the function $\text{dist}^+$ as a function of $N$ (multiples of the period) for different energy levels. The energy levels $H \in [H_-, H_+]$ are color-coded.

the positive harmonic,

$$A_1^+(I) = -i\mu \int_0^{-14\pi} \frac{\Delta H_{\text{ell}}^{1,+} \circ \gamma_I^3(\sigma)}{-1 + \mu \partial_G \Delta H_{\text{circ}} \gamma_I^3(\sigma)} e^{i\widetilde{\gamma}_I^3(\sigma)} d\sigma. \tag{99}$$

Notice that the denominator is the same one used in the previous section for the inner and outer dynamics of the circular problem. Next we give the numerator $i\Delta H_{\text{ell}}^{1,+}$ explicitly. Let

$$\begin{aligned} \Delta H_{\text{ell}}^1(L,\ell,G,g,t) = &-\frac{1-\mu}{\mu}\mathcal{B}_1\left(-\frac{r(L,\ell,G)}{\mu}, v(L,\ell,G), g, t\right) \\ &-\frac{\mu}{1-\mu}\mathcal{B}_1\left(\frac{r(L,\ell,G)}{1-\mu}, v(L,\ell,G), g, t\right), \end{aligned} \tag{100}$$

where $\mathcal{B}_1$ is the function defined in Lemma 4.1. Then it is straightforward to see that

$$\begin{aligned} \Delta H_{\text{ell}}^{1,+}(l,L,g,G) = &-\frac{1-\mu}{\mu}\mathcal{B}_1^+\left(-\frac{r(L,\ell,G)}{\mu}, v(L,\ell,G), g\right) \\ &-\frac{\mu}{1-\mu}\mathcal{B}_1^+\left(\frac{r(L,\ell,G)}{1-\mu}, v(L,\ell,G), g\right), \end{aligned} \tag{101}$$

where

$$\mathcal{B}_1^+(r,v,g) = -\frac{1 - r\cos(v+g) - i2r\sin(v+g)}{2\Delta^3(r, v+g)}.$$

The computed value of the function $A_1^+$ is shown in Figure 18.

For the outer map, we compute the functions $B^*(I)$. Similarly to $A_1$, it is only necessary to compute the positive harmonics $B^{*,+}$. Recall from Lemma 4.4 that the positive harmonics $B^{\text{f},+}(I)$ and $B^{\text{b},+}(I)$ are defined as

$$\begin{aligned} B^{\text{f},+}(I) &= B_{\text{out}}^{\text{f},+}(I) + B_{\text{in}}^{\text{f},+}(I) e^{i\mu\omega_{\text{out}}^{\text{f}}(I)} \\ B^{\text{b},+}(I) &= B_{\text{in}}^{\text{b},+}(I) + B_{\text{out}}^{\text{b},+}(I) e^{i\mu\omega_{\text{in}}^{\text{b}}(I)}, \end{aligned} \tag{102}$$

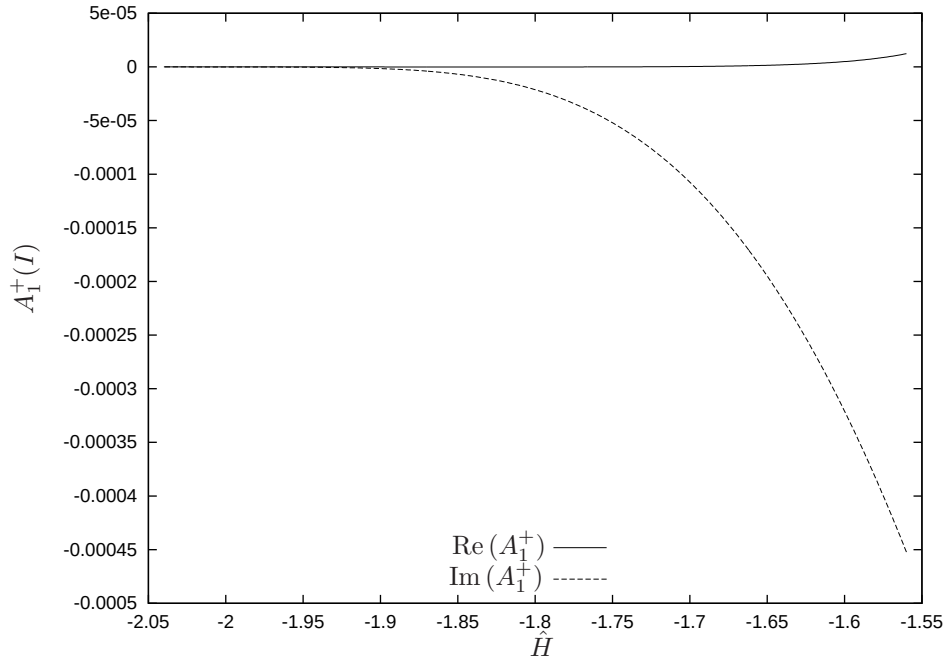


Figure 18: Function $A_1^+(I)$ (real and imaginary parts) involved in the definition of the inner map (58) of the elliptic problem as a function of the energy of the system in rotating coordinates $\hat{H}$. Recall that $\hat{H} = -I$.

where $\omega_{\mathrm{out}}^{\mathrm{f}}$ and $\omega_{\mathrm{in}}^{\mathrm{b}}$ were obtained in Section D.1. To obtain $B_{\mathrm{out}}^{*,+}$ and $B_{\mathrm{in}}^{*,+}$, we compute the integrals (71)–(75) numerically, using the same techniques as in the previous section D.1.

The computed values of the functions $B^{\mathrm{f},+}(I)$ and $B^{\mathrm{b},+}(I)$ are shown in Figure 19.

## D.3 Comparison of the inner and outer dynamics of the elliptic problem

Finally, we verify the non-degeneracy condition

$$\widetilde{B}^{*,\pm}(\mathcal{I}) \neq 0 \qquad \text{for } \mathcal{I} \in \mathcal{D}^* \tag{103}$$

stated in Lemma 5.2, which implies the existence of a transition chain of tori. Since $B^{*,+}$ and $B^{*,-}$ are complex-conjugate, it is only necessary to compute one of them. Let us compute the positive harmonic,

$$\widetilde{B}^{*,+}(\mathcal{I}) = B^{*,+}(\mathcal{I}) - \frac{e^{i\mu\omega^*(\mathcal{I})} - 1}{e^{i\mu\mathcal{T}_0(\mathcal{I})} - 1} A_1^+(\mathcal{I}).$$

All the functions involved in the expression above are known: $\mathcal{T}_0$ and $\omega^*$ are obtained in section D.1, $A_1^+$ and $B^{*,+}$ are obtained in section D.2.

The computed values of the functions $\widetilde{B}^{\mathrm{f},+}$ and $\widetilde{B}^{\mathrm{b},+}$ are shown in Figure 20. Therefore, we see that the functions $\widetilde{B}^{*,+}$ are not identically zero. This justifies the statement (88) in Lemma 5.2.

**Remark D.1.** *Figure 20 also shows that $\widetilde{B}^{\mathrm{f},+}$ and $\widetilde{B}^{\mathrm{b},+}$ are almost identical, which is surprising for the authors. However, this fact is not relevant for the argument in Lemma 5.2; we only need that these functions do not vanish identically.*

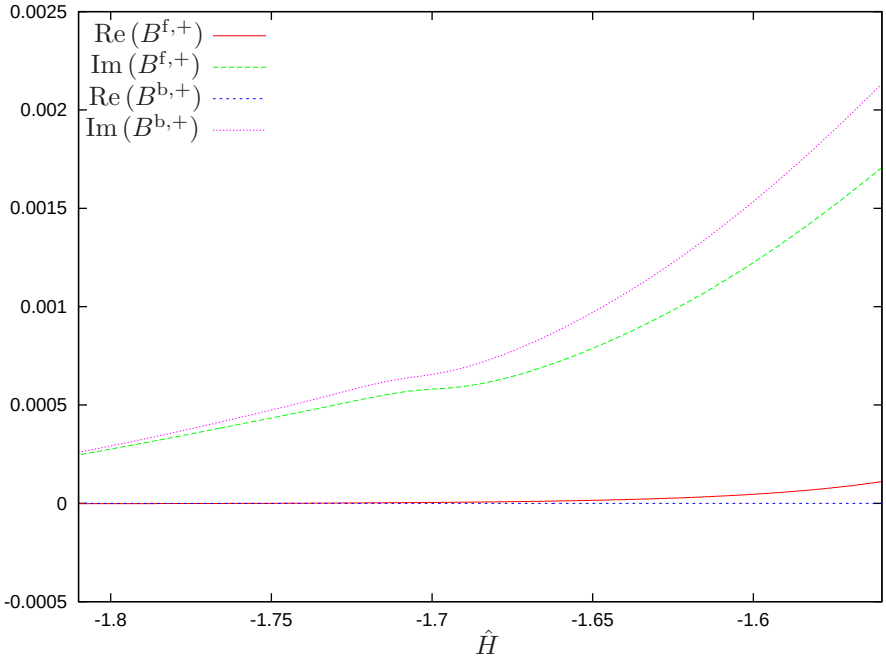


Figure 19: Functions $B^{\mathrm{f},+}$ and $B^{\mathrm{b},+}$ (real and imaginary parts) involved in the definition of the outer map (69) of the elliptic problem.

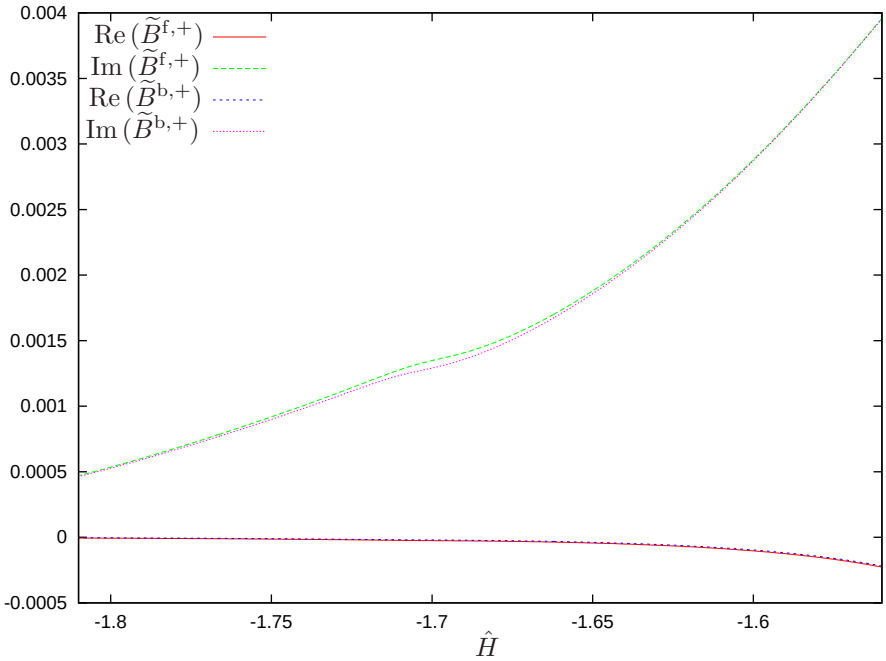


Figure 20: Functions $\widetilde{B}^{\mathrm{f},+}$ and $\widetilde{B}^{\mathrm{b},+}$ (real and imaginary parts).